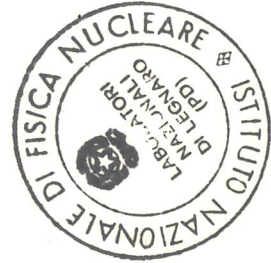# FEASIBILITY STUDY
of a
HADRON FACILITY

Conceptual Design Report

February 1992

ISTITUTO NAZIONALE DI FISICA NUCLEARE
LABORATORI NAZIONALI DI LEGNARO

FEASIBILITY STUDY
of a
HADRON FACILITY

Conceptual Design Report

February 1992

ISTITUTO NAZIONALE DI FISICA NUCLEARE
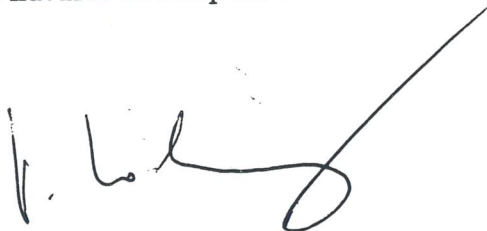### LABORATORI NAZIONALI DI LEGNARO

1

Contents

i

Preface

Beginning with a first meeting held in Trieste on october 1985 a study group was formed with scientists and experts in accelerator physics and technology from several european and american institutions to study the feasibility of a hadron facility for the production of 30 GeV proton beams at an intensity of 100 μA. The study lasted about three years and a dozen workshops on the subject were held in several countries; its ultimate purpose was to develop a conceptual outline of accelerator components, their characteristics and the cost associated. All this work has been summarized in a final report, the "Proposal for a European Hadron Facility" (May 1987), which did not make any reference to a specific site. This document is a valuable milestone, representing the state of the art for the realization of such a project.

The efforts of this international community continued the following two years; a new series of workshops were organized in Legnaro, Eindhoven and Lecce. During this period the emphasis shifted to include in the design a specific site and the Laboratori Nazionali di Legnaro were chosen as the reference. The scope of the study was then limited to a 1.2 GeV proton accelerator and expanded to include the acceleration of heavy ions, since LNL owns a Tandem and the post-accelerator ALPI.

During this second phase, a large amount of technical information was produced and gathered together; it is now very important to collect all of that information in this summary report, which is also addressed to the nuclear physics community, to make it aware of the variety of applications available with the project investigated. This document is therefore not intended as an official proposal for approval of construction and authorization of funding.

The valuable contribution of all of the participants listed in the next page is greatly aknowledged. A special thank goes to the experts, not only for solving crucial design issues, but also for spreading their knowledge to a young generation of scientists. It is the LNL intention to elaborate from this report a formal proposal to the proper authorities for the construction of a project sized to the needs for a natural developement of the laboratory in the near future.

Prof. Pietro Dalpiaz
Director of the Laboratori Nazionali di Legnaro

Legnaro, 10th February 1992

The following persons have contributed to the feasibility study:

G. Bassato	INFN-LNL
G. Benincasa	CERN, Geneve
G. Bisoffi	INFN-LNL
B. Blind	Los Alamos Nat. Lab.
K. Bongardt	KFA, Julich
H. Bothe	DESY, Hamburg
J. I. M. Botman	Tech. Hogeschool, Eindhoven
F. Bradamante	Trieste
M. Cavenago	INFN-LNL
F. Cervellera	INFN-LNL
M. Conte	Genova
M. Craddock	TRIUMF, Vancouver
J. F. Crawford	PSI, Villingen
A. Dainelli	INFN-LNL
P. Dalpiaz	INFN-LNL
M. J. A. de Voigt	Tech. Hogeschool, Eindhoven
H. Deitinghoff	Inst. fur Angewandte Phys., Frankfurt
G. Di Massa	Napoli
J. Doornbos	TRIUMF, Vancouver
A. Facco	INFN-LNL
S. Fazinic	Rudjer Boskovic Inst., Zagreb
G. Fortuna	INFN-LNL
D. Fiander	CERN, Geneve
F. Galluccio	CERN, Geneve
J. Griffin	Fermilab, Batavia
H. L. Hagedorn	Tech. Hogeschool, Eindhoven
G. Heritier	CERN, Geneve
H. Klein	Inst. fur Angewandte Phys., Frankfurt
P. Lapostolle	Neuilly sur Seine
Y. Y. Lee	Brookhaven Nat. Lab., Upton
A. Lombardi	INFN-LNL
G. Mancarella	Lecce
A. Massarotti	Trieste
M. R. Masullo	Napoli
M. F. Moisio	INFN-LNL
G. Moschini	Padova
M. Pabst	KFA, Julich
C. Planner	Rutherford Appleton Lab., Chilton Didcot
A. Pisent	INFN-LNL
A. M. Porcellato	INFN-LNL
M. Puglisi	Trieste
M. Pusterla	Padova
A. Ratti	Brookhaven Nat. Lab., Upton
G. Rees	Rutherford Appleton Lab., Chilton Didcot
P. L. Riboni	CERN, Geneve
C. Rossi Alvarez	INFN-LNL
A. G. Ruggiero	Brookhaven Nat. Lab., Upton
G. Schaffer	Los Alamos Nat. Lab.
H. Schonauer	CERN, Geneve
G. Soliani	Lecce
P. Spolaore	INFN-LNL
L. Tecchio	Torino
B. Tiveron	INFN-LNL
H. A. Thiessen	Los Alamos Nat. Lab.
V. Vaccaro	Napoli
M. Vretenar	CERN, Geneve
T. Weis	Inst. fur Angewandte Phys., Frankfurt
M. Weiss	CERN, Geneve

1
General Overview

A feasibility study of an accelerator complex, which takes the site of Laboratori Nazion-ali di Legnaro (LNL) as reference is described in this conceptual design report. The main components of the complex are a Heavy Ion Injection system and two rings, a Booster and a Decelerator, both with a maximum rigidity of 22.25 Tm, connected by a Transfer Line where exotic isotopes are produced and selected. The facility has two main goals:

a. Acceleration of stable ion species to kinetic energies of the order of few GeV/u, at a repetition rate of 10 Hz with intensities in excess of 10^{11} ions per second, for fixed target experiments in nuclear physics and for production of unstable isotopes.

b. Acceleration of protons to a kinetic energy of 5.8 GeV also at a repetition rate of 10 Hz for an average output current of 8 μA, or to 1.2 GeV at a repetition rate of 50 Hz for an average current of 40 μA.

With an upgrade of the proton injector, it is possible to raise the output current to about 100 μA, and the proposed complex of accelerators could then be used as the first stage of a larger hadron facility which would be able to produce high intensity beams of protons at 30 GeV, and beams of heavy ions such as gold with specific kinetic energies around 12 GeV/u.

1.1 The Hadron Facility

The individual components of the facility investigated are the following (Figure 1.1.1):

- a Heavy Ion Injector (XTU tandem and the ALPI post-accelerator);
- a Fast Cycling Synchrotron (Booster);
- a Slow Cycling Synchrotron (Decelerator);
- a Transfer Line (connecting the two rings);
- an Experimental Area;
- a H$^-$ High Intensity Linear Accelerator.

The location of the Hadron Facility on the LNL site is shown in Figure 1.1.2. The two accelerators have the same size and similar lattices. They can hold beams of particles with magnetic rigidity of 22.25 Tm, and are arranged in a vertical layout with the Decelerator exactly on top of the Booster and 2.5 metres above it. The lattices of the two rings have been designed to allow enough drift space for rf cavities, components for injection and

extraction, etc. (Table 1.1.1) A fourfold superperiodicity has been found convenient, with each superperiod made of a 90° arc and a 22 m long straight section. The arcs are made of FODO cells 11 metres long. The betatron tunes are 5.8 (H) and 3.8 (V), away from any low-order systematic resonance. Natural chromaticity is small and easily correctable with two families of sextupole magnets. The transition γ of 4.6 is high enough to be avoided by all acceleration cycles, except when protons are accelerated to 5.8 GeV at 10 Hz.
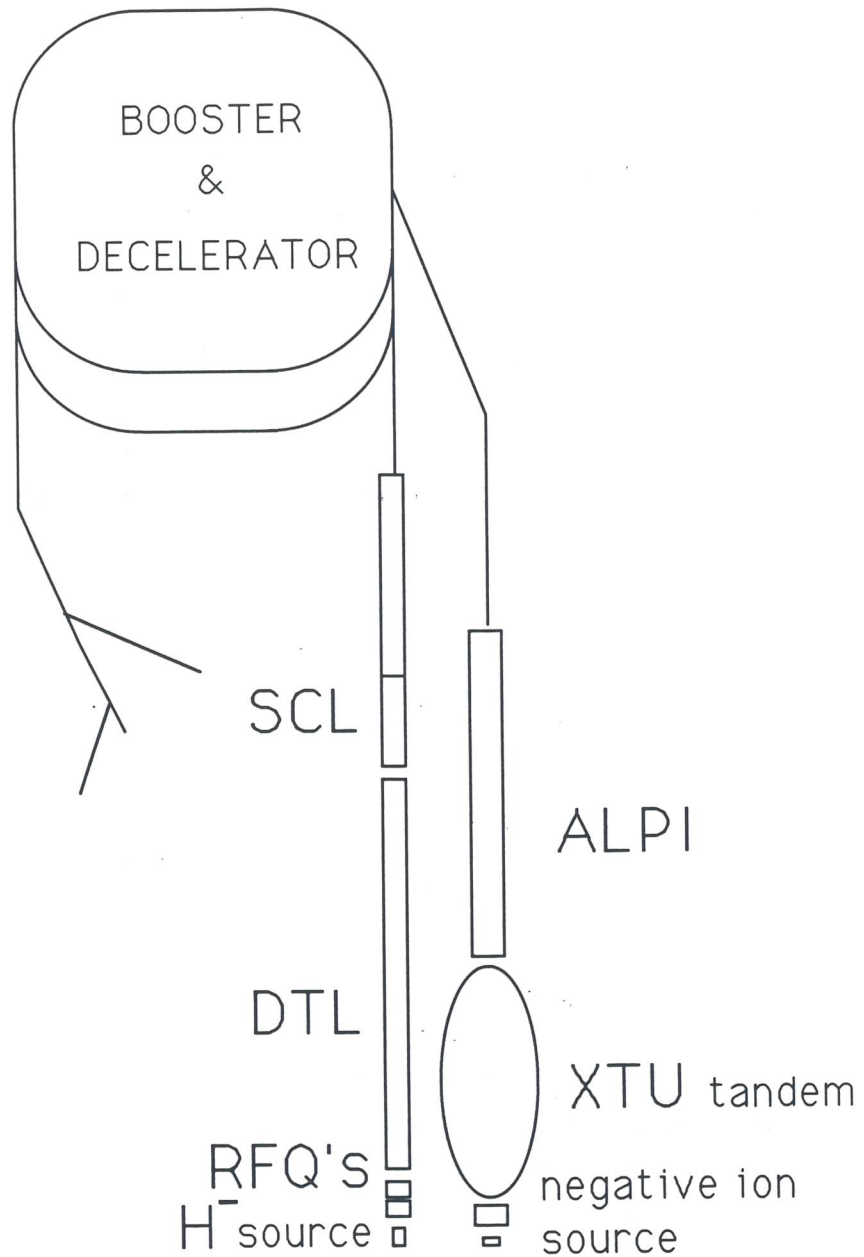

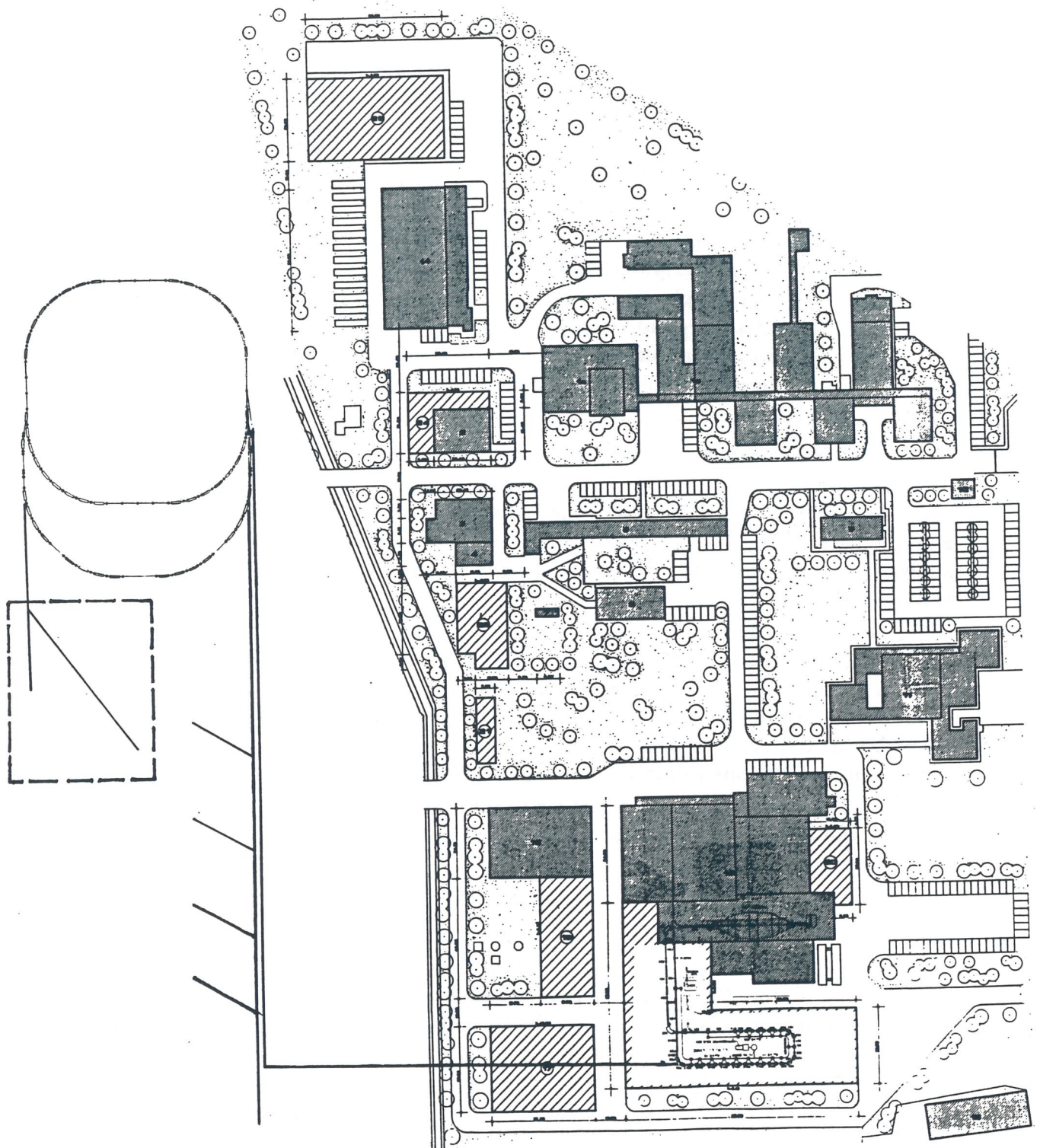Figure 1.1.1: Schematic layout of the Hadron Facility.

Figure 1.1.2: The Hadron Facility on the LNL site.

Table 1.1.1: General lattice parameters of the Facility rings.

Maximum Magnetic Rigidity		22.25	Tm
Circumference		266.6667	m
Bending Radius		17.62	m
Maximum Dipole Field		1.26	T
Dipole vertical gap		10	cm
Maximum Quadrupole gradient		9.0	T/m
Quadrupole bore radius		7	cm
Superperiodicity		4	
Transition Energy (γ_t)		4.6	
Betatron tunes:			
Horizontal plane	ν_h	5.8	
Vertical plane	ν_v	3.8	
Natural Chromaticity:			
Horizontal plane	ξ_h	-5.5	
Vertical plane	ξ_v	-4.9	

The Decelerator has basically the same lattice of the Booster, the same circumference and geometry, except for the long straight sections; a different quadrupole configuration allows a magnet-free drift space more than 11 m long, to accommodate electron cooling for heavy ions.

The dipole magnets have a gap of 10 cm, are 3.5 metres long and have a maximum field of 1.26 T. The physical aperture of the quadrupoles is circular with 7 cm radius. The number of power supply busses is minimized for easy tracking and tuning. A point of concern is the large rate of excitation of the dipole field, which is 38 T/s for both the proton and heavy ion modes of operation. The same maximum field excitation and variation rate allow acceleration of protons to 5.8 GeV.

In consideration of the dual nature of the project, which can accelerate heavy ions and protons, the two modes of operation are described separately.

1.2 Heavy Ion Cycle

The Laboratori Nazionali di Legnaro own and operate a Tandem Van de Graaff with a terminal voltage of 16 MV, used to accelerate continuous beams of heavy ions. Essentially all ion species up to lead can be accelerated at large intensities; acceleration of uranium requires source development. We propose a pulsed mode of operation of the Tandem, as already demonstrated successfully with a similar machine at Brookhaven National Laboratory. This mode of operation makes the Tandem the ideal injector for a heavy ion facility which employs a fast cycling synchrotron. A negative ion source is pulsed with a pulse duration of 360 μs at a repetition rate of 10 Hz. The following analysis is based on the example of gold. Negative-ion sources for gold in pulsed mode have been realized with peak currents in excess of 200 p-μA. In the scheme proposed here, the ions are accelerated towards the high voltage

terminal (+16 MV), where they hit a target and are partially stripped. In the case of gold an intermediate charge state of +13 is obtained, and the ions are further accelerated from the positive terminal toward ground where they exit the Tandem. Since the stripping efficiency is about 20%, the beam current in exit is decreased to 40 p-μA. One virtue of the Tandem is that it is able to deliver intense beams without sacrificing the small betatron emittance and momentum spread typical of electrostatic machines. The specific kinetic energy of Au^{+13} at the exit of the Tandem is about 1 MeV/u.

At the Laboratori Nazionali di Legnaro the construction of a linear accelerator (ALPI) is in a completion phase; the project is made of superconducting cavities with 80 and 160 MHz working frequencies for the equivalent of 40 MV accelerating voltage. The project will allow acceleration of heavy ions to an energy of 5-30 MeV/u depending on the species and charge state. For the proposal described here, ions of gold with charge state +13 are accelerated through a section corresponding to a total voltage of 36 MV; at the end of this section, where $\beta > 0.08$, they hit a second stripping target where a new charge state (+51) is produced with a reasonable efficiency of 15%. After acceleration through the final 4 MV section of the linear post-accelerator the final beam energy is 4.6 MeV/u, corresponding to $\beta \sim 0.1$.

Table 1.2.1: General parameters for the heavy ion acceleration mode.

	S	Cu	Au	U	
Atomic Number Z	16	29	79	92	
Mass Number A	32	63	197	238	
Charge State Q	16	27	51	54	
Injection Kinetic Energy	16.4	10.4	4.6	3.9	MeV/u
Extraction Kinetic Energy	2.53	2.08	1.03	0.85	GeV/u
Harmonic number	24	30	45	49	
Beam Intensity	2.0	1.8	0.7	0.7	10^{11} ions/s
Normalized Emittance	23	18	12	11	π mm-mrad
Bunch Area	0.017	0.011	0.005	0.005	eV/u - s

The time structure of the ALPI beam is generated by a 5 MHz pre-buncher located at the Tandem entrance, with a compression system (buncher) made of 80 and 160 MHz superconducting cavities located at the entrance of the post-accelerator. With this bunching system only one bucket in 32 at the exit of ALPI will be loaded. Assuming an overall transmission efficiency of 50% in addition to the stripping efficiencies, the beam current at the entrance of the Booster is 3 p-μA. The circumference of the Booster has been chosen to correspond to the injection of 45 bunches of gold ions per turn; the number of turns that can be injected is between 20 and 40. The rf harmonic at injection is also 45, corresponding to an injection frequency of 5 MHz, equal to the pre-buncher frequency. With this choice, all the rf buckets are occupied by beam bunches, except for the gap required for beam extraction. Each injected bunch is very short, about 1/50 of the length of the rf bucket.

Thus a "painting" procedure can be applied to the multi-turn injection of the heavy ions to fill the rf buckets uniformly. At the end of the process about 6×10^9 ions of gold have been injected. The resulting tune depression due to space charge is estimated to be 0.05, assuming that the beam fills essentially all the available aperture; this yields a normalized betatron emittance of 12 π mm-mrad. The beam is then accelerated to 1 GeV/u at a rate of 10 Hz, yielding 6×10^{10} ions of gold per second. Higher intensities are possible with source development; the ultimate intensity, which corresponds to the space-charge limit, is 3×10^{11} ions per second. Even higher intensities and energies can be obtained with lighter ions. The maximum dipole field required for this mode is less than 1.3 T, and the maximum rate of change is 38 T/s.

A peak voltage of 220 kV is required during the acceleration cycle; the beam velocity varies between $\beta = 0.1$ and $\beta = 0.9$ requiring a large frequency swing from 5 to 45 MHz. This is accomplished with two rf cavity systems: the first operates from 5 to 32 MHz, the second from 30 up to 50.5 MHz to allow also acceleration of protons.

Several modes of operation with heavy ions are possible. The beam can be extracted at the end of the acceleration cycle and sent toward external target stations, or it can be transferred to the Decelerator which can be used as a Stretcher with slow-spill extraction for 100% duty cycle. The possibility of producing ion fragments, for the study of fusion processes etc., is examined next.

A transfer line takes the beam from the Booster to the Decelerator. Along the transport the beam first encounters a target where fragments are produced, at about the same kinetic energy, with medium-to-large mass numbers, and completely stripped. Selection of the required fragment species is then obtained with a second target, called the *degrader*, placed in a region of large dispersion, with a system of collimators to select the desired species. The combination of the targeting and the focussing along the transport will allow the capture of a total momentum spread of 0.7% and a betatron emittance of 20 π mm-mrad in both planes. The expected yield can be as high as 1×10^{-4} fragments per incident ion. The secondary beam is then injected into the Decelerator. Here the bunches of fragments are captured by a 45 MHz rf system, rotated in the longitudinal phase space to present a smaller momentum spread (0.1%) and displaced by an additional rf system to an off-momentum trajectory at a distance of 1.2%, where they are allowed to debunch. The required voltage for the bunch operation is 1.4 MV, which can be obtained with two cavities.

Electron cooling is applied to the beam on the stacking orbit. A new pulse is injected every 100 ms, which has to be matched by the electron cooling rate. While both transverse and momentum cooling take place, the more important requirement is the reduction of the beam momentum spread by an order of magnitude. This process repeats until 12 pulses have been stacked (Figure 1.2.1); electron cooling then continues for a further 0.5 seconds, in conjunction with stochastic cooling. Finally the beam is decelerated from the energy of the fragments at production, down to about 5 MeV/u, which is near the Coulomb potential barrier energy at which fusion cross-sections are expected to be maximal. The deceleration lasts 0.3 s, and is followed by an interval of 0.1 s during which the field is reset to its initial value. At the end of the 2 second long cycle, the beam is extracted and directed to the experimental area. The beam momentum spread at this stage is 0.1%. A second step of electron cooling lasting about 100 ms can be applied just before extraction, for a further reduction of the beam momentum spread, for instance to 0.01%.

Tables 1.2.1 and 1.2.2 list the main parameters of the project for the acceleration and storage of heavy ions.
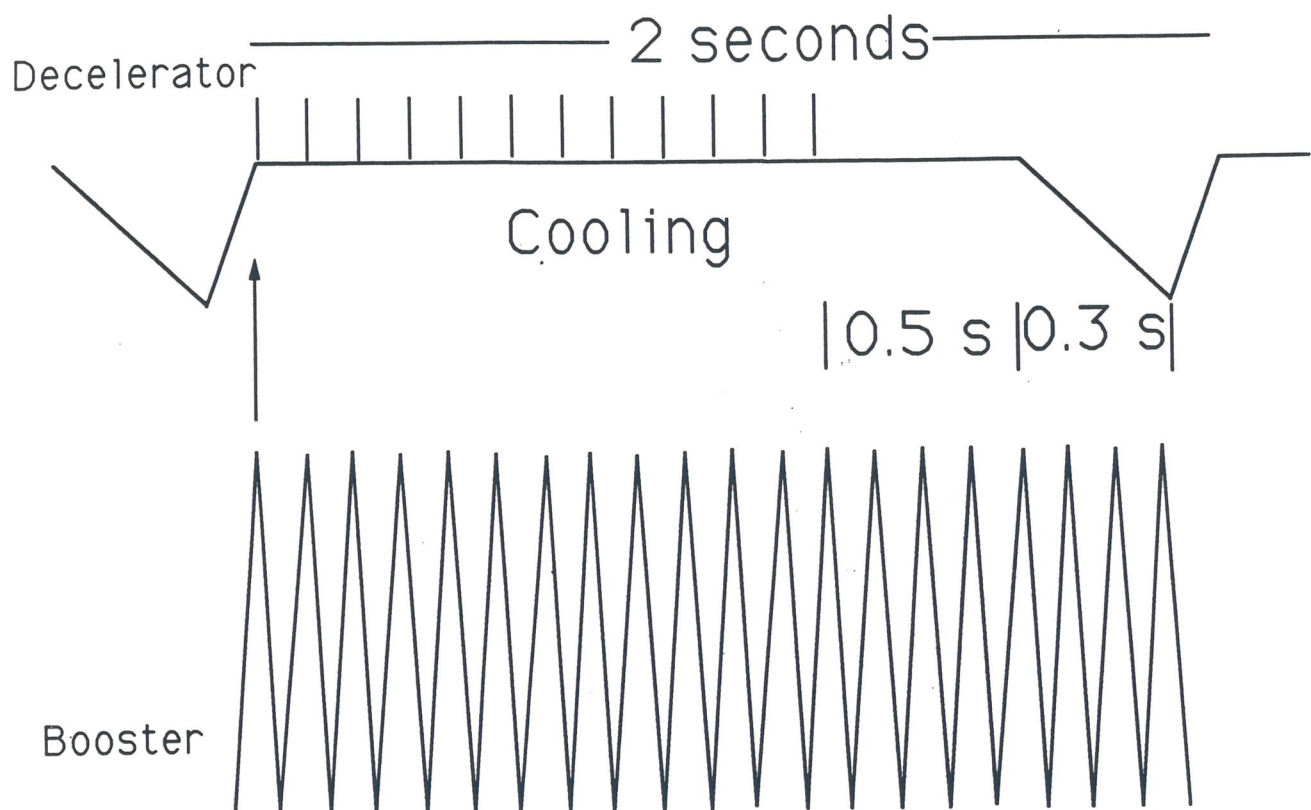
Figure 1.2.1: Magnetic cycle of the Hadron Facility.

Table 1.2.2: General parameters of the Cooling Systems.

Number of Ions	$1 \cdot 10^7$	
Mass Number, A	200	
Atomic Number, Z	80	
Specific Kinetic Energy	1.0	GeV/u
β	0.88	
Initial Emittance	20	π mm mrad
Initial Momentum Spread	0.28	%
Final Emittance	1	π mm mrad
Final Momentum Spread	0.01	%

Electron Cooling parameters

Length of e-beam	8	m
e-beam Diameter	10	mm
e-beam Current	12.5	Amp
Cooling Time	0.3	s
e-beam Energy	0.57	MeV
e-beam Power	7.1	MW

Stochastic Cooling parameters

Bandwith	1-2	GHz
Method	Notch Filter	
Number of Pickups	16	
Number of Kickers	32	
Schottky Power	1.0	kW
Thermal Power	negligible	
Amplifier Gain	160	dB
Cooling Time	0.3	s

1.3 Proton Cycle

It is possible to accelerate protons in the Booster at the same repetition rate of 10 Hz to a kinetic energy close to 6 GeV; the average expected intensity is about 8 μA. Apart from the addition of a proton linac, another requirement for the acceleration of protons is to add a few more rf cavities to cover the larger frequency band. No other modifications or additions are needed. At the nominal excitation, the dipole field is 1.26 T which corresponds to an energy of 5.8 GeV.

A further concept behind the design is to provide a proton source at 1.2 GeV to match the requirements of a possible future hadron facility with an average current of about 100 μA. In this mode of operation the Booster would work at a repetition rate of 50 Hz, accelerating

protons to 1.2 GeV in 10 ms. One pulse would then be stored in the Decelerator to wait for a second pulse to be accelerated in the Booster. At the end of this sequence, the two pulses would be transferred, one after the other, to a subsequent larger ring, which could operate at 25 Hz. For this mode of operation more rf cavities would have to be added, and the magnet power supply would have to be modified to allow cycling at 50 Hz. Moreover the maximum dipole field would be only 0.36 T, with a maximum rate of rise of 38 T/s, the same as in the 10 Hz mode of operation for heavy ions.

A further design goal is to provide a high beam-brilliance, which requires a normalized emittance in the Booster of 25 π mm-mrad corresponding to a space-charge tune-depression of 0.2 at the injection energy of 211 MeV.

Table 1.3.1 summarizes the mode of operation of the project for the acceleration of protons.

The proton injector consists of a negative-ion source, followed by two RFQs operating at frequencies of 32.5 and 130 MHz, then by a section of drift tube linac (DTL) for acceleration to 90 MeV at a frequency of 390 MHz, and finally by a short section of side-coupled linac (SCL) working at 1300 MHz for a final kinetic energy of 211 MeV. The longitudinal phase-space compression, due to the acceleration and proper matching sections, permits the required frequency jumps. The frequency of the first RFQ equals the rf at injection into the Booster, so that an individual bunch from the first RFQ can be transferred to an rf bucket of the Booster. Each of these bunches will be initially compressed to a length of about 1/40 of the Booster rf wavelength; this will constitute the "brush" for "painting" the rf buckets during injection into the Booster, to minimize losses and space-charge limitations.

The circumference of both the Booster and the Decelerator is 266.7 m. The rf for the acceleration cycle is chosen to be between 30 and 50 MHz, profitting from experience at the Fermilab Booster. To allow a 150 ns gap for injection/ejection, only 43 of the 50 rf buckets in the Booster are loaded; the remaining 7 are empty.

To maintain a space-charge tune-depression of not more than 0.2 and a beam normalized emittance of 25 π mm-mrad at injection into the Booster, a total of 5×10^{12} protons are accelerated per pulse, which corresponds to an average output current of 40 μA. Assuming an average current from the negative-ion source of 6.5 mA, 80 turns need to be injected, over $\sim$ 120 μs.

An average output current of 100 μA can be obtained with a larger injection energy into the Booster. Because of the uncertainties of the beam performance and of the actual space-charge limit in the Booster, the present proposal calls for a 211 MeV linac. Based upon operational experience, larger intensities could be obtained either by injecting more turns or by allowing larger beam emittances. A decision could then be reached on the energy upgrade of the linac in a second phase. It would indeed be possible to lengthen the SCL for further acceleration to 535 MeV. The space-charge limit at this injection energy value corresponds to a total of 1.1×10^{13} protons, which yields an average current of 88 μA. With a source current of 12.5 mA and no beam losses, 120 turns would have to be injected, over $\sim$ 140 μs in order to reach this intensity. At the design stage, enough space must be left for the addition of more SCL sections. Everything else remains unchanged, with the exception of the first RFQ which is replaced with another one operating at 43.3 MHz, the frequency at injection into the Booster at 535 MeV. In this case the width of the "brushes" is about 1/30 of the rf wavelength in the Booster.

The rf frequency range for acceleration from 211 MeV (535 MeV) to 1.2 GeV is 32.5 (43.3) - 50.5 MHz. Assuming a purely sinusoidal magnet cycle, a total peak rf voltage of

520 kV is required in the Booster. For acceleration to 5.8 GeV with 10 Hz repetition rate, the rf frequency has to be increased up to 56 MHz.

Table 1.3.1: General parameters for the proton acceleration mode.

Repetition Rate	10	50	Hz
Injection Energy	211	211	MeV
Extraction Energy	5.8	1.2	GeV
Number of Protons per Cycle	5×10^{12}	5×10^{12}	
Average Current	8	40	μA
Space-Charge Tune-Shift	0.2	0.2	
Harmonic Number	50	50	
rf Frequency	30-56	30-51	MHz
rf Voltage	330	520	kVolt
Normalized Emittance	25	25	π mm-mrad
Bunch Area	0.05	0.05	eV-s

At the injection energy of 211 MeV the actual beam emittance is 35 π mm-mrad. With a good field factor of 50% of the magnet vertical aperture, the required betatron acceptance is four times the beam emittance, i.e. 140 π mm-mrad. The required momentum aperture is expected to be 1%, for a total bunch area of 0.05 eV-s.

At the end of the acceleration cycle, the beam is ejected and transferred in a single turn into the Decelerator. There the beam is kept bunched and coasting with no energy change. The rf system has to operate at constant frequency and needs no more than 100 kV. It is also possible to send the beam directly to an experimental area for physics at 1.2 or 6 GeV, or to operate the Decelerator as a Stretcher where the beam is completely debunched and extracted over a 20 or 100 ms period with 100% duty cycle.

2

Injectors

2.1 Heavy Ion Injector

Heavy ions are injected into the Booster using the facilities at LNL: the existing XTU tandem and the ALPI superconducting post-accelerator now under construction [1]. The ALPI post-accelerator will be able to accelerate heavy ion beams to an energy equivalent to what would be delivered by a 40 MV electrostatic accelerator. The layout of the injector is shown in Figure 2.1.1.

The XTU tandem-ALPI combination is able to provide the short, high current pulses of heavy ions required to fill the Booster. Moreover the combination provides very good quality beams with small transverse emittance and momentum spread, which allows the injection of several beam turns into the reasonably small magnet aperture of the Booster.

It is also possible with this scheme to obtain beams with a wide range of mass numbers at sufficiently high charge states by using stripping targets at proper locations. The most demanding species to accelerate are of course the heaviest ones. In the following we take gold to be the reference case; however, other ions have also been considered (see Table 2.1.2).

2.1.1 The XTU Tandem

The XTU Tandem is an electrostatic accelerator of very reliable and established performance [2]; it is fed by a sputter source (Ionex 860) capable of delivering ions of any desired species (except the noble gases) with an initial charge state of -1. The negative ion source is currently operated in continuous mode, which is the conventional mode of operation of this device for most atomic and nuclear physics applications. But it is also possible to pulse the sputter source over short periods of time, at relatively high repetition rate. This mode of operation has been demonstrated at Brookhaven National Laboratory [3]; it is most useful when high peak currents are required for injection into a circular accelerator. For the complex in study the required repetition rate of the source is 10 Hz, equal to the repetition rate of the Booster, with a pulse duration of 360 μs corresponding to 40-turn injection, assuming gold ions. The peak current within a pulse can be taken to be 200 p-μA for all species, though this value can probably be exceeded with present sputter source technology. As described later, this value is still well below the space-charge limit at injection into the Booster, so that an increase in the source current would be most welcome because it would allow either a reduction in the pulse duration, and hence in the number of injection turns required for a given current, or alternatively a higher accelerated current.

In the first section of the Tandem, the beam is accelerated from the source towards the high-voltage terminal, which in the case of the XTU Tandem is at 16 MV. Since the charge state of the ions during this step is -1, the total kinetic energy at the terminal is just 16 MeV. At the terminal the beam hits the first stripping target where the ions are stripped of some of their electrons. For very light ions the stripping process is actually complete. In the following Q_T will denote the charge state acquired at the high-voltage terminal, and S_T the stripping efficiency, i.e. the fraction of the beam which survives.

In the second section of the Tandem, the beam is accelerated from the positive high-voltage terminal to ground potential at the downstream end of the accelerating column. The total kinetic energy gained in this section is $16 \cdot Q_T$ MeV, and the total kinetic energy from the entire Tandem $16 \cdot (Q_T + 1)$ MeV (plus the $150 \div 300$ keV from the injection platform).

The bunching operation for injection into the ALPI post-accelerator is performed with two main devices. The first, a double-drift buncher with a basic frequency of 5 MHz, is located between the high voltage platform housing the sputter source and the entrance to the Tandem; the second device (a time compressor) is located in front of the ALPI post-accelerator and actually consists of two superconducting Quarter Wave Resonators with operating frequencies of 80 and 160 MHz. The choice of 5 MHz for the operating frequency of the double-drift buncher gives for the case of a gold ion beam a 360 μs pulse made up of a train of 1800 bunches spaced by 200 ns.

The beam survival rate is 50% after the first pre-bunching, and essentially all of it passes through the superconducting time compressor.

A summary of beam parameters for different ion species is shown in Table 2.1.2 for comparison.

2.1.2 The ALPI post-accelerator

The ALPI post-accelerator is a series of superconducting Quarter Wave Resonators [4a] made of OFHC (Oxygen-Free High-Conductivity) copper electroplated with lead which, following the international experience, have been devoleped also at Legnaro since 1986 [4b,1,4c,4d]. The transverse focussing and the bending are done with normally conducting techniques. To accelerate heavy ions over a wide range of velocities, a broad Transit Time Factor curve is required; this is obtained with a two-gap cavity of the type shown in Figure 2.1.2. The central inner conductor is filled with liquid helium, and the cavity operates below the critical temperature of lead.

Each cavity is independently phased to enable the acceleration of ion species with very different velocities. Furthermore, the large β variation of a single ion species along the machine requires the use of different sections of the post-accelerator for different β ranges. This is achieved by means of three sections: a low-β section with 24 cavities ($\beta_{opt}=0.055$) operating at 80 MHz; a medium-β section with 48 cavities ($\beta_{opt}=0.11$) at 160 MHz; and a high-β section ($\beta_{opt}=0.15$) with 21 cavities also operating at 160 MHz. The average accelerating field is of the order of 3.0 MV/m with a quality factor of about 10^8 and a total dissipated power around 6 W per cavity. The kinetic energy gain per cavity is around 0.45 MeV per charge unit and the equivalent total accelerating voltage is about 40 MV. ALPI consists essentially of a series of similar modules of the type shown in Figure 2.1.3, each of which accommodates two cryostats containing four cavities, with a central room-temperature triplet for transverse focussing. General parameters are summarized in Table 2.1.1.

For the case of gold ions, the beam is injected into the ALPI post-accelerator with charge state +13, which is produced at the stripping target in the XTU tandem; acceleration then continues through a section equivalent to a total of 35 MV, the gold ions acquiring a specific kinetic energy of about 3.5 MeV/u; this corresponds to $\beta = 0.0864$, high enough for a second, highly efficient stripping stage. The location of the second stripping target is shown by a dot in Figure 2.1.1. The gold ions then acquire a new charge state $Q_F = 51$; the stripping efficiencies S_F for gold and other reference ions are shown in Table 2.1.3. The ions then traverse the remaining 5 MV section where their specific kinetic energy increases to a total of 4.58 MeV/u, which corresponds to $\beta = 0.0988$.

Table 2.1.3 also summarizes the expected beam characteristics at the end of acceleration in ALPI for several ion species. Light ions like sulphur will already be completely stripped by the second target. The beam transverse emittance and momentum spread depends mostly on multiple scattering effects in the stripping targets. A final rms emittance of 1 π mm-mrad is assumed here. For design purposes, the second stripping target is taken to be at the same position in the ALPI post-accelerator for all ion species; the location chosen corresponds to a net voltage of 35 MV. Of course during design optimization, and also during machine operation, the stripping location can be easily changed from species to species. Carbon foils are used for stripping targets, both in the XTU tandem and the ALPI post-accelerator, with a thickness of a few tens of $\mu g/cm^2$ optimized to yield the charge state which corresponds to the largest efficiency estimated with conventional formulae [5]; some corrections are required [6], but under the present conditions they are small and are therefore ignored.

Finally, each beam pulse is made of a train of micro-bunches which, during acceleration in the 160 MHz section of ALPI, occupy 1 in 32 rf buckets. The required pulse lengths for other ion species are also given in Table 2.1.3; they are estimated assuming 40-turn injection into the Booster. The same source current of 200 p-μA is assumed for all ion species. The average current in a beam pulse is then obtained by multiplying the source current by the stripping target efficiencies (10÷80% according to ion masses), and by the bunching and transport efficiencies, which have been taken to be 50% total. The Tandem-ALPI combination operates at a repetition rate of 10 Hz for all ion species, matching the repetition rate of the Booster.

2.1.3 The Ion Transfer Line (ITL) between ALPI and the Booster

As shown in Figure 2.1.4, the extraction point from the ALPI post-accelerator and the injection point of the Booster are separated by a 360 m long transport line consisting of focussing quadrupoles, a few bending magnets and one debuncher cavity. Between extraction from ALPI and injection into the Booster, the beam must be bent by 90° to the right and then by 25° to the left. This is accomplished by two magnets of 45° each and one of 25°.

The transport line is designed to provide matching of the lattice functions at both upstream and downstream ends, avoiding unnecessary dilution of the beam emittances. The design of the line takes advantage of the concept of standard FODO cells with about 90° phase advance per cell, with special matching doublets or triplets at the ends. The magnet elements are listed in Table 2.1.4. As far as possible, quadrupoles are all of the same length, cross-section and strength, and are similar to those employed in the ALPI project.

To minimize civil construction, the ITL is located in the same building housing the

proton linac. Thus, the heavy ion beam goes from the ALPI post-accelerator towards the proton linac; after a bend of 90°, it runs parallel to the proton linac from south to north. At the end of the linac the proton and heavy ion transfer lines merge for final transport to injection into the Booster.

Table 2.1.1 Acceleration in the ALPI Complex. General Parameters

XTU Tandem Terminal Voltage	16	MV
ALPI Post Accelerator		
Average Accelerating Field	3.0	MV/m
Synchronous Phase	-20	deg
Maximum Magnetic Rigidity	3.3	Tm
Length	~80	m
Number of Cavities :		
Low Beta Section $\beta = 0.055$	24	
Medium Beta Section $\beta = 0.09$	48	
High Beta Section $\beta = 0.15$	21	
Length of Modules :		
'Short' Modules	4.06	m
'Long' Modules	4.30	m
Number of Cavities per Module :		
Low- & Medium-β Sections	8	
High-β Section	6	
Number of Cryostats per Module	2	
Resonant Frequency :		
Low-β Section	80	MHz
Medium- & High-β Sections	160	MHz

Table 2.1.2 Beam Parameters at the exit of the XTU tandem.

Ion Species	S	Cu	I	Au	U
Atomic Number	16	29	53	79	92
Mass Number	32	63	127	197	238
Rest Energy (GeV/u)	0.93047	0.93029	0.93068	0.93126	0.93161
Q_T	9	11	12	13	13
S_T	0.34	0.27	0.20	0.20	0.20
Kinetic En. (MeV/u)	5.00	3.05	1.64	1.14	0.94
β_T	0.1033	0.0808	0.0593	0.0494	0.0449
Current (p-μA)	34	27	20	20	20

Table 2.1.3 Beam Parameters at the exit of the ALPI post-accelerator.

Ion Species	S	Cu	I	Au	U
Q_F	16	27	40	51	54
S_F	0.50	0.46	0.21	0.16	0.14
β_S	0.1776	0.1402	0.1033	0.0864	0.0786
Kinetic En. (MeV/u)	16.40	10.39	6.11	4.58	3.86
β_F	0.1853	0.1483	0.1140	0.0988	0.0908
Pulse length (μs)	192	240	312	360	392
Energy Spread			10^{-4}		
Transverse Emittance (rms)			1π mm-mrad		
Current (p-μA)	17.0	12.4	4.2	3.2	2.8

Table 2.1.4 List of components for the ITL.

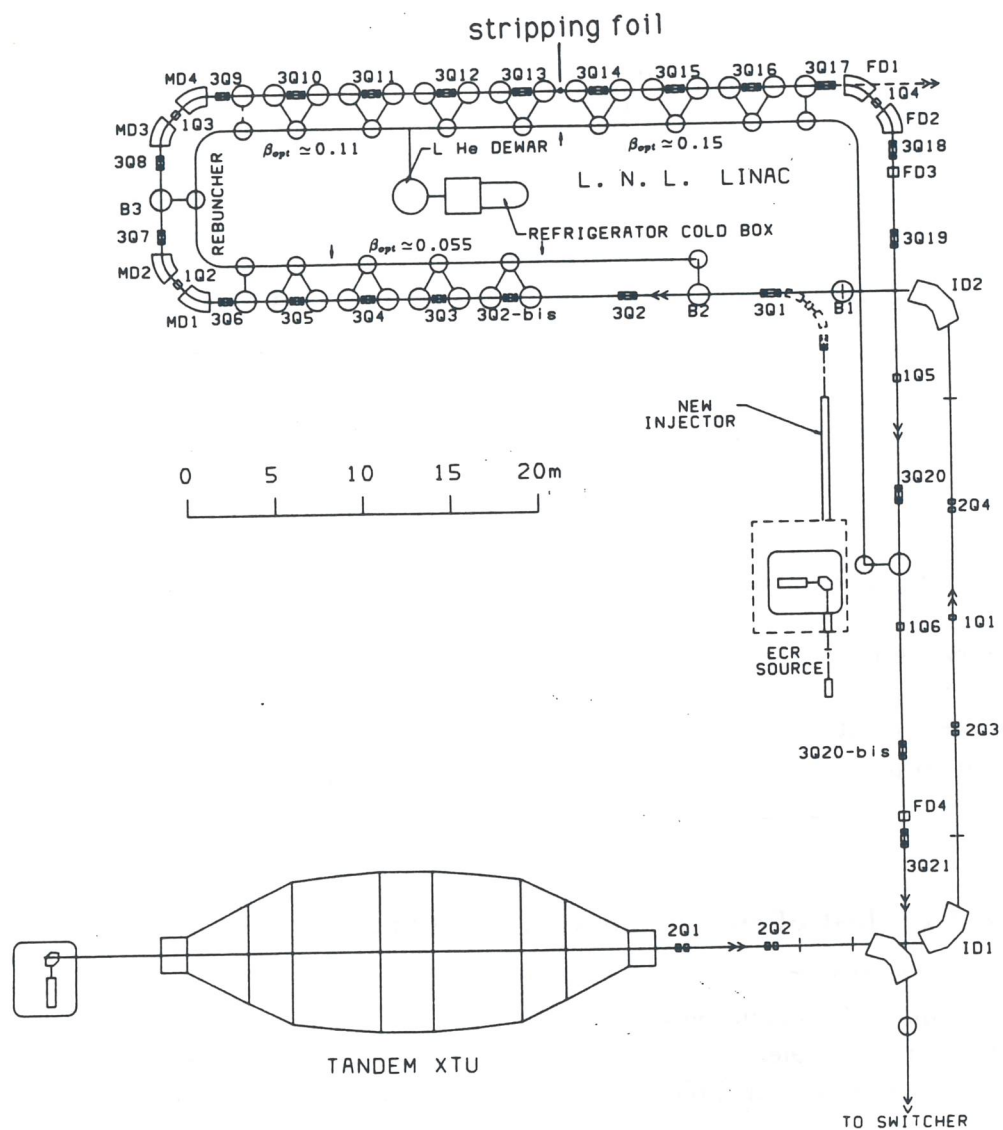|	
Total number of quadrupoles	50
Length of quadrupoles	0.8 m
Bore diameter of quadrupole	50 mm
Dipole magnets:	
45° Bend, number	2
25° Bend, number	1
vertical gap	50 mm
Number of steering dipoles	50

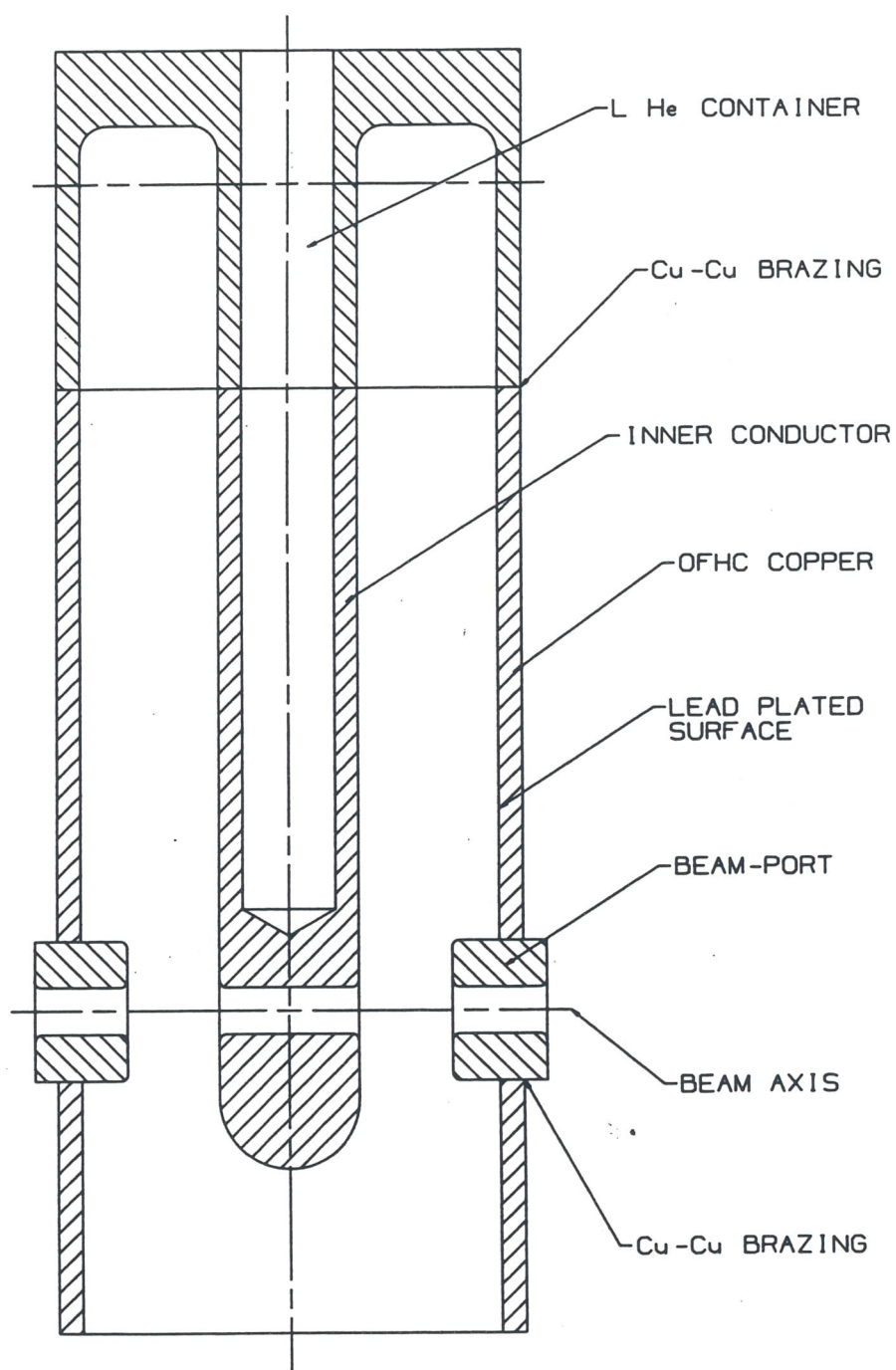Figure 2.1.1: Layout of the ALPI complex project.

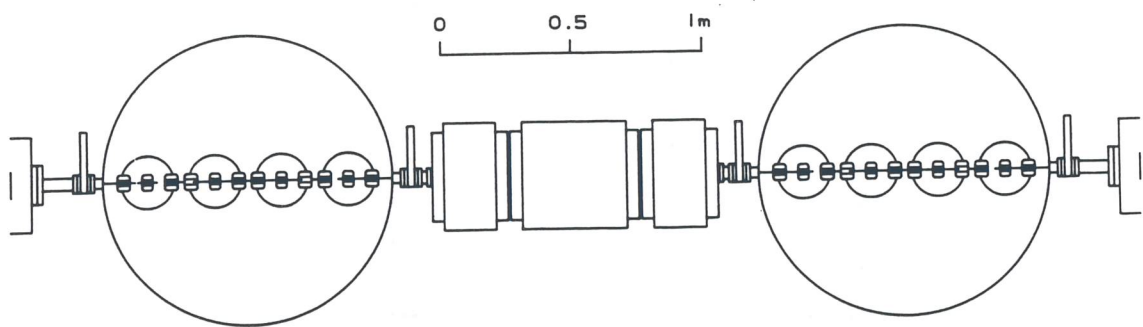Figure 2.1.2: Quarter-Wave Resonator of the ALPI post-accelerator.

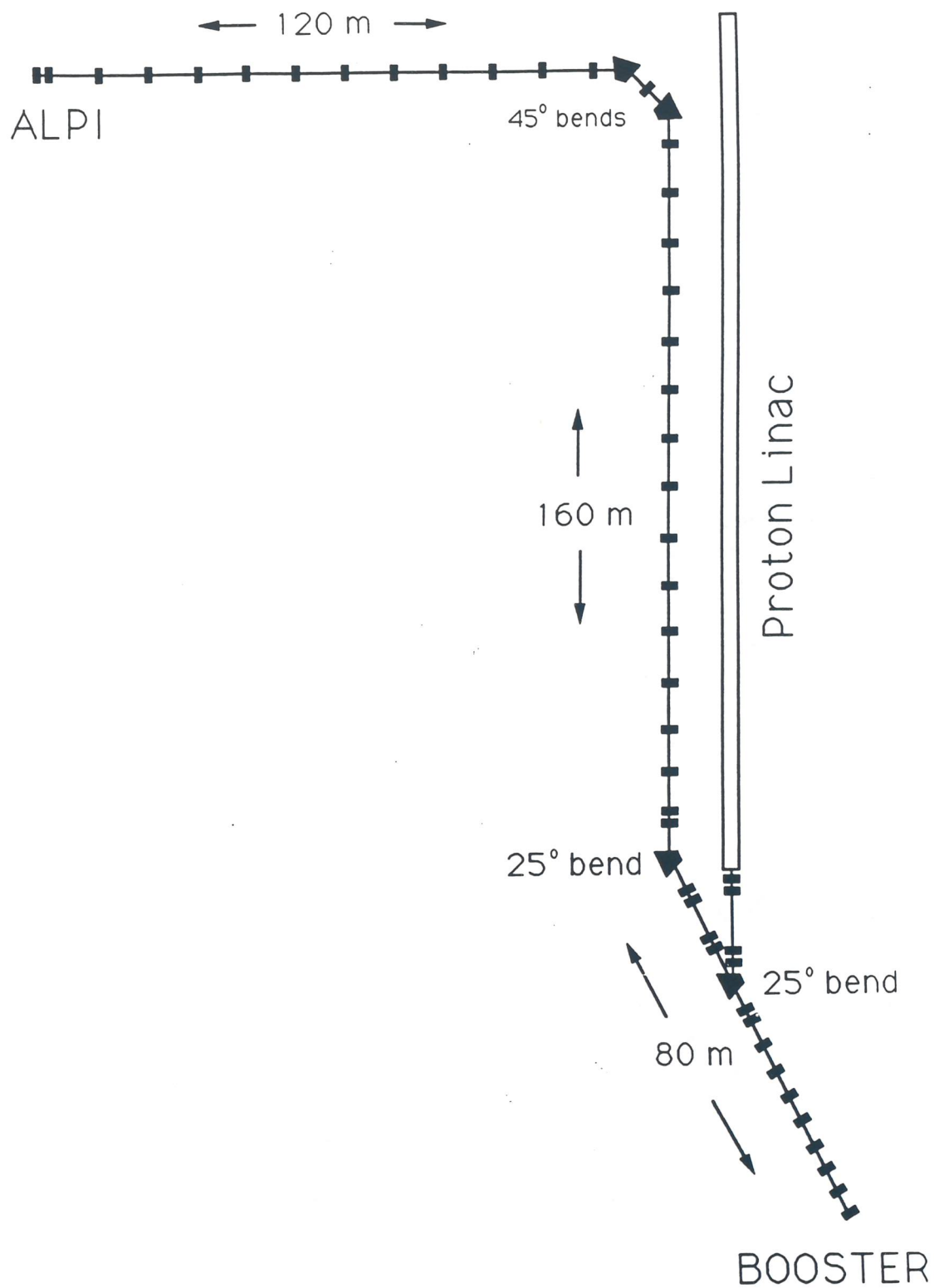Figure 2.1.3: Schematic drawing of the ALPI module.

Figure 2.1.4: Transfer Line (ITL) from ALPI to the Booster.

2.2 Proton Linac

The proton beam injector, shown in Figure 2.2.1, is a conventional linear accelerator [7,8]. Two RFQs accelerate the beam from an H^- source to 2 MeV and prepare its dimensions and bunching for a Drift Tube Linac (DTL) which accelerates the beam to 90 MeV, after which a Side Coupled Linac (SCL) raises the energy to 211 MeV in a more efficient fashion.

The choice of the frequencies for acceleration is important in order to match the required bunch configuration at injection into the Booster. The scenario is based on the choice of 50 for the rf harmonic number in the Booster, which corresponds to a frequency of 32.5 MHz for an injection energy of 211 MeV (43.3 MHz for injection at 535 MeV). For proper bunch-to-bucket injection, the beam must be bunched at the Booster injection rf frequency. This defines the frequency of the first RFQ to be 32.5 MHz (43.3 MHz).

The frequencies of the subsequent sections of the linac, chosen to be compatible with both energy schemes, are 130, 390 and 1300 MHz in the second RFQ, the DTL and the SCL respectively. One out of forty SCL buckets are filled in the 211 MeV configuration, whereas at the higher 535 MeV energy, one bucket out of thirty is full.

In the transfer lines which transport the beam from one section to the following, matching is preserved both transversely (transverse emittances) and longitudinally (bunch length and momentum spread). A beam chopper, located after the second RFQ, provides a 150 ns gap to match the rise time of the Booster extraction kicker. The total length of the linac, including an allowance for transfer lines and H^- source, is about 167 m for the 211 MeV version, and 250 m after the upgrade to 535 MeV.

2.2.1 The Negative-Ion Source and the RFQs

A negative-ion source operating at 10 kV generates a beam pulse with a peak current of 6.5 mA at a repetition rate of either 10 or 50 Hz, corresponding to the two modes of operations proposed for proton acceleration in the complex. Achieving the design intensity requires 80 injection turns into the Booster, corresponding to a source pulse duration of 123.5 μs.

The H^- beam is transferred to the first RFQ (RFQ1), where it is adiabatically bunched, focussed and accelerated to 0.2 MeV at a frequency of 32.5 MHz. RFQ1 is designed to control the space-charge effects in order to optimize the beam transfer efficiency and to limit the increase in transverse emittance. An overall capture efficiency of 90% is expected with a normalized rms emittance of 0.06 to 0.12 πmm-mrad.

The bunching achieved with RFQ1 is good enough to allow injecting the beam directly into the second RFQ (RFQ2), which operates at 130 MHz, four times higher, with a 100% bunch-to-bucket transfer. One bucket out of four is therefore occupied by the beam. The output energy of the RFQ2 is 2 MeV.

A transfer line, consisting of 130 MHz bunching cavities and triplet units for transverse focusing, allows the installation of the chopping and collecting elements. The line can handle

up to 100 μA peak current and it is insensitive to current fluctuations [9].

The phase compression in RFQ2 permits loss-free transfer in a bunch-to-bucket mode to the next section, the Drift Tube Linac.

2.2.2 The Drift Tube Linac (DTL)

The DTL consists of four tanks operating at 390 MHz. After this frequency jump, one out of twelve buckets will be filled. The first tank accelerates to 22.5 MeV, the whole section to 90 MeV.

At the beginning of the first tank the rf phase is adjusted to $-45°$, which provides an rf bucket large enough to capture the beam bunches from RFQ2 with a low accelerating gradient [9]. Within the first tank, the rf phase is increased linearly to $-25°$, achieving a higher accelerating gradient; the bucket area decreases accordingly, while the bunch phase is compressed by the energy gain, preserving longitudinal emittance. In the other three tanks the synchronous phase is kept constant at $-25°$.

The geometrical design of the tanks is optimized to maximize the shunt impedance, and the accelerating gradient is kept constant throughout the accelerating structure.

2.2.3 The Side Coupled Linac (SCL)

The SCL comprises three modules, each of which contains four cavities driven by a high power 1300 MHz klystron [7]. Klystrons with peak power of 10 MW and average power of 100 kW are commercially available. This frequency is 31/3 times larger than the DTL one, i.e. 40 times the RFQ1 one, and thus allows acceleration of one beam bunch every 40 rf buckets. The transition between the DTL and the SCL is at 90 MeV.

The SCL is designed with a constant number of tanks per module and a constant number of cells per tank through the whole section, which therefore has shorter tanks at the beginning than at the end. With this scheme, the phase slippage due to the rapid increase of the beam velocity in the tanks at the low energy end, is strongly reduced. This also compensates for the reduced shunt impedance at low velocity, keeping the mean accelerating field nearly constant along the whole structure. The number of cells per module is determined by the choice of three full modules in the first stage (211 MeV), with all the cells in a single tank identical.

Tanks in one module are connected together by bridge couplers, to provide the space for focussing elements and for beam diagnostic devices between tanks. Each module thus forms an independent rf structure, while the field levels and phases are the same in all tanks. A five-cell disc-loaded cavity operating in the $\pi/2$ mode is considered to be an adequate bridge coupler. It exactly replicates the behaviour of the side-coupled structure; with 5% inter-cell coupling, the rf group velocity in the bridge is the same as in the tanks. By increasing the coupling between the tank and the bridge coupler, it is possible to reduce the fields in the latter, keeping its power losses to 2% of the overall cavity dissipation.

Beam focussing is provided by quadrupole doublets between the tanks. Short tanks allow for a reduced beam size, and therefore a smaller bore and a higher shunt impedance; a larger number of tanks increases the complexity of the structure. The optimal number of

tanks is then a compromise between these effects.

The layout of the SCL is determined by computer optimization programs, and checked by beam dynamics simulations which include multi-particle tracking. The values of the input emittances are 0.6 πmm-mrad for the transverse normalized rms emittance, and 5 πdeg-MeV for the longitudinal one at 1300 MHz. The emittances increase by less than 20% both transversely and longitudinally and, when alignment errors are included, the increases are expected to be less than 30%. No particular effort has been made to reduce emittance growth, because the present values are satisfactory. Beam transmission in the SCL is about 100%.

Table 2.2.1 summarizes design, beam dynamics and structure parameters of the three linac sections.

2.2.4 The Linac Energy Upgrade

It is possible to raise the extraction energy of the linac to 535 MeV by adding a new SCL section to the proton linac, allowing for higher current capabilities of the complex. In this new configuration, the rf frequency at injection into the Booster increases to 43.3 MHz and a new RFQ1, operating at that frequency, is required. The other RFQ2, the DTL and the first section of the SCL remain unchanged. One bucket in three is now occupied by the beam at the exit of RFQ2, one in nine at the exit of the DTL, and one in thirty in the SCL. The chopper between RFQ2 and the DTL has to be modified. The new accelerating section of the SCL also operates at 1300 MHz.

This configuration is intended to increase the average beam intensity provided by the Booster to 100 μA; the negative ion source must therefore provide a higher current of 12.5 mA. The expected performance, design and beam dynamics parameters are shown in Table 2.2.2.

In order to raise the linac energy to 535 MeV six additional SCL modules must be added at the end of the linac. After completion of the first stage at 211 MeV, the first module of the new SCL section could be used to raise the energy to 250 MeV for possible medical applications in cancer therapy.

2.2.5 The Proton Transfer Line (PTL)

The proton linac lies along a path from north to south on the LNL site. Enough space is left for the SCL to be upgraded to 535 MeV in a second phase. At the end of the linac the beam is taken through a transport line into the Booster. The transfer lines for heavy ions and protons merge in a 25° bending magnet upstream of the final transport line, from which point the two beams share the same elements. The proton linac building is 7 m wide so that it can also house the heavy ion transport line. Both the proton and the heavy ion beam lines are at the same elevation, about 4 m below ground level, which is the same as that of the Booster. With this configuration the beams are bent and injected into the Booster in the horizontal plane.

The proton transfer line is about 80 m long; it includes a section with a debunching system for the rotation of the bunches prior to injection into the Booster [10]. The de-

buncher consists of two rf cavities operating at 1300 MHz; its main purpose is to trade off bunch length, which is due to the long drift length and to space-charge phenomena, against momentum spread. The actual location of the debuncher depends on the linac final energy and beam intensity. At injection, the length of each linac bunch is about 1/40 or 1/30 of the Booster accelerating rf buckets at injection energies of 211 or 535 MeV respectively.

2.2.6 Experimental Facilities

The possibility of the addition of a single module, to raise the output energy to 250 MeV in one step, has already been mentioned (see section 2.2.4). This proton energy is ideal for cancer therapy and other medical applications.

The DTL is divided into four sections corresponding to output energies of 24, 46, 68 and 90 MeV, as shown schematically in Figure 1.1.2. Between adjacent sections it is possible to extract the beam for isotope production. Beams of any of these energies, or 250 MeV, are then taken to the experimental building.

Table 2.2.1 General Parameters for Phase 1.

	RFQ1	RFQ2	DTL	SCL	
Input Energy	0.01	0.2	2	90	MeV
Output Energy	0.2	2	90	211	MeV
Frequency	32.55	130.2	390	1300	MHz
Length	3.3	3.4	41	26	m
Peak Current	6.5	24	60	200	mA
Peak rf Power	0.005	0.21	7.1	23.4	MW

Table 2.2.2 General Parameters for Phase 2.

	RFQ1	RFQ2	DTL	SCL	
Input Energy	0.01	0.2	2	90	MeV
Output Energy	0.2	2	90	535	MeV
Frequency	43.3	130.2	390	1300	MHz
Length	2.6	3.4	41	109	m
Peak Current	12.5	40	100	330	mA
Peak rf Power	0.006	0.21	7.1	23.4	MW

Table 2.2.3 Parameters of the RFQs

	RFQ1	RFQ2	RFQ1	
	Phase 1		Upgrade	
Frequency	32.55	130.2	43.3	MHz
Intervane Voltage	30	100	35	kV
Input Kinetic Energy	0.01	0.2	0.01	MeV
Output Kinetic Energy	0.2	2.	0.2	MeV
Synchronous Phase	90 - 35	75 - 24	90 - 35	deg
Aperture Radius	1	0.6	0.9	cm
Length	3.3	3.4	2.6	m
Peak Power	5	210	5.5	kW
Phase Advance σ_{ot}	75 - 72	40 - 33	80 - 75	deg
Transmission	$\geq$90	$\geq$90	$\geq$90	%

Normalized Input Emittance for the whole chain

0.7 $\qquad$ π mm mrad

Normalized Output Emittance for the whole chain

$\leq$1.8 $\qquad$ π mm mrad

Longitudinal Output Emittance for the whole chain (rms, at 130 MHz)

$\leq$300 $\qquad$ $\leq$200 $\qquad$ deg keV

Table 2.2.4 Parameters of the DTL and SCL

	DTL	SCL	SCL	
	Phase 1		Upgrade	
Input Kinetic Energy	2	90	211	MeV
Output Kinetic Energy	90	211	535	MeV
Resonant Frequency	390	1300	1300	MHz
Number of Tanks	4	12	24	
Number of cells	216	304	816	
Number of Klystron	4	3	6	
Acc. Field ($E_0 T$)	2.4	7	5.8	MV/m
Synchronous Phase	45 - 25	28	28	deg
Shunt impedance	28 - 51	36 - 46	46 - 49	MΩ/m

H⁻ Source

RF frequency at injection into the Booster

(43.3)
32.5   130   390 [MHz]   1.3 [GHz]

RFQ₁   RFQ₂   DTL   SCL   to Booster

211 MeV   535 MeV
40 μA   88 μA
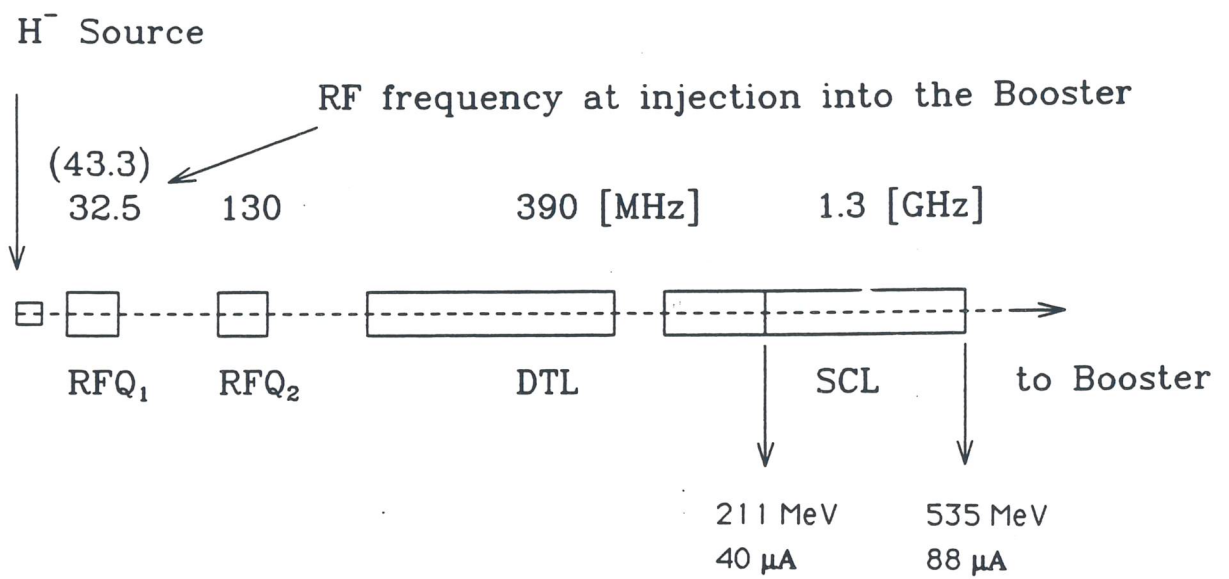
Figure 2.2.1: Schematic Layout of the H⁻ Injector.

References

[1] G. Fortuna et al.," The ALPI project at the Laboratori Nazionali di Legnaro", Nucl. Instr. and Meth. A-287 (1990)253-256.

[2] R. A. Ricci and C. Signorini, Nucl. Instr. and Meth., 184 (1981) 35.

[3] P. Thieberger et al., Nucl. Instr. and Meth. A-268 (1988) 513-521.

[4a] I. Ben-Zvi and J. M. Brennan, Nucl. Instr. and Meth. 212 (1983) 73.

[4b] P. Boccaccio, LNL Annual Report 1986 LNL-INFN (REP) 002/87.

[4c] I. Ben-Zvi,E. Chiaveri, B.V. Elkonin, A. Facco and J. S. Sokolowski, Proceedings of the 2nd European Particle Accelerator Conference, Nice, June 1990, pag. 1103-1105.

[4d] A. Porcellato et al., Proceedings of the Twenty-fourth Symposium of North Eastern Accelerator Personnel, Kansas State University, October 1990, pag 259-277.

[5] K. Shima, T. Ishihara and T. Mikumo, Nucl. Instr. and Meth. 200(1982) 605.

[6] M. A. McMahan, R.F. Lebed and B. Feinberg, Proceedings of the 1989 IEEE Particle Accelerator Conf., Chicago IL, 1 (1989) pag 536.

[7] P. Lapostolle, M. Vretenar, M. Weiss, "The High Energy Proton Linac", Proceedings of the XV Workshop on EHF, Lecce 9-14 October 1989, (EHF-89-59).

[8] P. Lapostolle, "Report from working group on Linac", same Proceedings, (EHF-89-76).

[9] M. Pabst, K. Bongardt, "Some remarks on transfer line RFQ2 DTL and DTL", same Proceedings, (EHF-89-60).

[10] K. Bongardt,"The high energy transfer line Linac-Booster", same Proceedings, (EHF-89-61).

3
Booster Ring

3.1 Lattice and General Layout

The overall size of the ring has been determined by general considerations such as the highest specific kinetic energy of the heaviest ion to be accelerated, compatibility with the heavy ion injector, and the available space on site. The maximum specific energy has been fixed at 1 GeV/u for gold ions, corresponding to a magnetic rigidity of 22.25 Tm.

The ALPI injector provides 200 ns bunch spacing, and the rf matching requires the Booster circumference to be a multiple of the incoming bunch spacing; this multiple has been chosen to be 45 for gold ions; this, together with the output velocity ($\beta=0.098834$), gives a total length of 266.6667 m, consistent with the area available on site.

The shape and symmetry of the ring has been determined by the need for many straight sections to accommodate devices for beam handling, namely injection and extraction systems, and acceleration cavities. This need for many straight sections, combined with the high periodicity required to avoid crossing systematic betatron resonances, suggests the choice of a fourfold symmetry (Figure 3.1.1), which also allows a reasonably high dipole magnet packing factor. Given the periodicity of the lattice it is important to fix the choice of the betatron tunes to stay clear of the following major systematic resonances:

$$\nu_h = i, \quad \nu_v = j$$

$$2\nu_h = k, \quad 2\nu_v = l$$

$$\nu_h + \nu_v = m, \quad \nu_h - \nu_v = n$$

(with i, j, k, l, m and n natural integers).

While several sets of values can satisfy these requirements, general considerations of technical feasibility and machine operation make the choice of $\nu_h=5.8$ and $\nu_v=3.8$ the preferred one. This solution allows a betatron phase advance per cell of about 90° in the horizontal plane and 60° in the vertical plane. This can be considered good from the point of view of chromatic and aberration effects, and operational aspects such as the positioning of diagnostics devices. The resulting cell half-length is over five metres, which can accommodate a dipole magnet about 3.5 m long.

In the high intensity mode, one can expect a considerable tune depression from space charge, which shifts the tune values closer to half-integral resonances; for instance in the

horizontal plane from 5.8 down to 5.6. This is believed to be better than the situation with the unperturbed tune just below a half-integral value (such as 5.3 or 3.3) because in that case the shift would bring the tune values closer to integral resonances.

Larger values of tunes than those given above would require either a larger betatron phase advance per cell, endangering beam stability, or a shorter cell length, reducing considerably the packing factor and the attainable magnetic rigidity. On the other hand, lower tune values are not acceptable because they would lead to large beam envelopes which require unreasonably large magnet apertures.

To ensure good stability of the betatron motion, a separated function FODO focussing structure has been chosen for the basic cell. The choice of the FODO cell also gives very good chromatic properties, and in principle a higher momentum acceptance.

Each superperiod, which is mirror-symmetric about its mid point, consists of an arc and two half straight sections; four bending cells make up the arc, while the two half straight sections consist of a basic cell without the bending dipoles.

The total number of cells is therefore fixed at 24, eight of which are without dipole magnets, and the resulting length of the basic cell is 11.11 m. The maximum magnetic field (1.26 T) and beam rigidity accepted, together with the total number of bending dipoles (32), set the length of the dipole magnets at 3.46 m.

The dipoles are sector magnets with zero entrance and exit angles; because of the large sagitta ($\sim$8.5 cm), they have to be curved. Apart from some large-aperture quadrupoles at the injection point, only two types are used: 0.6 m long focussing (QF) and 0.5 m long defocussing (QD), in the horizontal plane. Their lengths are different so that the required strengths, which are different in the two types, can be produced by the same excitation current; they can then be operated on a common power supply if required. The drift spaces between dipoles and quadrupoles are 0.7728 m long.

This configuration allows a 'transparent' arc with a betatron phase advance of almost 360° in the horizontal plane, which also makes the dispersion function vanish at the ends; the dispersion remains zero along the full length of the long straight section.

The overall magnet layout of the Booster is shown in Figure 3.1.1, that of a FODO cell in Figure 3.1.2; a summary of the lattice and FODO cell parameters is given in Tables 3.1.1 and 3.1.2. Lattice and dispersion functions are shown in Figure 3.1.3 for one fourth of the machine. It can be seen that while the periodicity of the β functions exactly matches the cell periodicity, the dispersion function follows the superperiodicity of the structure. Table 3.1.1 also shows that the transition γ is high enough to be well above the whole accelerating cycle. Transition energy crossing occurs only when protons are accelerated to 6 GeV.

Both horizontal and vertical envelopes are shown in Figure 3.1.4; they correspond to a full emittance of 140 πmm-mrad and a momentum spread of $\pm$0.5% combined quadratically. It is seen that the largest vertical height and horizontal width are about 100 mm.

The proposed lattice has relatively weak focussing with a natural chromaticity value close to the betatron tunes which can be corrected with a modest sextupole scheme. The effect of the uncorrected chromaticity on the tune variation with momentum is shown in Figure 3.1.5. It is not clear whether this is tolerable; correction can be done if necessary by placing two families of sextupoles (SF and SD) next to quadrupoles with large dispersion (see Figure 3.1.3). The result of the correction, shown in Figure 3.1.5, can be obtained with a sextupole strength of $(B"l/B\rho) = \pm 0.2$ m^{-2}. Figure 3.1.6 shows the variation of the lattice

functions with momentum at the centre of one of the QF quadrupoles near the middle of an arc.

The presence of sextupoles for chromaticity correction causes a tune variation with the amplitude of the motion which never exceeds 0.001.

The positioning of the magnets in the tunnel requires special care. The following alignment rms errors are considered to be within the present state of the art: 0.3 mm for quadrupole lateral displacement and 0.3 mrad for dipole axial rotation. In addition, an integrated dipole field error of 3×10^{-4} rms can be expected. This causes an uncorrected closed orbit distortion with an expected value of about 5 mm rms in the quadrupoles, ensuring that the the closed orbit is within the available aperture at the start of operations. The initial use of a small-size beam can then allow detection and correction of the closed orbit distortion. For this purpose, two families of beam position monitors and steering magnets are located next to all QF and QD quadrupoles.

Similarly, quadrupoles have a maximum axial rotation error of 0.3 mrad rms, set by the effects of the betatron coupling, and a maximum integrated gradient error of 10^{-3}, which could cause a half-integral stop-band width of 0.004 rms.

Table 3.1.1: Lattice parameters of the Booster.

Ring Length		266.6667	m
Lattice Periodicity		4	
Maximum Magnetic Rigidity		22.25	Tm
Magnetic Bending Radius		17.6216	m
Total Number of Cells		24	
Number of Cells per Arc		4	
Phase Advance per Cell			
	Horizontal	90°	
	Vertical	60°	
Transition γ		4.6	
Betatron Tunes			
	ν_h	5.8	
	ν_v	3.8	
Natural Chromaticity			
	ξ_h	-5.45305	
	ξ_v	-4.89149	
β_H, max		16.0 m	
β_V, max		21.6 m	
Dispersion, max		4.95 m	

Figure 3.1.1: Magnetic layout of the Booster.

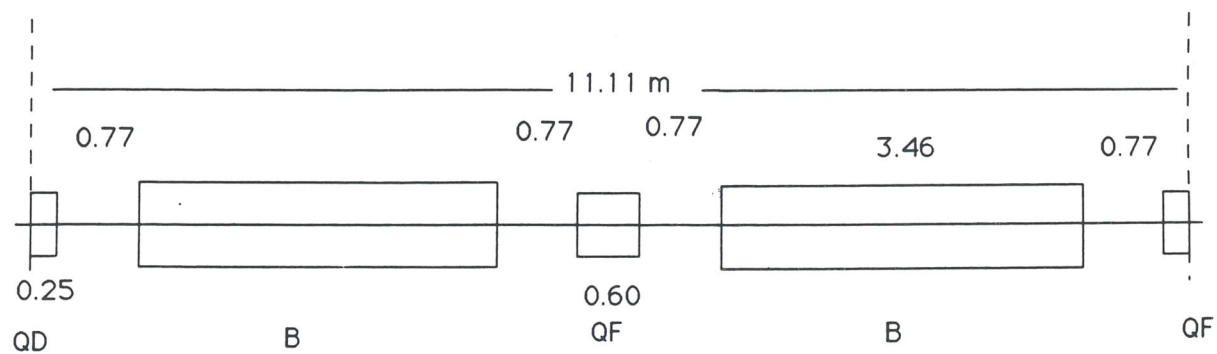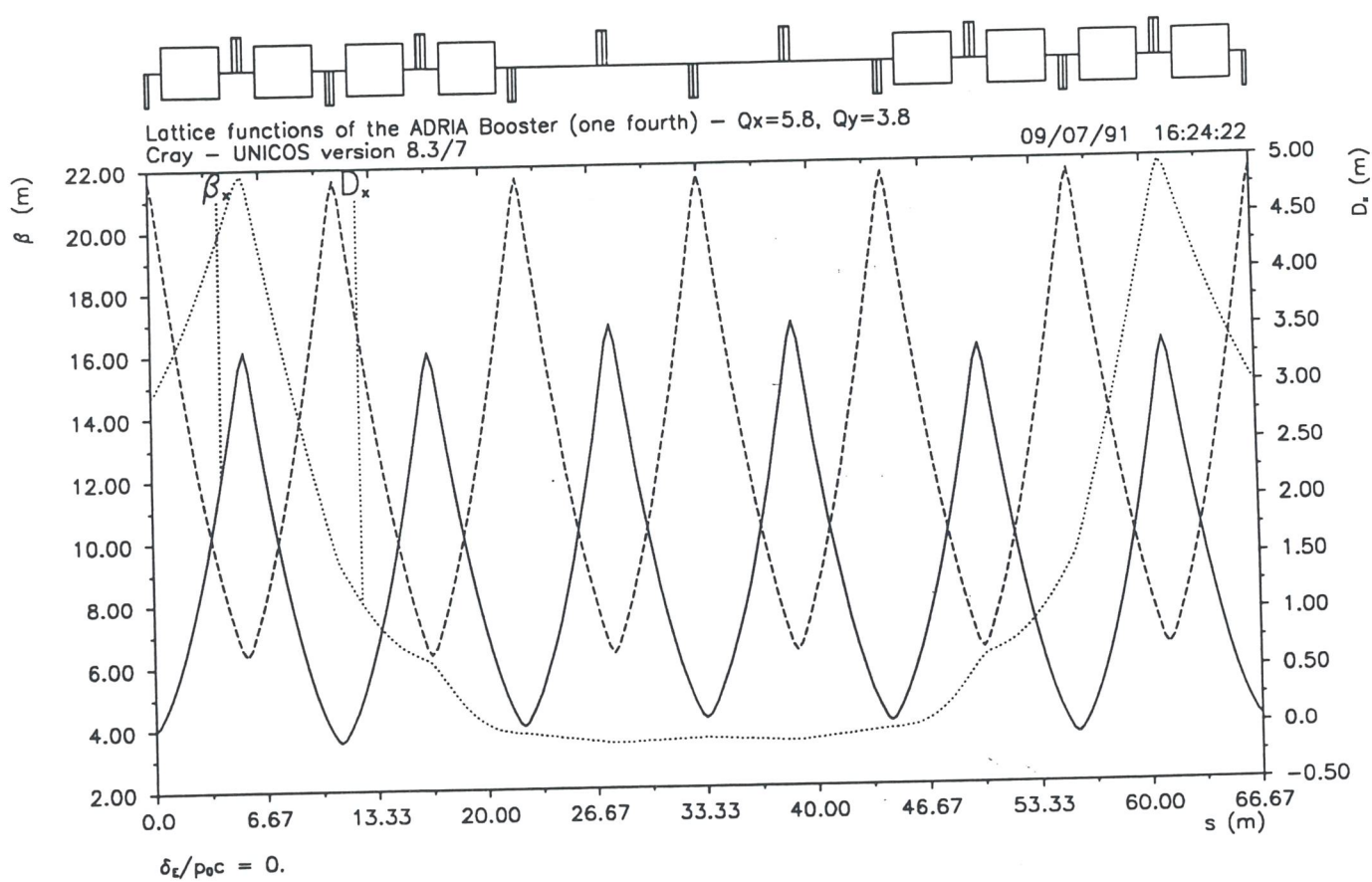Figure 3.1.2: The FODO cell of the Booster.

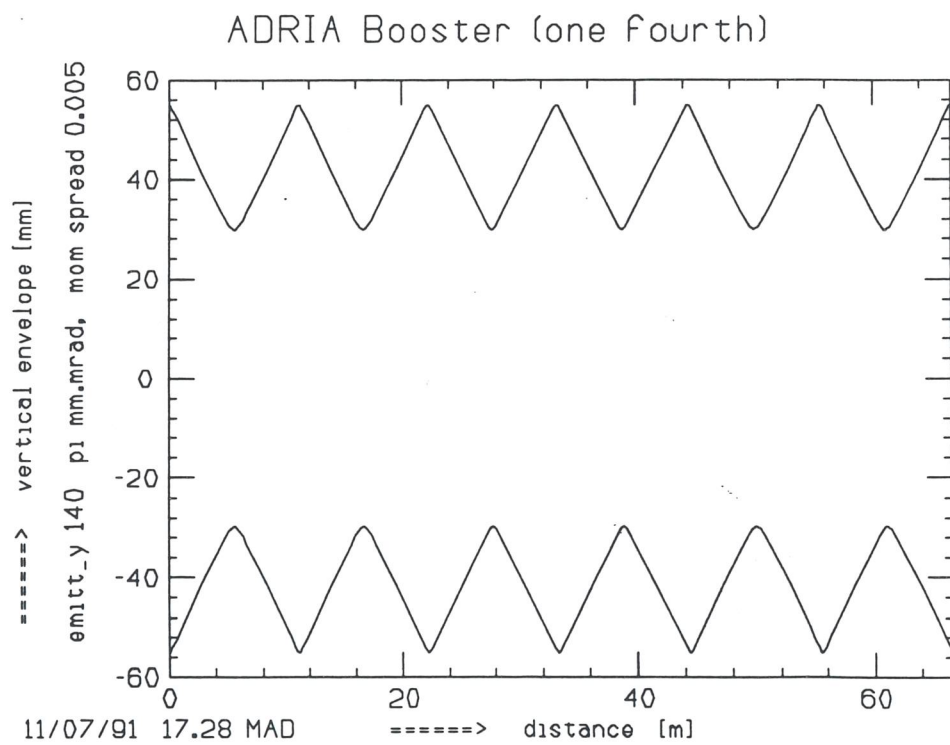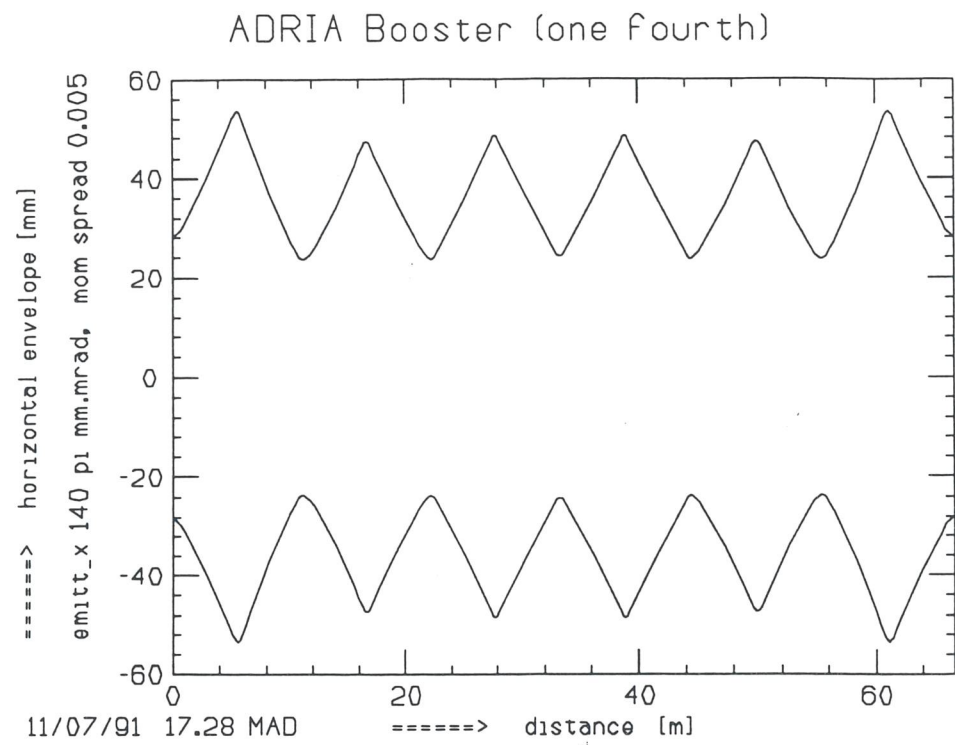Figure 3.1.3: Lattice functions of the Booster (one fourth).

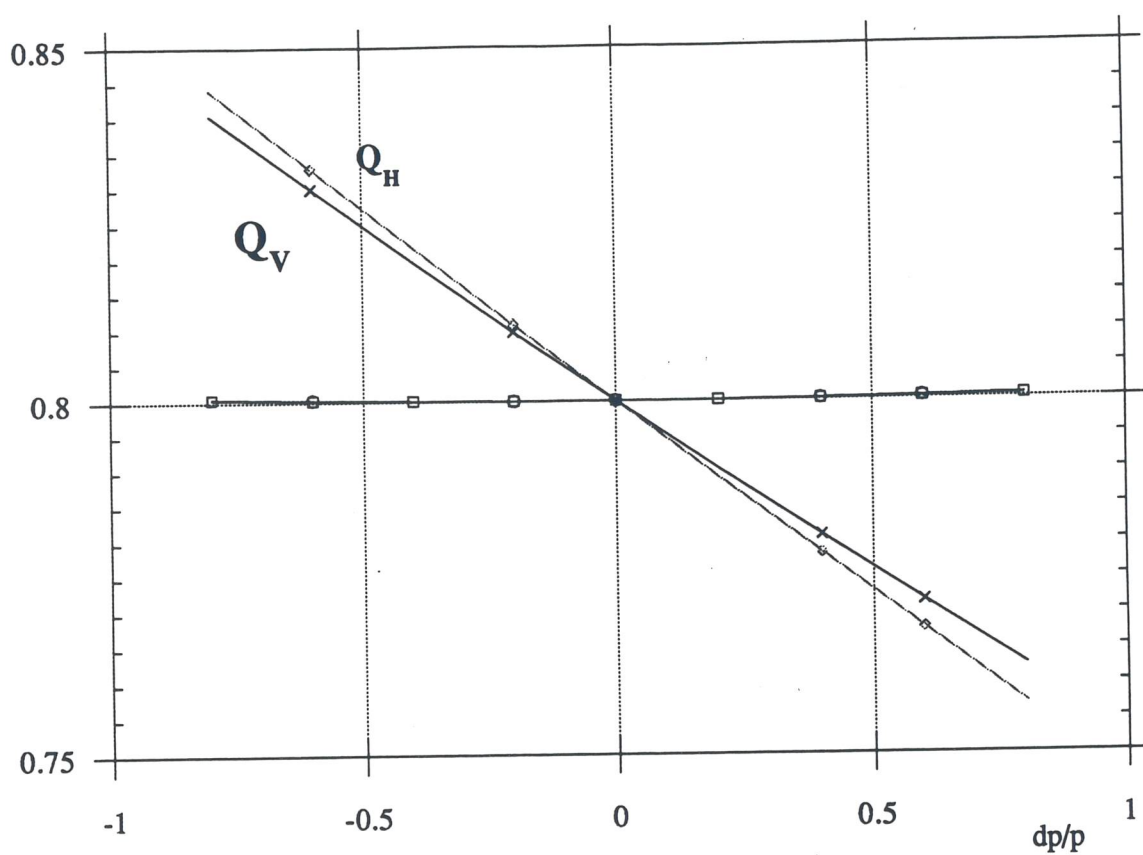Figure 3.1.4: Beam envelopes for the Booster (one fourth).
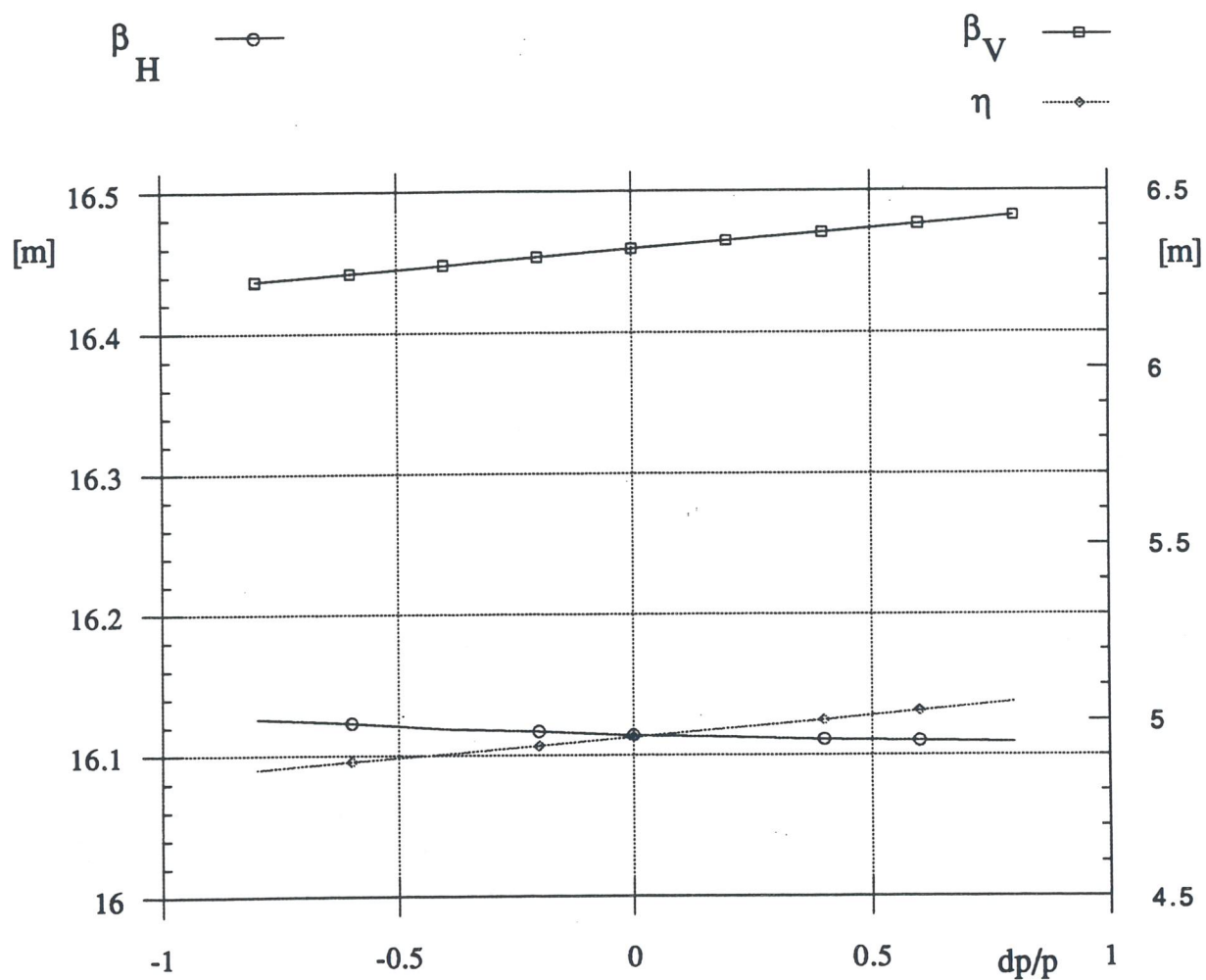
Figure 3.1.5: Horizontal and Vertical tunes vs. momentum deviation.

Figure 3.1.6: Lattice Functions vs. momentum deviation in the QF near the middle of the arc.

Table 3.1.2: Parameters of the FODO Cells.

Cell Length	11.1111	m
Dipoles:		
Dipole Length	3.4600	m
Bending Angle	11.25°	
Bending Radius	17.6216	m
Sagitta	8.48	cm
Vertical Gap	10	cm
Drifts:		
Drift Length	0.7728	m
Quadrupoles:		
QF Length	0.6000	m
Gradient	8.77	T/m
QD Length	0.5000	m
Gradient	8.77	T/m
Bore Radius	7.0	cm

3.2 Injection

Injection of either heavy ions or protons takes place in a long straight section, as shown in Figures 1.1.1 and 1.1.2. The components for injection and extraction are shown in more details in Figure 3.7.14. While several injection turns are required in both cases to reach the desired beam intensities, the methods proposed are different for heavy ions and protons. In the case of heavy ions the final intensity is limited by the ion source before the Tandem, whereas in the case of protons the limit is set by space charge. It is thus highly desirable to develop higher current heavy ion sources.

3.2.1 Injection of Heavy Ions

To obtain the required beam intensities, several beam turns of heavy ions from the Tandem and ALPI are injected into the Booster. It is not possible to use the method of charge exchange as in the case of protons. For heavy ions, multi-turn injection is accomplished by placing consecutive turns next to each other in betatron phase space. After n turns have been injected the beam emittance is $\epsilon = n\epsilon_0/\eta_n$, where ϵ_0 is the emittance of a single turn and $\eta_n < 1$ is the injection efficiency, which depends on the number n of turns already injected. High efficiency requires good matching of the transfer line to the Booster, and also proper shaping of the beam cross-section.

For a given total beam emittance there is a limit to the maximum intensity, given by the maximum allowable tune-depression $\Delta\nu$ due to space-charge forces, taken here to be 0.2. The relation between $\Delta\nu$, the total beam emittance ϵ, and the total number N of particles is [1a,1b,1c]

$$\Delta\nu = \frac{N r_p Q^2}{2\beta^2 \gamma^3 B A \epsilon} \tag{3.2.1}$$

where Q is the charge state, A the mass number, $r_p = 1.535 \times 10^{-18}$ m and B the bunching factor defined as the ratio of the average beam current to the peak current. Since the physical acceptance of the Booster is 140 π mm-mrad, a safe value for the total beam emittance is 100 π mm-mrad. Thus, for the case of gold (Q=51, A=197) we derive $N = 3 \times 10^{10}$, which at the repetition rate of 10 Hz corresponds to 3×10^{11} ions per second. With ion sources available at present, this would require injection of 100 turns.

Estimates for the achievable currents with the XTU and ALPI injector are given in Table 3.2.1, in which a current of 200 p-μAmp and 40 injection turns have been assumed for each species. Different final currents result from different transmission efficiencies and different pulse lengths determined by the velocities at injection. It can be seen from the same table that currents are not limited by space-charge phenomena. There is therefore considerable scope for future source development. The injection of 40 turns in one plane is probably difficult. As a comparison, it seems possible to inject about 28 turns into the AGS Booster at Brookhaven [2].

Beam is injected in the horizontal plane via a Lambertson magnet located next to the quadrupole QD at the centre of the long straight section (see Figure 3.2.1). A horizontal orbit bump is first generated with special dipole magnets located at both ends of the long straight section. At the injection point, which is at the end of the Lambertson magnet, a narrow beam is required, i.e. a low value for β_h. Taking $\beta_h = 6$ m, the beam width at injection is 8 mm, to which 3 mm for the septum thickness has to be added. The first turn is injected 11 mm from the bumped closed orbit, which is initially displaced by 29 mm. The inner side of the septum is at a distance of 33 mm from the reference closed orbit; this will not reduce the acceptance of the ring. The orbit bump is turned off at a rate fast enough to avoid for any single pulse hitting the injection septum, but also slow enough to allow the maximum number of turns to be injected. For 20-turn injection, the orbit bump magnets must be turned off in 70 μs for very light ions, and in 180 μs for gold ions. The required magnet components for multi-turn injection of heavy ions are listed in Table 3.2.2.

3.2.2 Injection of Protons

The most efficient method of multi-turn injection is to provide a beam of H$^-$ ions from the Linac [3a,3b,3c]. In the Booster this beam traverses a thin foil where protons are stripped of the electrons and are then trapped in orbit. The charge exchange method provides good efficiency and, in principle, constant beam cross-section as the intensity increases. The method does not violate Liouville's theorem since circulating and injected particles have different charge state at the moment they merge. The beam parameters at the exit of the Linac for injection into the Booster are shown in Table 3.2.3. As one can see, in order to reach the required intensity, 80 turns are required for injection at 211 MeV.

In practice the beam dimensions will grow during charge-exchange injection due to the following effects: the movement of the injection bump, and multiple scattering of the particles during repeated passage through the stripping foil. The efficiency can be increased by properly rotating the injected beam cross-section at injection, and by carefully matching the end of the transfer line to the injection point in the Booster. The number of foil traversals can be minimized by suitably locating the foil and by modulating the orbit bump with time to move the beam off the foil expeditiously. Finally, the beam will be diluted by space charge. To keep this dilution under control a "painting" technique can be applied as explained below.

Figure 3.2.2 shows the layout of the magnets required for injection, and Table 3.2.4 lists their specifications. They provide a very localized horizontal orbit bump entirely confined within the two quadrupoles of one half-cell in a long straight section. The four magnets that provide the orbit bump are identical in length, cross-section and field. They have an effective length of 0.5 m and are 0.5 m apart, placed symmetrically between quadrupoles. The foil can be made of vitreous carbon or alumina about 200 μg/cm^2 thick, and is placed at the centre of the one-metre long central region of the bump. It is important that the location of the foil does not limit the physical acceptance, which is required to be 140 π mm-mrad. Since the foil is located in a region where $\beta_h \sim \beta_v \sim$ 10 m, its edge should be at least 37 mm away from the central reference orbit. The orbit bump should displace the circulating beam by this amount plus a quantity at least equal to half the beam width, which is estimated to be 7 mm, corresponding to a total emittance of 5 π mm-mrad. This can be obtained with a field in the bump-magnets of 0.2 T at an injection energy of 211 MeV. If the injection energy is raised to 535 MeV the strength of the bump-magnets also has to be increased correspondingly to 0.34 T.

At the start of injection, the orbit bump magnets are already at maximum field. During the injection process, which lasts 123.5 μs, the magnets are slowly turned off so as to bring part of the already circulating beam off the stripping foil. This will minimize the number of foil traversal and reduce the amount of emittance growth due to multiple scattering.

Whereas the circulating beam goes through all four bump-magnets, the injected beam enters the second magnet from the outside and merges with the circulating beam at its exit (Figure 3.2.2). To allow the beam to enter in this way, the dipoles can be made C-shaped. The incoming beam may have then to pass through the yoke of the previous bump dipole and of the Booster quadrupole (QD).

To remove electrons left over from the stripping, clearing electrodes are located on each side of the foil to remove the electrons before they are trapped in the fringe field of the dipole magnets.

During the stripping process, atoms of hydrogen (H$^\circ$) will also be produced. They cannot be removed with magnets, but will travel in a straight line until they encounter the first downstream dipole of the Booster, where they continue undeflected through a pipe inserted tangentially into the yoke of the magnet. They can then be collected for diagnostic purposes and other applications. Similarly, the negative ions that remain unstripped after traversing the foil can be removed by the following bump magnet which will deflect them out of the machine. The total inefficiency (H$^-$ and H$^\circ$) of the stripping process is typically a few percent.

During injection the beam intensity increases and the beam size will increase accordingly. The requirement is a normalized beam emittance of 25 π mm-mrad at a beam intensity of 1.1×10^{11} protons per bunch for 211 MeV injection, and 2.7×10^{11} for 535 MeV injec-

tion energy. In either case the space-charge tune-depression should not exceed 0.2. This is calculated according to Equation (3.2.1), which assumes that the beam bunches have a gaussian particle distribution in each dimension. Assuming that rf buckets are essentially full at the end of injection and the rf capturing process, the space-charge tune-shift during the accelerating cycle is plotted in Figures 3.2.3 (a,b) for the two repetition rates of 10 and 50 Hz.

Space-charge effects can also be controlled by the "painting" technique [4,5], i.e. by the use of small beam bunches from the linac to fill up the rf buckets uniformly. This is also required to insure nearly loss-free transfer of the beam bunches from the linac to the Booster rf buckets. Shaping the beam to a uniform longitudinal distribution has a twofold effect: it reduces the space-charge tune-shift by a factor of two, and it also reduces the amount of tune spread across the bunch, which is believed to be the main factor in beam stability. Clearly some sort of transverse "painting" would also be useful for the same reasons, but this appears to be more difficult to realize. Longitudinal "painting" is made easier by the short length of the linac bunches (about 1/30 of the length of the rf buckets), and by the small bunch momentum spread (about 1/4 of the rf bucket height). For convenience, injection occurs in a region with essentially no dispersion; this does not cause any inconvenience to the "painting strategy"; because of the relatively low number of turns to be injected, we rely on selection by phase rather than by momentum.

Table 3.2.1: Heavy Ion Beam Parameters after Injection into the Booster.

	S	Cu	I	Au	U	
Mass Number	32	63	127	197	238	
Atomic Number	16	29	53	79	92	
Charge State	16	27	40	51	54	
β	0.1853	0.1483	0.1140	0.0988	0.0908	
Kinetic Energy	16.4	10.4	6.1	4.6	3.9	MeV/u
Orbit Period	4.8	6.0	7.8	9.0	9.8	μs
Harmonic No.	24	30	39	45	49	
Ions per Cycle	2.0	1.8	0.79	0.68	0.68	$\times 10^{10}$
Normal. Emittance	22.6	18.0	13.8	11.9	10.9	π mm mrad
Bucket Area	0.0086	0.0055	0.0035	0.0026	0.0024	eV/u-s
Space-Charge, ΔQ	0.053	0.068	0.060	0.070	0.074	
Q_s	0.035	0.045	0.073	0.097	0.117	

Table 3.2.2: Magnetic Elements Specifications for Heavy Ion Injection.

Initial Orbit Bump	29	mm
Bump Fall-off Period	70-200	μs
Number of Injected Turns	≥ 20	
Lambertson Magnet:		
Length	1	m
Field	0.2	T
Aperture (H×V)	2×4	cm^2
Septum Thickness	3	mm

Table 3.2.3: Proton Beam Parameters at Injection into the Booster.

Injection Energy	211	535	MeV
β	0.577	0.771	
Magnetic Rigidity	2.21	3.79	T m
Normalized Emittance	25	25	π mm-mrad
Bunch Area	0.050	0.075	eV-s
Space-Charge ΔQ (max)	0.2	0.2	
Q_s (max)	0.06	–	

Table 3.2.4: Magnetic Elements Specifications for Proton Injection.

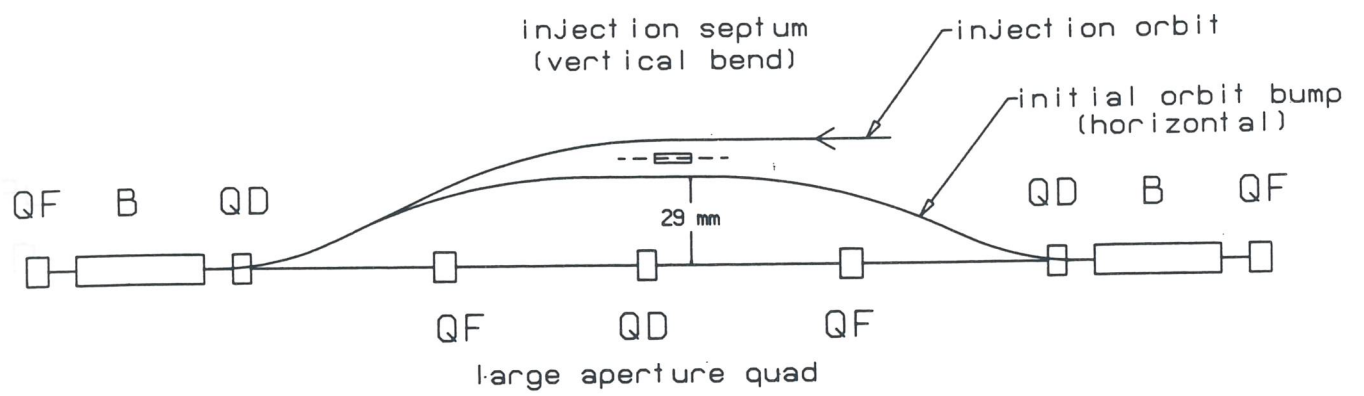|				
Injection Energy	211		535	MeV
Injection orbit bump		50		mm
Number of injection turns	80		120	
Bump fall-off period	123.5		138.4	μs
Bump Magnets:				
Number		4		
Length		0.5		m
Field	0.1		0.15	T

Figure 3.2.1: Layout of the Injection System for Heavy Ions.
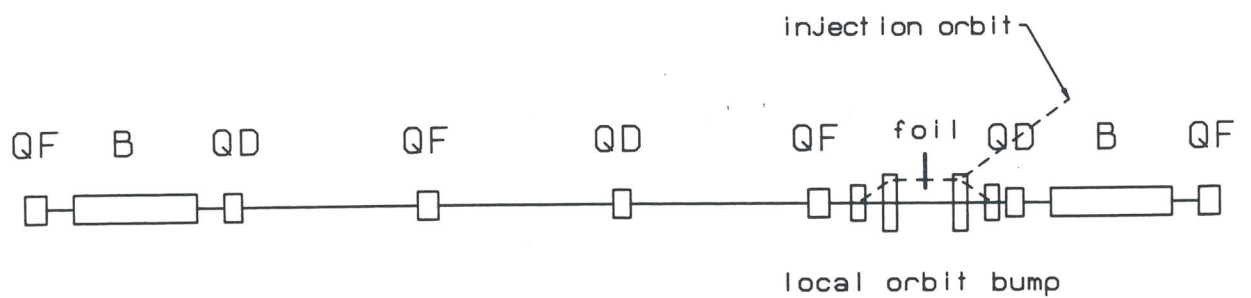
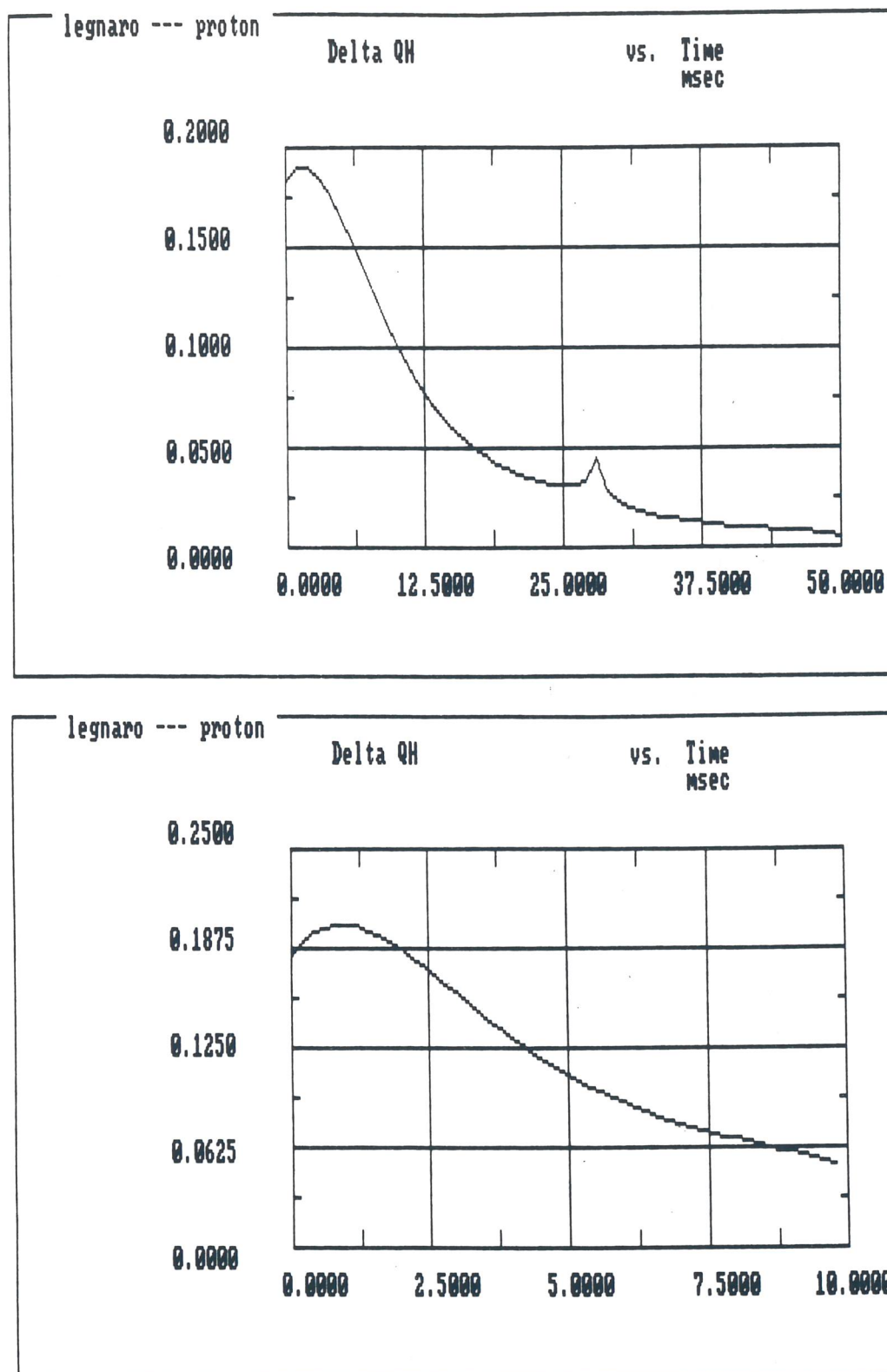Figure 3.2.2: Layout of the Injection System for Protons.

legnaro --- proton   Delta QH   vs. Time
                                            msec

0.2000

0.1500

0.1000

0.0500

0.0000
       0.0000   12.5000   25.0000   37.5000   50.0000

legnaro --- proton   Delta QH   vs. Time
                                            msec

0.2500

0.1875

0.1250

0.0625

0.0000
       0.0000   2.5000   5.0000   7.5000   10.0000

Figure 3.2.3: Space-Charge Tune-Shift During Acceleration of Protons.

3.3 Extraction

Both heavy-ion and proton beams are extracted from the Booster in single-turn mode. If slow-spill extraction is required, this can be accomplished in the Decelerator, after transferring and debunching.

Extraction takes place in the straight section opposite the injection straight, as shown in Figures 3.3.1 and 3.7.14. It starts with a fast kicker magnet, located upstream of the straight section, which displaces the beam vertically by 60 mm at the entrance to a Lambertson magnet that moves the beam horizontally. The septum of the Lambertson magnet is 10 mm thick and is located 32 mm away from the central orbit in order not to restrict the required physical acceptance. The angular deviation generated by the kicker is large enough to extract the full beam at all energies. The main parameters of the magnetic extraction components are given in Table 3.3.1.

To reduce the required kicker strength, it is proposed to use the steering magnets in the long extraction straight to create a local vertical bump that can be turned on slowly, after which the kicker is fired to extract the beam. This technique will be more useful at high energies, where the beam dimensions are small.

The rise time of the kicker magnet is about 150 ns, with dimensions and field strength as specified in Table 3.3.1. Since the bunch spacing at extraction for either heavy ions or protons is about 20 ns, it is necessary to create before injection a gap in the beam of about 7 empty buckets to match the kicker rise time. The undesired bunches can be removed at the exit of the ALPI with a beam chopper or a modulated deflector which can send them to other areas where they can be used for a low energy experimental program.

Beam abort can be accomplished in the same way, through the same extraction channel: a pulsed magnet when turned on will direct the beam to the required underground area for dumping in a dedicated target.

Table 3.3.1: Magnetic Element Specifications for the Extraction channel.

Lambertson Magnet		
(Horizontal Bend)		
Length	3.5	m
Field	1.0	T
Aperture (H×V)	5×5	cm^2
Kicker Magnet		
(Vertical Bend)		
Length	3.5	m
Field	0.04	T
Aperture (H×V)	10×15	cm^2
Rise Time	150	ns

extraction kicker
(vertical)

lambertson magnet
(horizontal)

QF   B   QD   QF   QD   QF   QD   B   QF
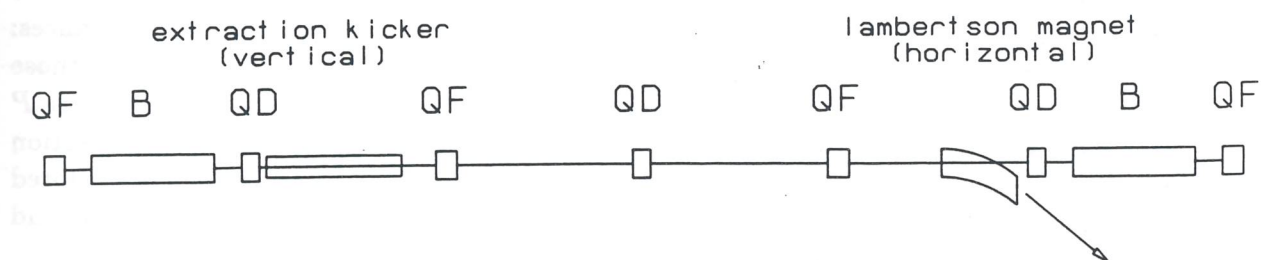
Figure 3.3.1: Layout of the Extraction from the Booster.

3.4 Polarized Proton Beams

It is possible to accelerate beams of polarized protons in the Booster. Optically-pumped sources are capable of delivering typically 60% polarized beams of H^- with currents of about 20 μA [6]. Polarized protons can be accelerated in the Linac, injected into the Booster over about 100 turns and accelerated further as described for the unpolarized beam. However special care has to be taken to avoid too many traversals of the stripping foil, since excessive depolarization may result. Because the total current will be lower, no difficulties are expected from space-charge effects.

The polarized proton beam circulates with its polarization aligned vertically, along the direction of the guiding magnetic field. Depolarization can occur if the particles traverse regions with magnetic field in the horizontal direction; thus, to preserve a high degree of polarization, it is important to minimize all magnet imperfections which produce horizontal field components. These are the same ones which produce vertical closed orbit distortions. The horizontal field components necessary for vertical focussing cannot be avoided. In addition, injection and extraction systems involving horizontally bending magnets have to be carefully designed.

The spin of the particles precesses around the direction of the guiding field by an angle $2\pi\gamma G$ per turn, where $G = 1.7928$ is the anomalous magnetic moment of the proton and γ the relativistic energy factor. Resonances may occur which will move the spin away from the vertical direction, resulting in an effective depolarization. There are two types of resonances: intrinsic ones and those caused by imperfections. Intrinsic resonances correspond to those values of energy in the acceleration cycle which satisfy the condition $\gamma G = kP \pm \nu_v$ where P is the lattice periodicity, ν_v the vertical betatron tune, and k any integer. The imperfection resonances occur when $\gamma G = k$, and, to first order, can be excited only by vertical closed orbit distortions. Higher order resonances, caused by non-linear magnet imperfections and weak betatron coupling, can be neglected in a fast cycling synchrotron.

A resonance is described by a strength ϵ, a dimensionless quantity which depends on the lattice of the accelerator, the betatron tune, the amplitude of motion and closed orbit distortions. The asymptotic depolarization caused by the traversal of a single resonance can be calculated using the Froissart & Stora formula [7]:

$$P_f = \left[2\exp\left(-\frac{(\pi\epsilon)^2}{G\Delta\gamma \pm \Delta\nu_v}\right) - 1\right]P_i \qquad (3.4.1)$$

where P_i and P_f are the polarization coefficients before and after the crossing of the resonance, $\Delta\gamma$ is the energy gain per turn, and $\Delta\nu_v$ is a possible change of tune per turn which may be added in the case of an intrinsic resonance.

For polarized protons, there are again two modes of acceleration: to 1.2 GeV at a repetition rate of 50 Hz, and to 5.8 GeV at 10 Hz. In the first mode, the only intrinsic resonance corresponds to k = 0 and an energy of about 1 GeV if the betatron tune is ν_v=3.8. Its strength, calculated with the help of the code DEPOL [8], is ϵ=0.0055 for a normalized emittance of 10 π mm-mrad. In the high repetition rate mode, this resonance can be avoided by running the Booster lattice at a somewhat larger tune value, taking advantage of the low Laslett tune shift; in this way the depolarization caused by betatron motion is virtually zero.

In the 6 GeV cycle six intrinsic resonances have to be crossed. The strongest are at $G\gamma = \nu_v$ (the fundamental) and $G\gamma = 16 - \nu_v$, corresponding to an energy of 5.5 GeV;

in this latter case the depolarizing contributions of the 16 bending cells add coherently. A careful choice of the tune can help keep polarization above 50%. The implementation of a tune-jump system appears difficult due to the high repetition rate.

Eleven imperfection resonances are expected in the energy range up to 6 GeV, of which only two (0.63 and 1.15 GeV) are below 1.2 GeV. Nevertheless computations show significative depolarization only for vertical closed orbit distortions larger than 0.5 mm rms; as explained in section 3.1, this distortion can be corrected practically to zero.

3.5 The Magnet System

The Booster lattice consists of 24 cells with 24 horizontally focussing quadrupoles (QF), 24 horizontally defocussing quadrupoles (QD) and 32 bending dipoles (2 bending dipoles for each of the 16 cells in the arcs). Provision is made for two families of sextupoles for chromaticity correction.

The beam envelopes in Figure 3.1.4 shows a maximum beam dimension of 100 mm in the dipoles, and imply a dipole vertical aperture of 100 mm. The magnetic length of the dipole magnet is 3.46 m and the bending angle per magnet is 11.25° (0.1963 rads). The radius of curvature is $\rho = 17.6216$ m, and the designed maximum bending field is $B_{max} = 1.26$ T. The bending magnets are of sector type and are curved to accommodate the sagitta of 84.8 mm. As a consequence the vacuum chamber and the coils are also curved.

The QF and QD focussing elements have a magnetic length of 0.6 m and 0.5 m respectively, their bore diameter is 140 mm and the maximum design field gradient is $G = \pm 8.77$ T/m with a field at the pole tip of 0.62 T.

The high repetition rate of the machine requires a high dipole field rate of change $\dot{B} = 38$ T/s which, to avoid eddy current effects in the iron core, implies thin laminations for all the magnetic elements in the ring.

3.5.1 Dipole Design.

The H-type bending magnet design has been chosen for both Booster and Decelerator [9,10,11,12,13,14]. The cross-section of a dipole magnet is shown in Figure 3.5.1, while Table 3.5.1 lists the fundamental parameters.

To achieve the correct curvature, lamination foils are packed in 14 rectangular blocks 250 mm long (except for the two external ones of a shorter length to be determined after a more detailed design) which, to obtain the overall bending angle of 11.25°, are assembled with an angle of 0.9375° between each other. The blocks are kept together by straps welded on the top and bottom edges and by two stainless steel end plates. The straps will not shunt the eddy currents because of their small size and their position in a low field region. Each dipole weights 15 tons. The laminations, 0.35 mm thick, are made of iron characterized by a low remanent field in order to obtain high field quality at low excitation, and with good saturation properties. They are stacked randomly to minimize the effect of magnetic and construction imperfections.

The coils are arranged in four pancakes, two around the upper pole and two around the lower one, with 5 turns each for a total of 20 per magnet. Each conductor has a rectangular cross-section of 18.0×80.0 mm^2, each of 10 subconductors 8.0×15.0 mm^2 with a central cooling hole 3.5 mm diameter, carrying a maximum current density of 4.61 A/mm^2; the mean density, which sets the Joule losses, is 2.9 A/mm^2 (see Figure 3.5.1).

The inductance of the dipole is 5.50 mH and the corresponding maximum peak stored energy is $\frac{1}{2}LI^2 = 71.$ kJ. The ohmic resistance is 2.9 mΩ per dipole. The current range is between $I_{min} = 287.$ A and $I_{max} = 5086.$ A. The maximum current rate of change is $\dot{I}_{max} = 151.1$ kA/s. These numbers correspond to the 10 Hz operation rate.

The total dissipated power in the dipole system is 1.3 MW.

3.5.2 Quadrupole Design

The lengths of the quadrupoles in the Booster ring are adjusted to equalize the excitation currents in the two families as closely as possible. The QF quadrupoles have 0.6 m magnetic length and have a maximum design gradient of 8.7720 T/m, while the QD quadrupoles are 0.5 m long and have a maximum design gradient of 8.768 T/m. The calculated beam envelopes (Figure 3.1.4) give a bore diameter of 140 mm which, together with the design gradients, gives an easily achieved magnetic field at the pole tip of 0.62 T.

Because of the high repetition rate of the machine, the laminations are 0.35 mm thick, as for the dipoles. The quadrupole laminations, being four-fold symmetric, are cut in four identical pieces for convenience.

The proposed design has four turns per coil. The cross-section of the conductor is 18.0×52.0 mm^2, formed by two subconductors with 16.0×25.0 mm^2 cross-section with a central cooling hole with 6.5 mm diameter. With this design the same subconductor can be used for both the quadrupole and dipole coils. It is possible to increase the number of the quadrupole subconductors maintaining the same coil dimensions and to reduce the dissipated power.

The bore aperture of 140 mm implies a maximum excitation current of 4.42 kA (QF). The total power dissipated in the quadrupole system (QF+QD) does not exceed 0.3 MW.

The quadrupole parameters are given in Tables 3.5.2-3. The cross-section of the quadrupole magnets is shown in Figure 3.5.2.

3.5.3 Sextupole Magnets

Sextupoles, to be installed at a later stage to control the machine chromaticity, would form two families: 6 (SF) next to QF quadrupoles and 12 (SD) next to the QD quadrupoles in the arcs. The magnetic length has been set at 0.2 m and the aperture is circular with 140 mm diameter to match the quadrupoles. The field at the pole tip is less than 0.06 T.

Their design maximum strength is relatively weak (B''= 24 T/m^2) and their use can in principle be avoided. The accelerator can be operated in the first instance without them, and if required they can be added in a subsequent phase. The single coil wound around the six poles consists of a single turn with a cross-section of 15.0×30.0 mm^2, with no water cooling, carrying at most 1.2 kA. The sextupoles can be fed a with a constant current with a value optimized for the initial part of the accelerating cycle, where the chromatic corrections are most important.

Table 3.5.1: List of parameters for the Booster dipole magnets.

Parameter	Unit			
Type of magnet			Curved H	
Number of Magnets			32	
Bending Angle	degrees		11.25	
Bending Radius	m		17.60	
Core Length	mm		3360	
Magnetic Length	mm		3460	
Gap Height	mm		100	
No. Pancakes per Magnet			4	
No. Turns per Pancake			5	
Conductor Dimensions	mm^2		18.0×80.0	
Repetition Frequency	Hz	10		50
Injection Field	T	0.0690		0.1250
Extraction Field	T	1.2643		0.3600
Injection Current	A	276.8		503.7
Extraction Current	A	5085.7		1444.0
Current (rms)	A	3175.0		974.0
Current Density (rms)	A/mm^2	2.88		0.93
Max $\dot{I}$	kA/s	151.1		147.7
DC Resistance	mΩ		2.91	
Inductance	mH		5.50	
Dissipated Power	kW	41.10		17.50
Copper Weight	ton		1.45	
Iron Weight	ton		13.6	
Dissipated Power,total	MW	1.315		0.560
Stored Energy,total	MJ	2.3		0.2

Table 3.5.2: List of parameters for the Booster quadrupole magnets QF.

Parameter	Unit			
Type of magnet			QF	
Number of Magnets			24	
Core Length	mm		530	
Magnetic Length	mm		600	
Pole Tip Radius	mm		70	
No. Turns per Pole			4	
Conductor Dimensions	mm^2		17.0×52.0	
Pulse Rep. Frequency	Hz	10		50
Minimum Gradient	T/m	0.479		0.871
Maximum Gradient	T/m	8.772		2.525
Minimum Current	A	240.1		437.0
Maximum Current	A	4419.2		1264.0
Current (rms)	A	2759.0		899.4
Max $\dot{I}$	kA/s	131.3		129.9
Current Density (rms)	A/mm^2	3.76		1.23
DC Resistance	mΩ		0.764	
Inductance	mH		0.340	
Dissipated Power	kW	6.5		6.0
Copper Weight	kg		185	
Iron Weight	kg		680	
Dissipated Power,total	MW	0.160		0.144
Stored Energy,total	kJ	80.		6.5

Table 3.5.3: List of parameters for the Booster quadrupole magnets QD.

Parameter	Unit			
Type of magnet			QD	
Number of Magnets			24	
Core Length	mm		430	
Magnetic Length	mm		500	
Pole Tip Radius	mm		70	
No. Turns per Pole			4	
Conductor Dimensions	mm^2		17.0×52.0	
Pulse Rep. Frequency	Hz	10		50
Minimum Gradient	T/m	0.479		0.871
Maximum Gradient	T/m	8.768		2.525
Minimum Current	A	240.1		437.0
Maximum Current	A	4419.2		1264.0
Current (rms)	A	2759.0		899.4
Max $\dot{I}$	kA/s	131.3		129.9
Current Density (rms)	A/mm^2	3.76		1.23
DC Resistance	mΩ		0.655	
Inductance	mH		0.280	
Dissipated Power	kW	5.6		5.0
Copper Weight	kg		160	
Iron Weight	kg		550	
Dissipated Power,total	MW	0.135		0.120
Stored Energy,total	kJ	66.		5.4

tie
straps

pancake 1

pancake 2

subconductors

15 mm

80 mm

3.5

18 mm

b)

792 mm

100 mm

860 mm
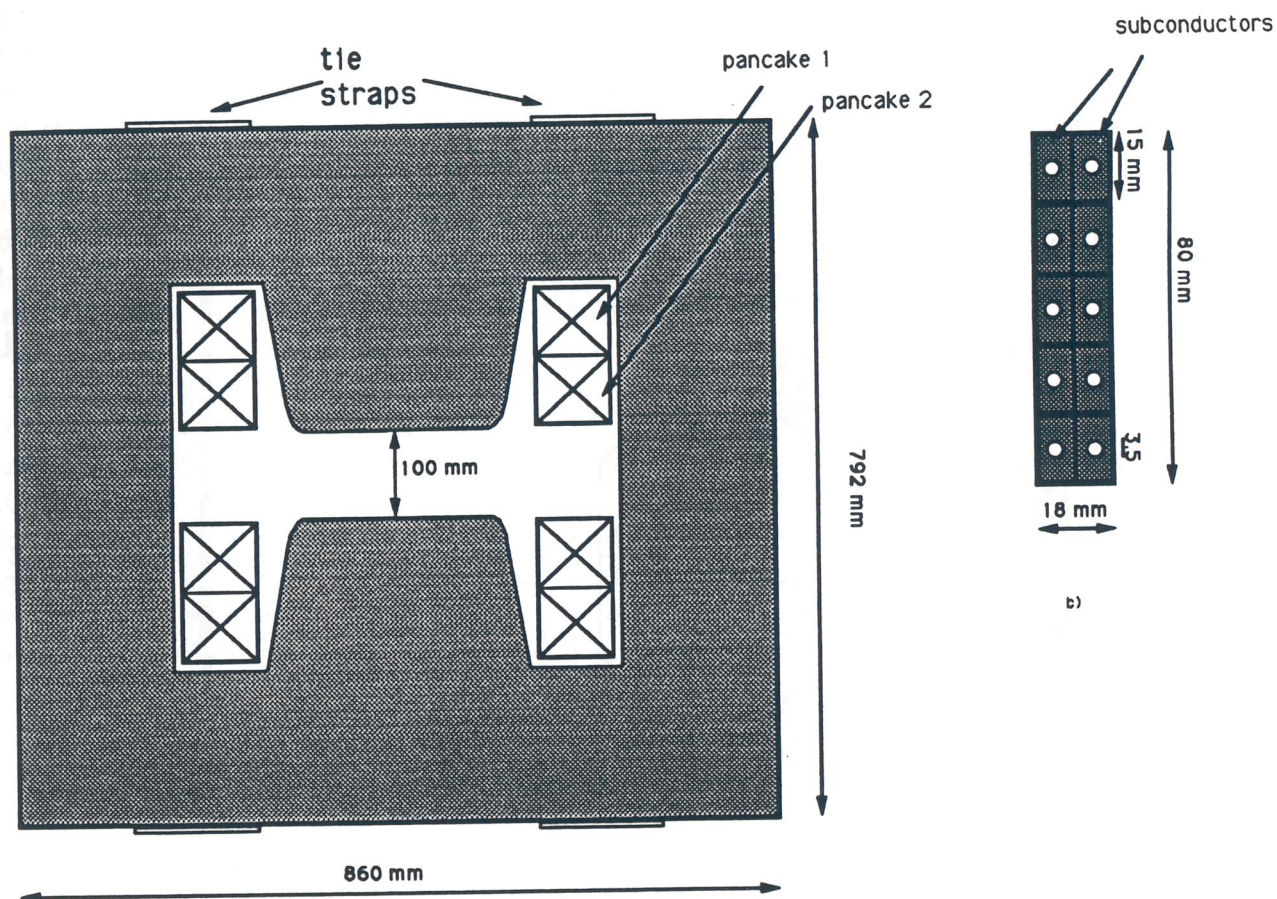
Figure 3.5.1: a) Cross-Section of the Dipole Magnets;
b) Cross-Section of the Dipole Conductor.
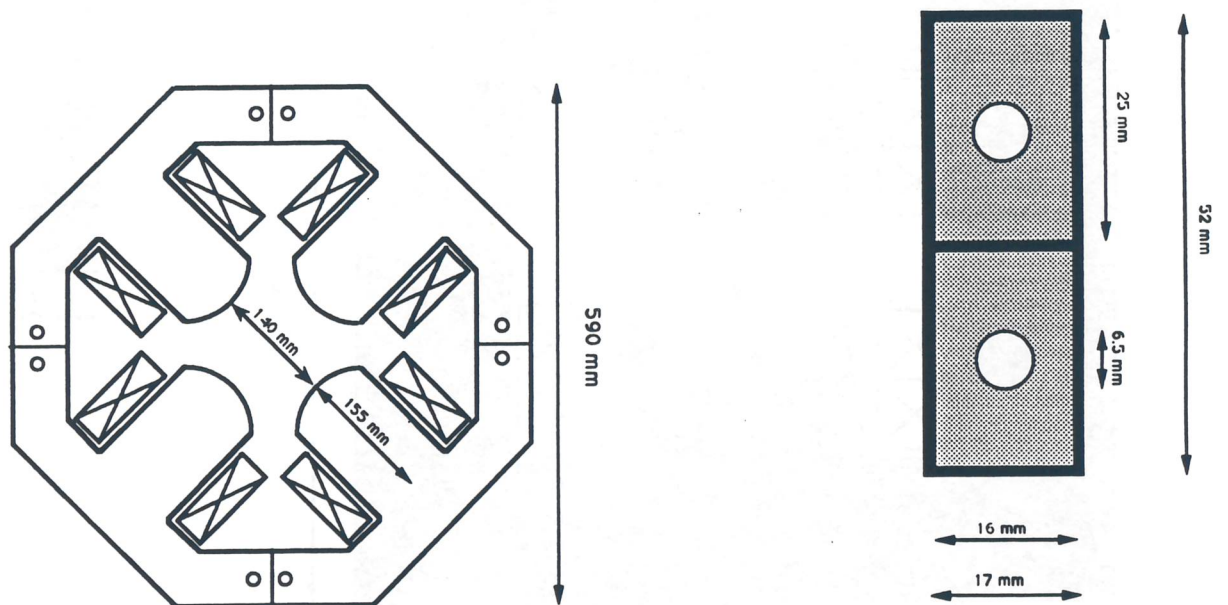
Figure 3.5.2: a) Cross-Section of the Quadrupole Magnets;
b) Cross-section of the Quadrupole Conductor.

3.6 Power Supplies

The high operating frequencies of 10 Hz and 50 Hz can be achieved only with a resonating power supply in which the inductances of the magnets are made to resonate in parallel with a capacitor bank. Only the case of a pure single resonating frequency is considered here; the addition of a second frequency to lengthen the acceleration cycle is not advantageous since it requires a more complicated power supply circuit and saves only a marginal amount of rf during acceleration.

The proposed solution is to provide three power supply busses, one each for the QF and QD quadrupoles and one for the dipoles separately. Table 3.6.1 summarizes the main parameters of the three power supply busses. Figure 3.6.1 shows the magnet and circuit arrangement for the dipoles. Selecting the 10 or 50 Hz operation cycle is obtained by switching the power supply network to the required capacitor bank as shown in the figure. Since the load is large, the dipole circuit is divided into four identical cells, each corresponding to a superperiod of the magnet lattice, with all 8 dipoles of the superperiod connected to the same bus transformer. There are four virtual ground reference points. As shown in Figure 3.6.2, the quadrupoles are arranged similarly, except that since they provide a smaller load they can be included in only two cells, one each for QF and QD types. The total power required to operate the booster magnets is 1.7 MW.

When magnets are ramped on different power supply busses, good power supply regulation is required. In order to maintain a betatron tune stable to less than 0.01 throughout the cycle, a current regulation of one part in 10^4 is required between the different busses. Similarly power supply ripple is of the same magnitude or less to avoid unacceptable tune oscillations.

Connection of the sextupole magnets is considerably easier. They are divided into two families (SF and SD) each of which is connected in series to a single independent bus. It may even not be necessary to power the sextupoles in AC mode, but rather to leave them at a constant excitation corresponding to injection energy, when they are most needed. For this case the circulating current is 1.2 kA with a negligible voltage.
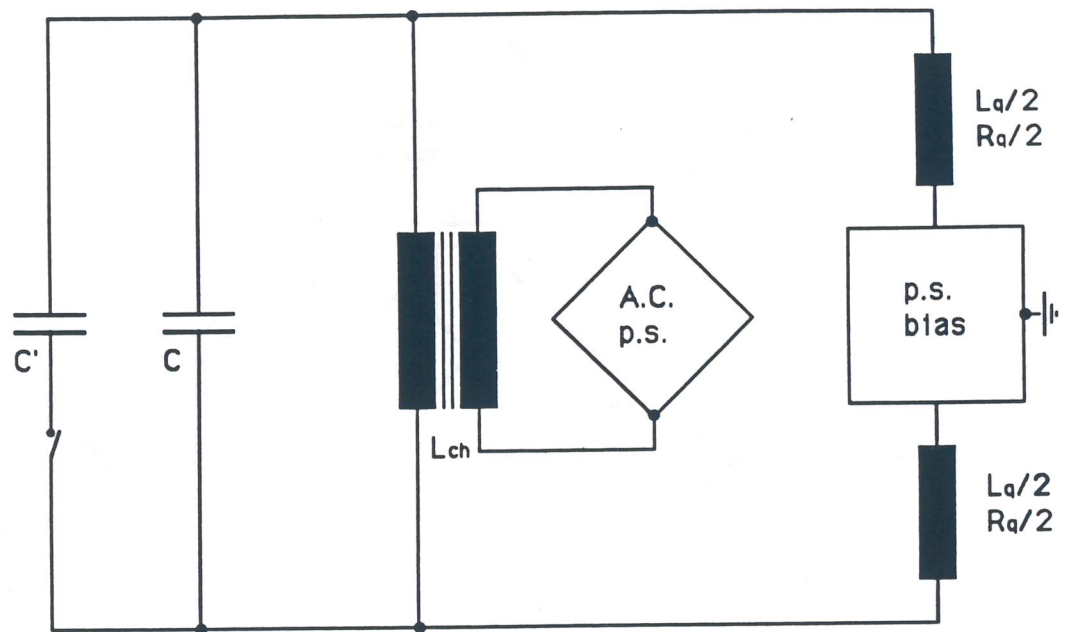
Table 3.6.1: Main dipole and quadrupole power supply system requirements.

	Peak Voltage kV	Dissipated Power MW
Dipoles:		
10 Hz	26.8	1.315
50 Hz	26.0	0.560
Quadrupoles (QF):		
10 Hz	1.11	0.160
50 Hz	1.08	0.144
Quadrupoles (QD):		
10 Hz	0.92	0.135
50 Hz	0.88	0.120

Figure 3.6.1: Power Supply arrangement for Dipole Magnets.

C : Cres(10 Hz)
C'||C : Cres(50 Hz)
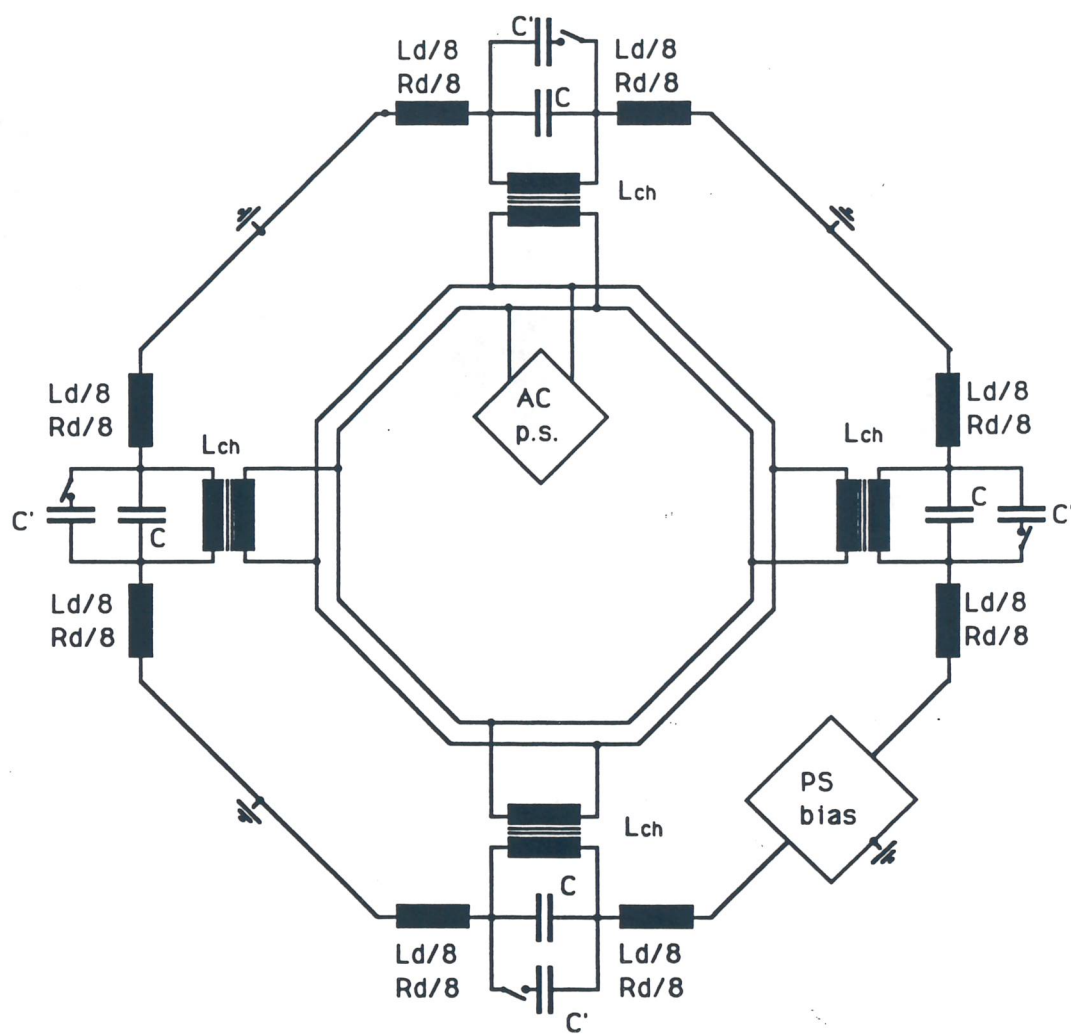
C : C_{res}(10 Hz)
C'||C : C_{res}(50 Hz)

Figure 3.6.2: Power Supply arrangement for Quadrupole Magnets.

3.7 The rf System

The purpose of the rf system in the Booster is twofold. The first task is the acceleration of different species of heavy ions from ALPI to an energy which corresponds to the maximum magnetic rigidity $B\rho = 22.25$ Tm of the ring, at a repetition rate of 10 Hz. This corresponds to 1 GeV/u for gold ions and to 2.5 GeV/u for ions as light as carbon.

The second task is the acceleration of intense beams of protons from the injection energy of 211 MeV to a maximum kinetic energy of 5.8 GeV, which again corresponds to the maximum magnetic rigidity at the same repetition rate of 10 Hz. Protons can also be accelerated at the repetition rate of 50 Hz to 1.2 GeV, the limit being set by the maximum dipole field rate of change of 38 T/s, thus increasing the average beam intensity by a factor of five.

To cope with the large frequency swings required for the acceleration of both heavy ions and protons, the operating range is covered by: a low frequency system (LFRF) sweeping from 5 to 32 MHz and a high frequency system (HFRF) ranging from 30 to 51 MHz. For the acceleration of protons to 6 GeV in 50 ms, a third set of cavities (VHRF) must be added to the Booster to cover the 50 to 56 MHz range.

Both LFRF and HFRF systems use several double-gap cavities, tuned by applying a longitudinal biasing field to a set of Ni-Zn ferrite rings. These resonators are characterized by quality factors typically below 100, and are driven by tetrodes housed inside the cavity structure with an output power of the order of 100 kW.

3.7.1 Acceleration of Heavy Ions

Table 3.7.1 summarizes the rf requirements for the acceleration of different ion species. The use of a constant harmonic number is the most convenient mode of operation, in which a low bunching factor and space-charge tune-depression are obtained, since all the buckets are occupied. The rf frequency at injection is always 5 MHz, the frequency of the ALPI prebuncher; the resulting bunch separation at injection is then 200 ns for all species. Since different ions are injected with different velocities, appropriate harmonic numbers are chosen as shown in Table 3.7.1. The largest rf swing is required for the very heavy ions: in the case of uranium, the ratio between frequencies at extraction and at injection is 9.4, whereas for the acceleration of sulfur a ratio of only 5.2 is required.

Figure 3.7.1 gives the required rf peak voltage versus rf frequency in a 10 Hz cycle for different ion species. It can be seen that elements up to copper require a frequency swing of only 5 to 32 MHz. For the heavier ions like iodine, gold and uranium, the frequency required is from 5 to 47 MHz, with voltages not exceeding 220 kVolt. This is taken into account in the choice of the two rf systems.

The peak voltage depends on the acceleration rate and on the size of the rf buckets. The bucket area is determined by the painting techniques used with multi-turn injection to fill the buckets uniformly. Since the bucket length is about 200 ns, the bucket area is then specified by the bucket height, which is chosen to be at least a factor of 3 larger than the momentum spread of the bunches injected from ALPI. Table 3.7.1 gives a summary of their dimensions and the required bucket area and height. In absolute energy units, the variation from one species to another is small, as one would expect from the operation of the ALPI injector, while in specific energy units, there is a very substantial variation. The bucket area

is only 0.0024 eV/u-s for uranium and 0.049 eV/u-s for deuterium.

The actual total voltage program during an acceleration cycle is shown in Figure 3.7.2 for deuterium and in Figure 3.7.3 for uranium, assuming that the buckets are filled at injection and that they increase in area quadratically with time by a factor of two during the cycle. Most of the voltage is required for the acceleration proper and only a small fraction to generate the bucket area.

3.7.2 Acceleration of Protons

In the complex described here, the acceleration of protons is assumed for an injection energy of 211 MeV. This is a more demanding case which requires the largest frequency swing and accelerating voltage; a higher energy linac can alleviate the requirements in the rf system.

A harmonic number $h = 50$ during the acceleration cycle is chosen for two reasons: it implies a frequency range which coincides with the HFRF system for the acceleration of very heavy ions, and it provides natural rf matching for a second stage accelerator.

As already mentioned, protons can be accelerated according to two schemes. In the case of 50 Hz to the kinetic energy of 1.2 GeV, the rf ranges from 30 to 50.5 MHz as shown in Figure 3.7.4. The required rf voltage is shown in Figure 3.7.5 for buckets with an area of 0.05 eV-s completely filled at injection. A quadratic variation of the bucket area with time and an increase of a factor of two during the acceleration cycle have again been assumed.

The frequency modulation and the voltage program for acceleration at 10 Hz to 5.8 GeV are shown in Figure 3.7.6 and 3.7.7. The rf frequency now ranges from 30 to 56 MHz; to cover the last interval from 50 to 56 MHz, a third cavity system (VHRF) providing a maximum voltage of 270 kV is required. During this acceleration cycle, the particles cross transition at $\gamma_t = 4.59$. The crossing is fast and very few consequences are expected. Even with an intensity of 2.5×10^{11} protons per bunch the Soerenssen parameter, which measures the mismatch between the longitudinal space-charge forces and the rf focussing, is estimated to be less than one, provided that the inductive contribution of the beam-wall coupling impedance is large enough (40 Ω) to compensate for the space-charge impedance. It is also estimated that the negative-mass instability will cause the bunch area to grow by no more than a few percent.

3.7.3 The rf cavities

Both the LFRF and the HFRF use double-gap cavities, in which the Transit Time Factor (TTF) is a concern. The distance between the two gaps is chosen to accommodate the widest spectrum of accelerated ions.

The TTF is the parameter that indicates how efficiently particles of velocity β are accelerated through two gaps a distance L apart. When the two gaps are exactly π radians apart, the TTF is:

$$TTF = sin\ \frac{\pi L}{\beta \lambda} \tag{3.7.1}$$

where λ is the rf wavelength. The same expression can be also written to show its dependence

on the harmonic number h as:

$$TTF = sin \, \frac{\pi L h}{2\pi R} \tag{3.7.2}$$

where the denominator is the circumference of the ring. It is clearly desirable to have a TTF as close as possible to unity for the widest range of species. A summary of the TTF for both systems is listed in Table 3.7.2 for several ions, and in Table 3.7.3 for the two proton scenarios. In the case of a double-gap cavity in which the two gaps are exactly in phase (the so called 0 mode) the expression for the TTF becomes:

$$TTF = cos \, \frac{\pi L h}{2\pi R} \tag{3.7.3}$$

In Table 3.7.2, the factors listed for the low frequency system are calculated with this expression, since it is proposed to run the cavities in 0 mode. While for heavy ions only six cavities are required in the HFRF, for the acceleration of protons to 5.8 GeV at 10 Hz two more are needed, and a total of 12 must be used for acceleration to 1.2 GeV at 50 Hz.

3.7.3.1 The low frequency rf system

The low frequency rf system consists of cavities operating between 5 and 32 MHz, and is used only for acceleration of heavy ions.

The cavities can be modelled using as a reference those built for the Princeton-Pennsylvania accelerator (PPA, shown in Figure 3.7.8), which tuned from 6 to 30 MHz and were capable of 7 kV per gap [15,16]. The voltages now required are considerably higher:

20 kV/gap @ 15 - 32 MHz (for all ion species)
5 kV/gap @ 6 MHz (10 kV for Deuterium)
1 kV/gap @ 5 MHz (2 kV for Deuterium)

This scenario has been calculated assuming that 6 double-gap cavities are used. The gap-to-gap distance is 0.8 m, as required by the TTF considerations described above, and each cavity is therefore about 1.6 m long. This implies that the LFRF system occupies 3 drift regions, each 5 m long; two cavities will be installed in each drift space, leaving enough room for diagnostics, vacuum ports and instrumentation.

The voltage that can be obtained depends on the rf flux, and therefore on the magnetic field that can be stored in the ferrite. Considering that 7 kV were obtained in the PPA cavities with an rf field of only 20 Gauss, while with new types of ferrites it is now possible to exceed 100 Gauss (as in the rf system for the AGS Booster at Brookhaven National Laboratory), the required rf voltage for the Booster LFRF system seems practicable.

The TTF calculated in Table 3.7.2 apply to the frequency range 6 to 32 In the lowest frequency band, fromfor the 0 mode apply to the 6-32 MHz range. In the lowest frequency band, from 5 to 6 MHz, which was not covered by the PPA cavity, the voltage requirements are smaller. One possible way to cover this frequency interval is to couple two adjacent cells with a transmission line to increase the inductive load, and to run the pair in 0 mode.

3.7.3.2 The high frequency rf system

The high frequency rf system ranges from 30 to 50.5 MHz; it is used to accelerate both heavy ions and protons, with the following voltage requirements:

23 kV/gap @ 30-40 MHz in heavy ions cycle
24 kV/gap @ mid-band in proton - 10 Hz cycle
25 kV/gap @ mid-band in proton - 50 Hz cycle

A very similar rf system, using the cavity shown in Figure 3.7.9, is in operation in the Fermilab Booster [17].

Three tuners are connected to the beam-pipe in the center of the cavity to compensate for the capacitive reactance of the resonator at that point. There are two main contributions to this capacitance: the first comes from the two gaps, as seen at the end of the coaxial transmission line formed by the beam-pipe and the outer conductor; the second comes from the power amplifier, which is directly coupled to the cavity. A water-cooled tetrode is installed in a stub as the final stage. To reach the TTF listed in Tables 3.7.2 and 3.7.3, the gap distance is 1.6 m and the cavities are run in a π mode. The voltage requirements listed above have been calculated assuming the use of 6 double-gap cavities for heavy ions and either 8 or 12 for protons. Six double-gap cavities will occupy 3 drift regions.

One parameter of concern is the power delivered to the beam. In the case of the acceleration of heavy ions, the beam power requirements are modest compared to losses in the cavities. The situation is more critical for protons: more than 10^{13} particles are accelerated in each cycle of the Booster. The power delivered to the proton beam is plotted in Figure 3.7.10. Although beam loading effects have been studied and compensated for in existing accelerators for similar conditions, they must be carefully considered in the design of the Booster rf system.

3.7.3.3 The 50-56 MHz system for 5.8 GeV protons

The acceleration of protons to 5.8 GeV at 10 Hz requires an additional rf system able to deliver a total voltage of 270 kV in a frequency range from 50 to 56 MHz.

For this purpose, it is possible to build a single-gap cavity tuned by perpendicularly biased garnets, a scheme that has recently been successfully tested as a prototype by the Los Alamos-TRIUMF collaboration, and is also being adopted in the SSC-LEB design [18,19]. The substantial advantage of this cavity is that the quality factors involved are above 1000, and it is therefore possible to achieve much greater voltages for the same amount of dissipated power. Because the overall length is about a metre, it is possible to fit up to four of them in a five metre drift space to obtain the required voltage. A drawing of this type of cavity is shown in Figure 3.7.11.

3.7.4 The Cavity Arrangement

The variation of the ratio Q_s of the synchrotron frequency to the revolution frequency is plotted versus time in Figures 3.7.12 and 3.7.13 for gold ions and for protons. This value is largest soon after injection but never exceeds 0.06, which is considered safe from

the beam dynamics point of view. Nevertheless to minimize the possible enhancement of betatron-synchrotron coupling, the rf cavities are located as symmetrically as possible in low dispersion regions. The proposed locations of the rf cavities in the Booster ring are shown in Figure 3.7.14

Table 3.7.1: rf Parameters for some Heavy Ion Scenarios.

	S	Cu	I	Au	U	
Mass Number	32	63	127	197	238	
Charge State	16	27	40	51	54	
Kinetic Energy						
@ injection	16.40	10.39	6.11	4.58	3.86	MeV/u
@ extraction	2.53	2.08	1.37	1.03	0.85	GeV/u
β						
@ injection	0.1853	0.1483	0.1140	0.0988	0.0908	
@ extraction	0.9632	0.9509	0.9143	0.8802	0.8516	
Orbit Period						
@ injection	4.8	6.0	7.8	9.0	9.8	μs
@ extraction	0.9235	0.9354	0.9729	1.0106	1.0445	μs
Harmonic No.	24	30	39	45	49	
rf Frequency						
@ injection	5	5	5	5	5	MHz
@ extraction	25.99	32.07	40.09	44.53	46.91	MHz
Full $\frac{\Delta p}{p}$ Bucket						
@ injection	0.038	0.031	0.026	0.022	0.022	%
Bucket Area						
@ injection	0.0086	0.0055	0.0035	0.0026	0.0024	eV/u-s

Table 3.7.2: Transit Time Factors for Cavities (Heavy Ions).

LFRF System:		HFRF System:	
5-32 MHz	0-mode	30-50.5 MHz	πmode
Gap Distance	0.8 m	Gap Distance	1.8m
Cavity Length	1.6 m	Cavity Length	2.2 m
No. of Cavities	6	No. of Cavities	6

	S	Cu	I	Au	U	
Harmonic No.	24	30	39	45	49	
LFRF System						
Effective Voltage	195	200	200	210	220	kV
TTF	0.975	0.960	0.933	0.911	0.895	
Required Voltage	200	208	214	230	246	kV
Voltage/Gap	16.7	17.4	17.9	19.2	20.5	kV
HFRF System						
Effective Voltage	-	-	200	210	220	kV
TTF	-	-	0.736	0.816	0.862	
Required Voltage	-	-	272	257	255	kV
Voltage/Gap	-	-	22.6	21.4	21.3	kV

Table 3.7.3: rf Cavities for Acceleration of Protons.

Harmonic Number = 50

Repetition Rate	10	50	Hz

HFRF System

(30-50.5 MHz in π mode)

Number of Cavities	8	12	
Effective Voltage	330	520	kV
TTF	0.872	0.872	
Required Voltage	378	378	kV
Voltage/Gap	23.6	24.8	kV

VHRF System

(50-56 MHz Single Gap)

Number of Cavities	4	-	
Total Voltage	270	-	kV
Cavity Length	1	-	m
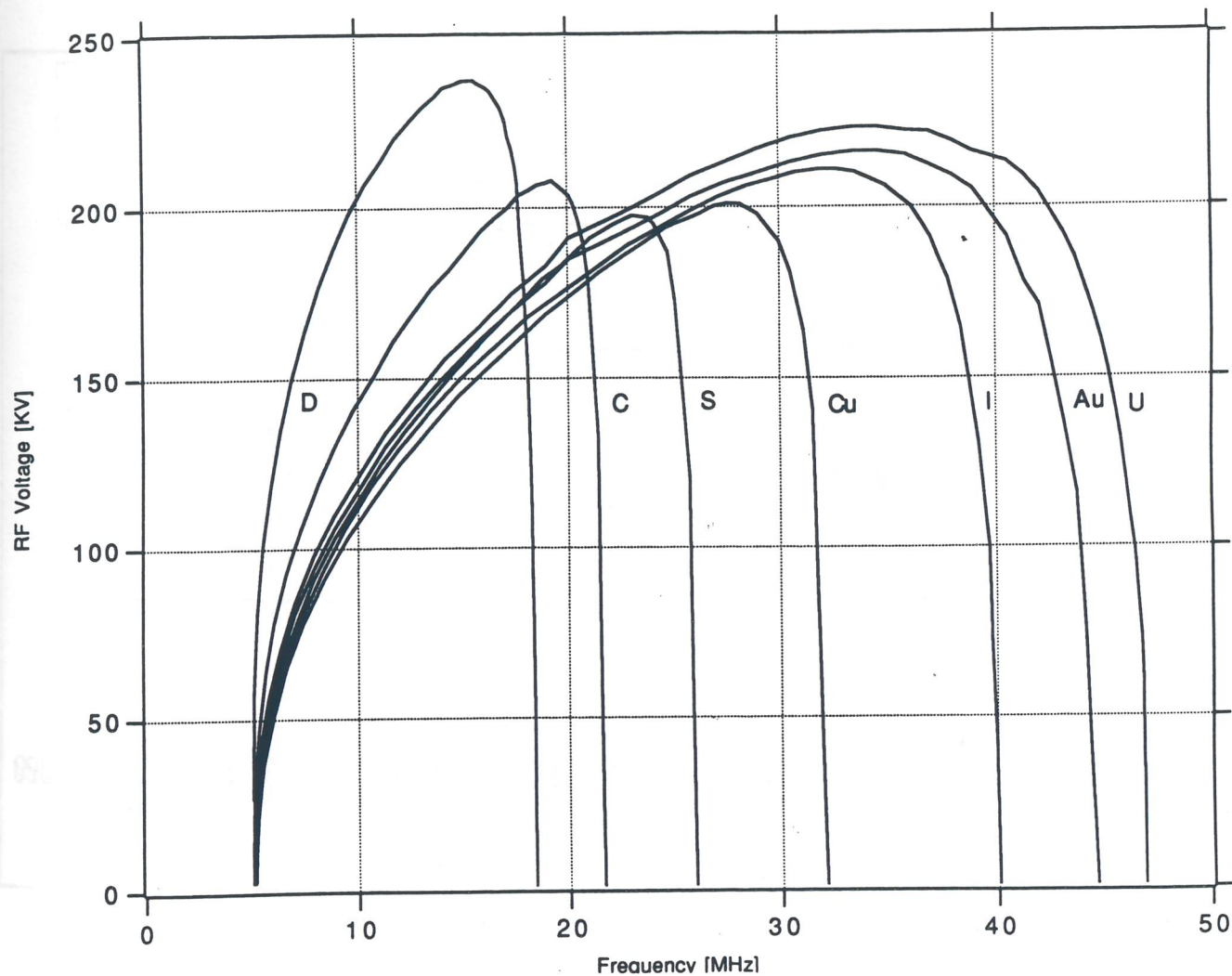
Figure 3.7.1: Required rf voltage vs. frequency for Heavy Ions acceleration.
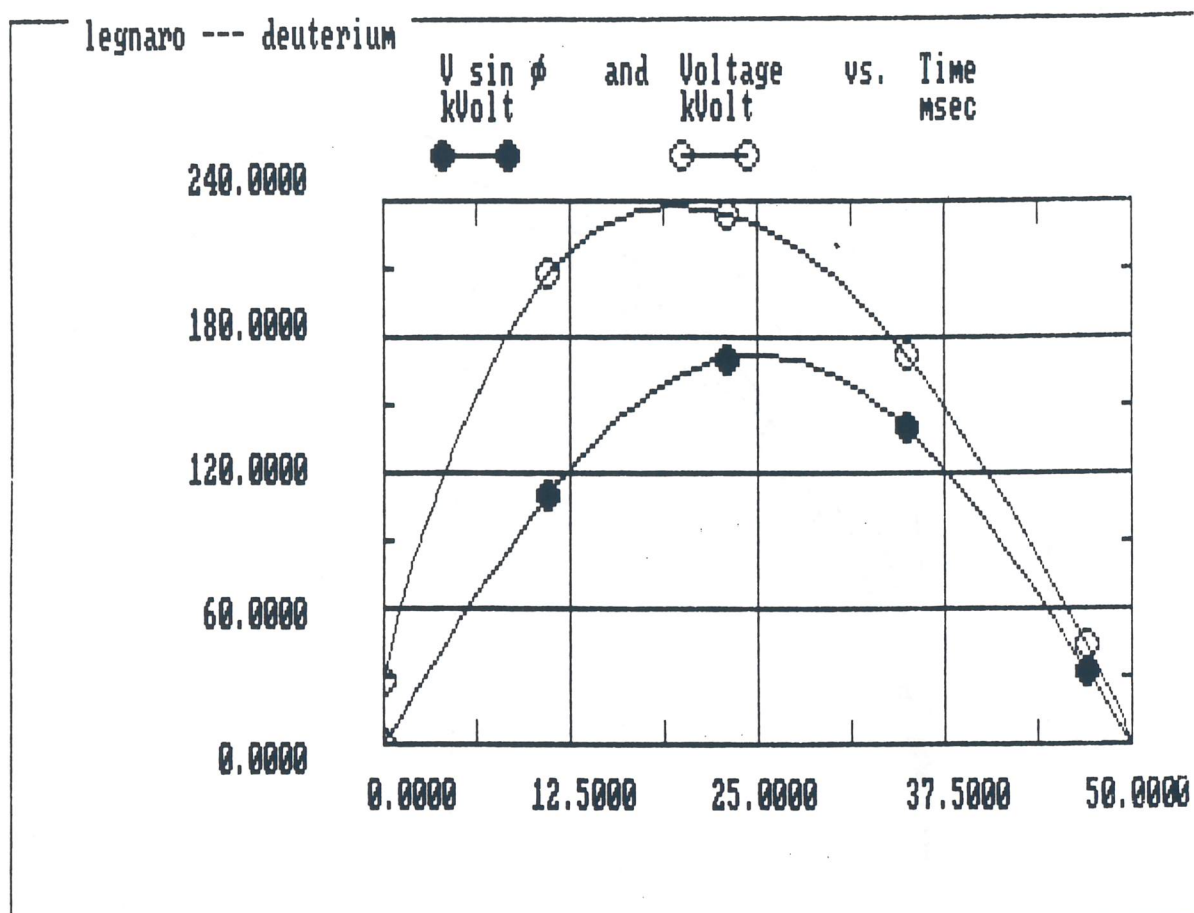
Figure 3.7.2: Voltage program for the acceleration of Deuterium.
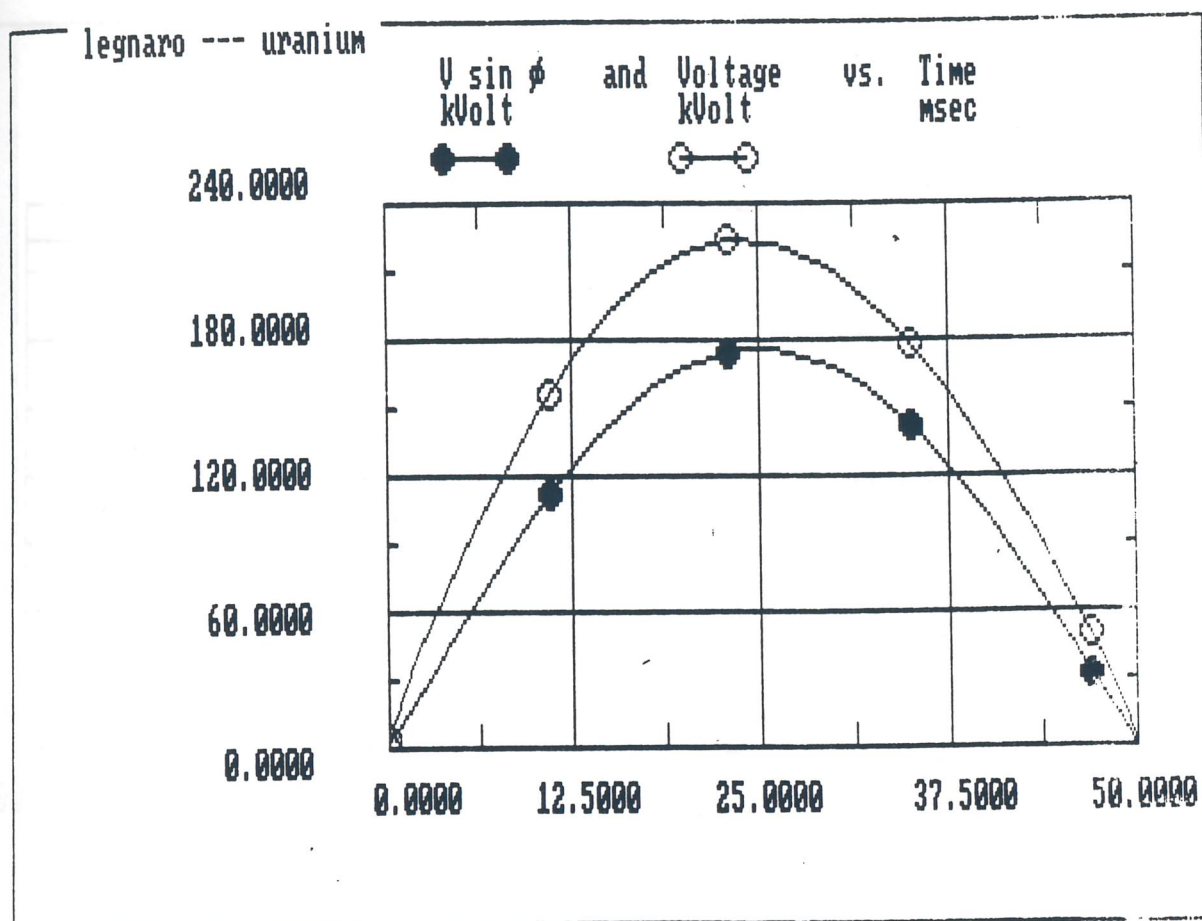
Figure 3.7.3: Voltage program for the acceleration of Uranium.
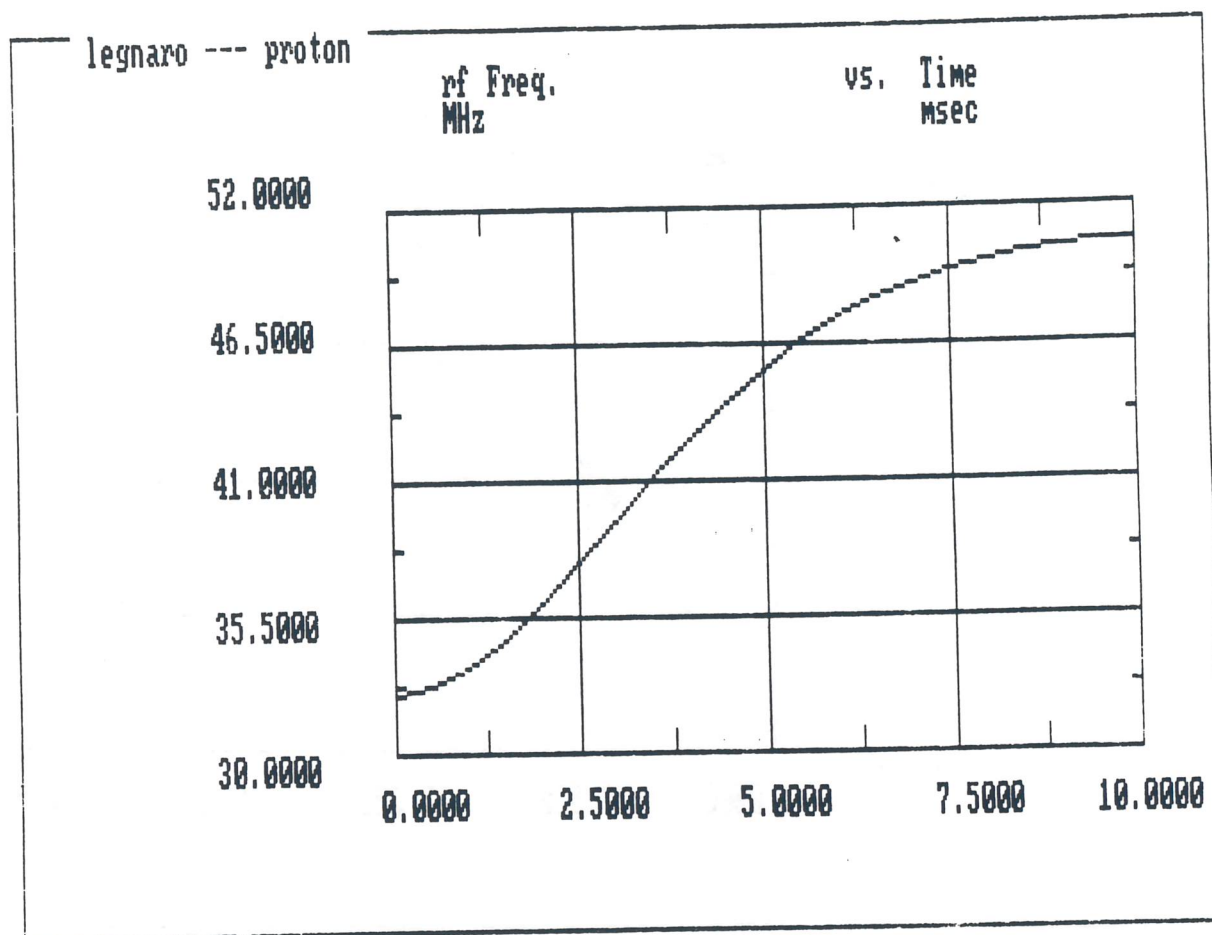
Figure 3.7.4: Frequency program for the acceleration of Protons (50 Hz).
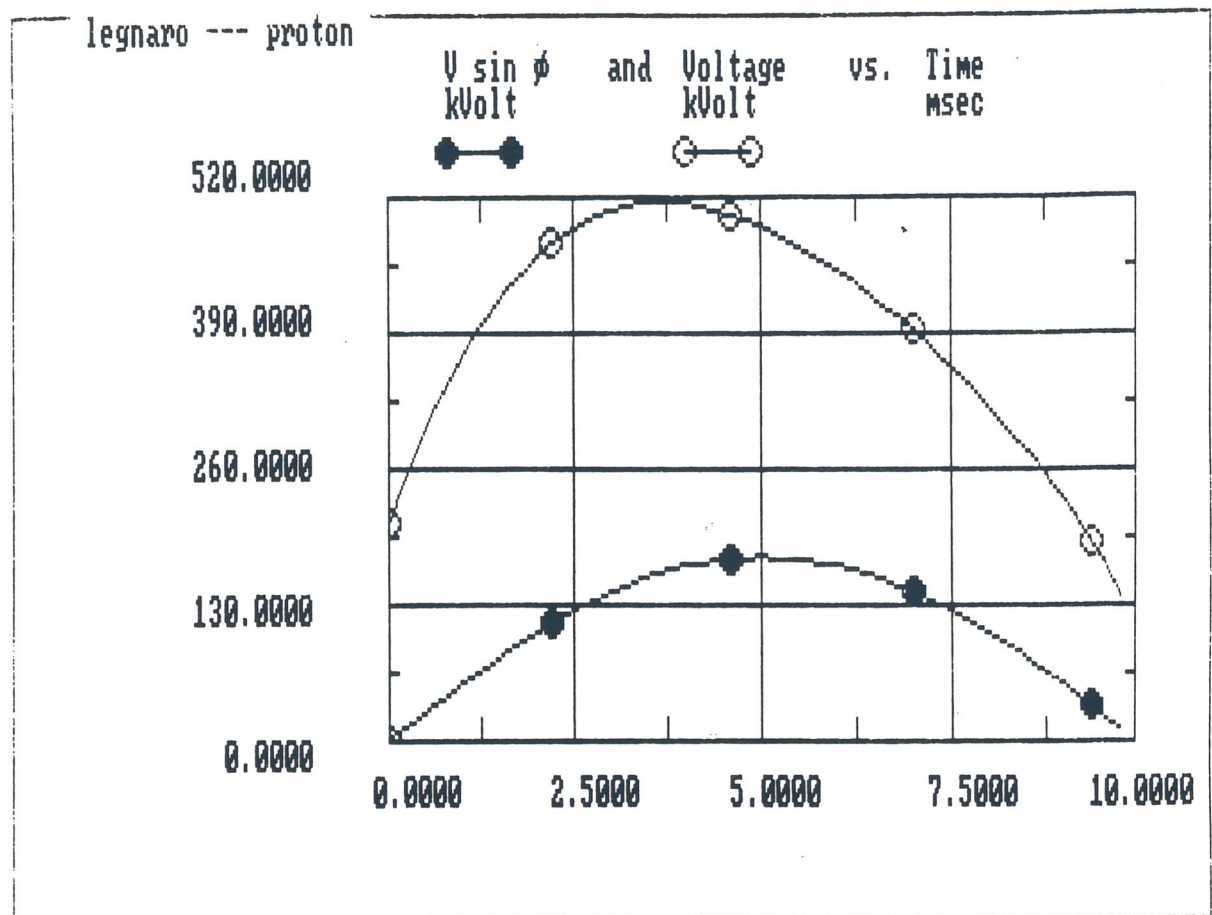
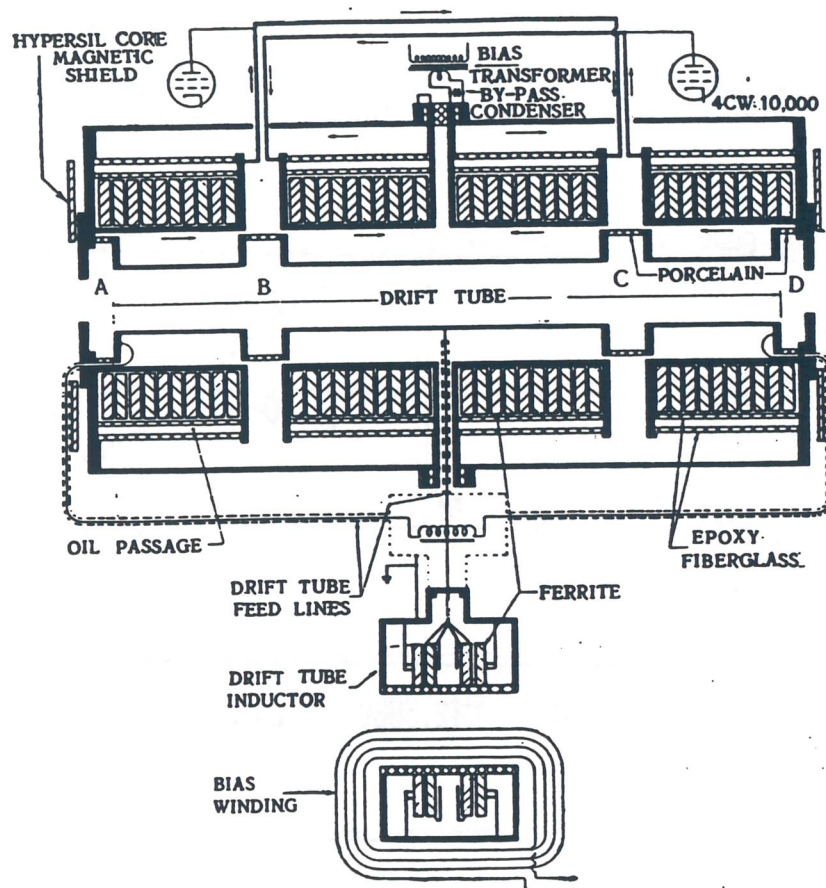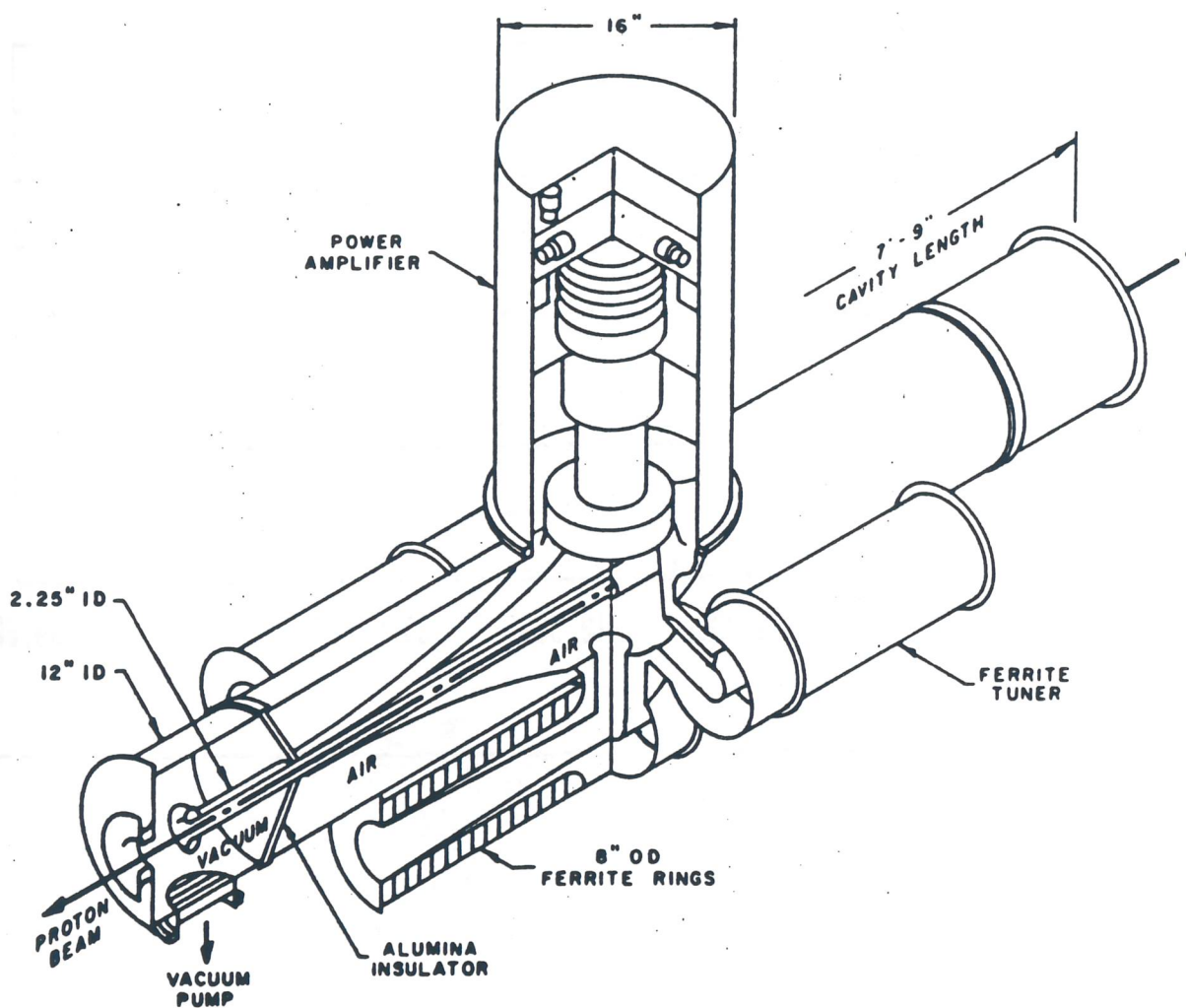Figure 3.7.5: Voltage program for the acceleration of Protons (50 Hz).
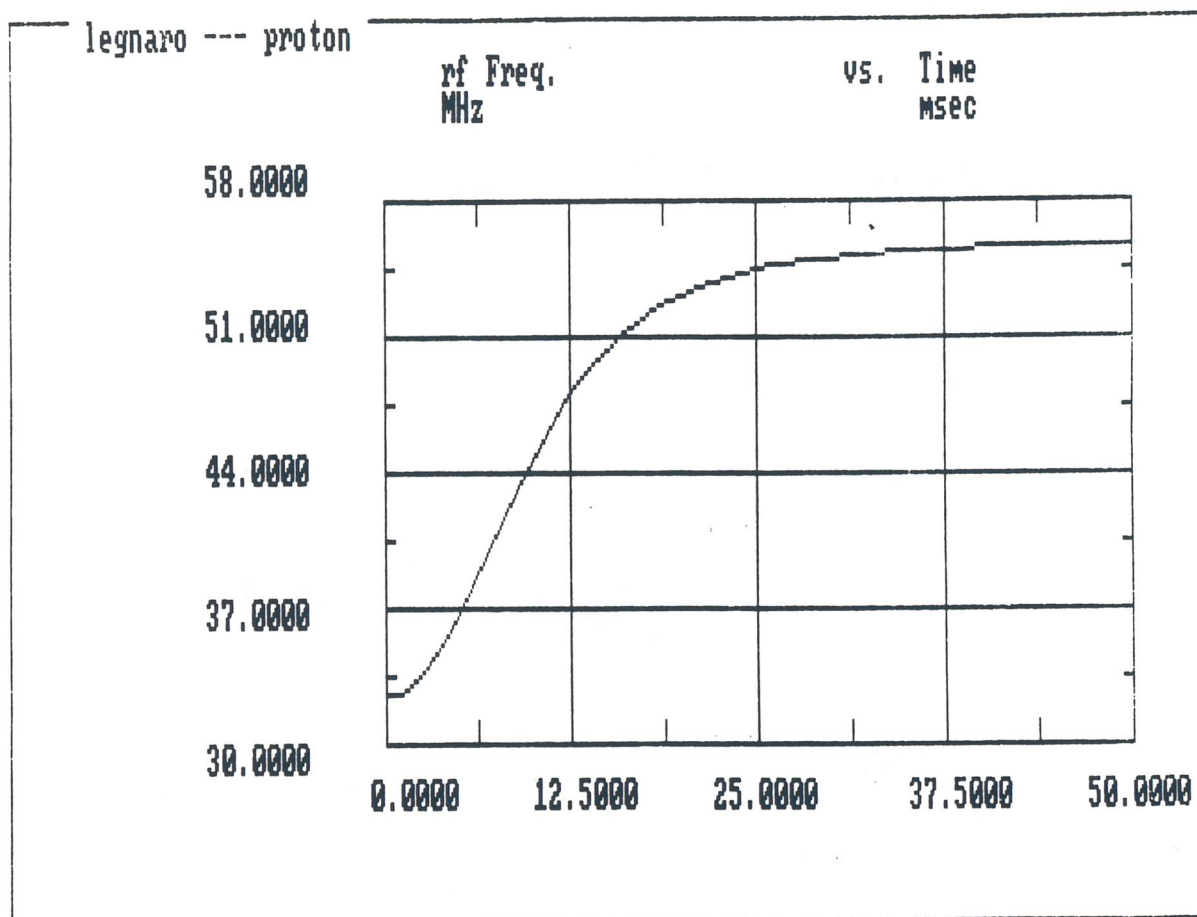
Figure 3.7.6: Frequency program for the acceleration of Protons (10 Hz).
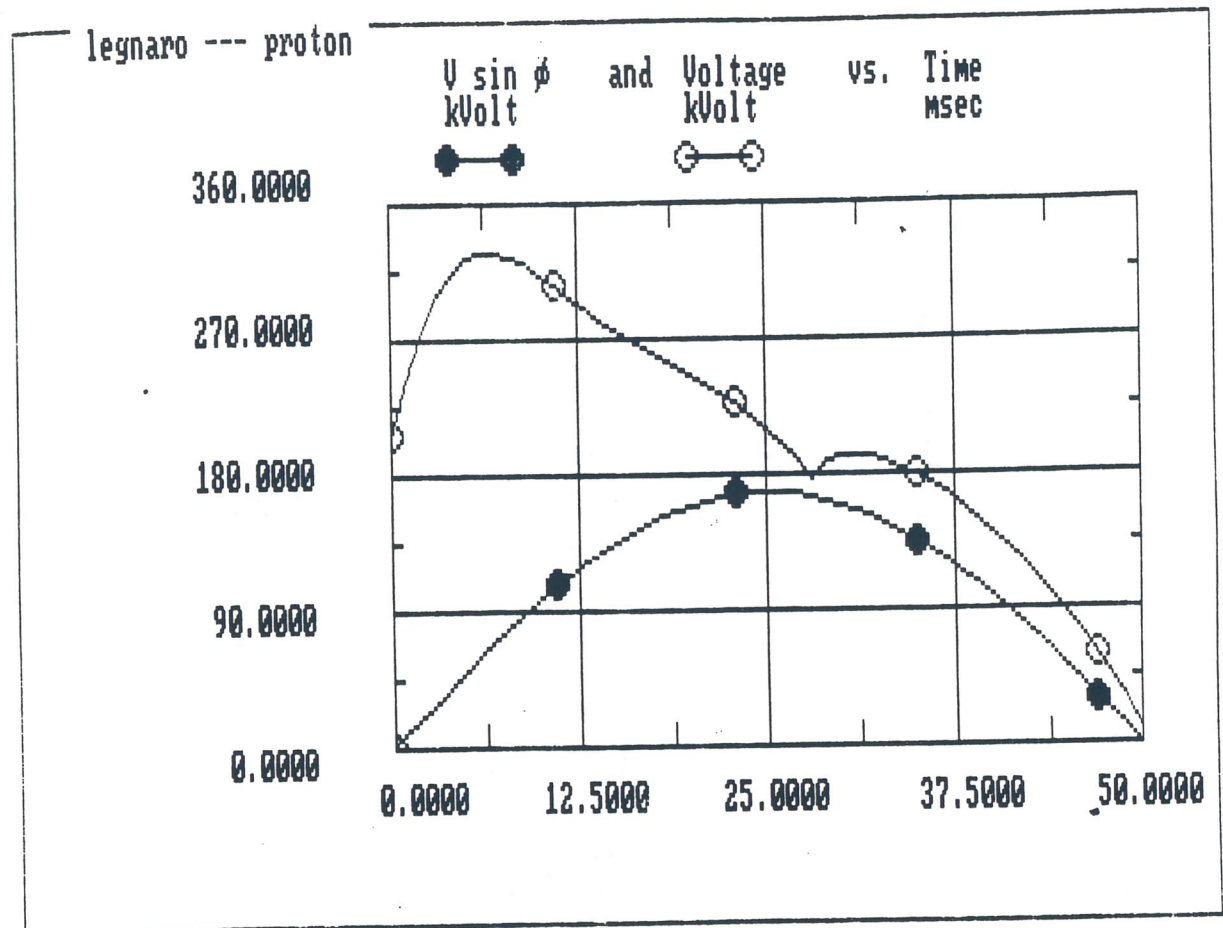
Figure 3.7.7: Voltage program for the acceleration of Protons (10 Hz).

Figure 3.7.8: The PPA rf cavity.
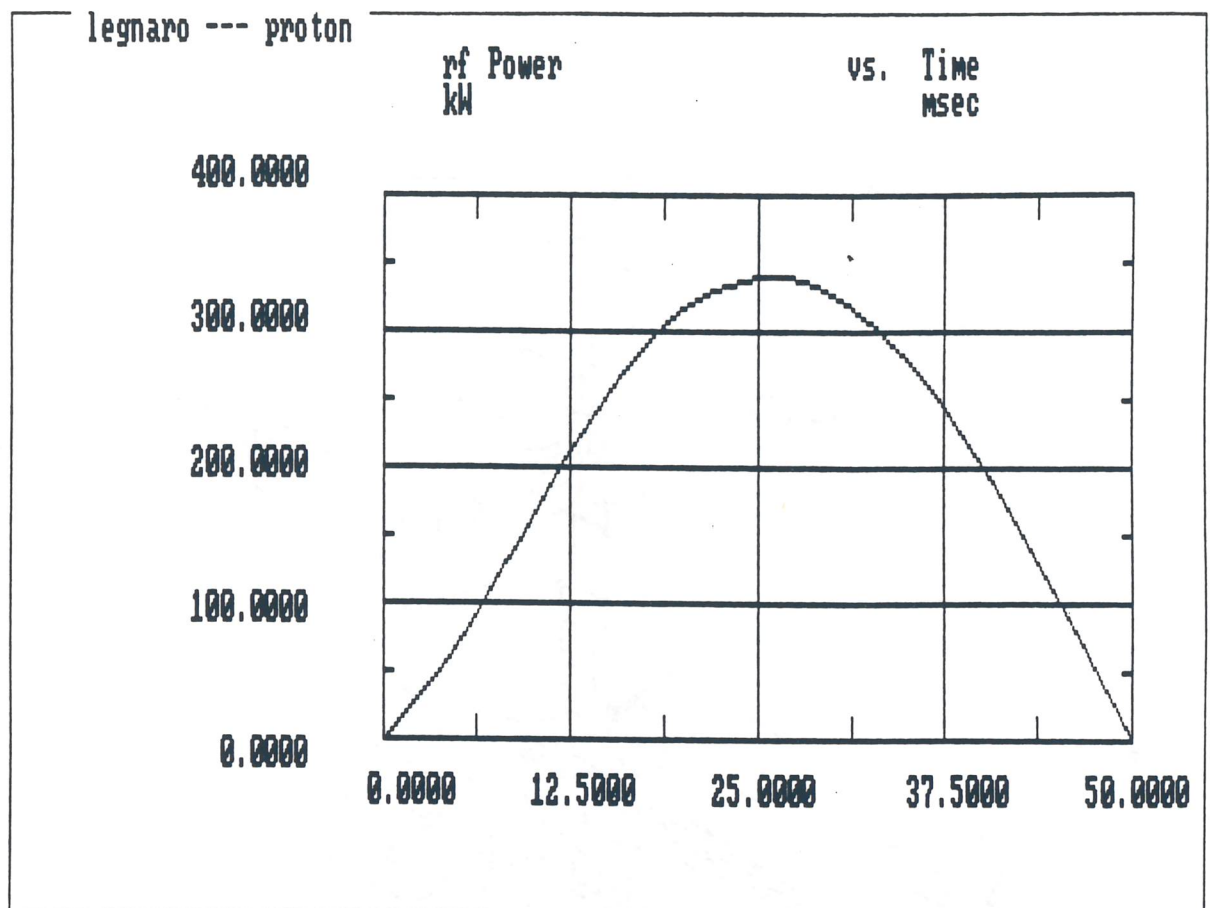
Figure 3.7.9: The Fermilab Booster rf cavity.

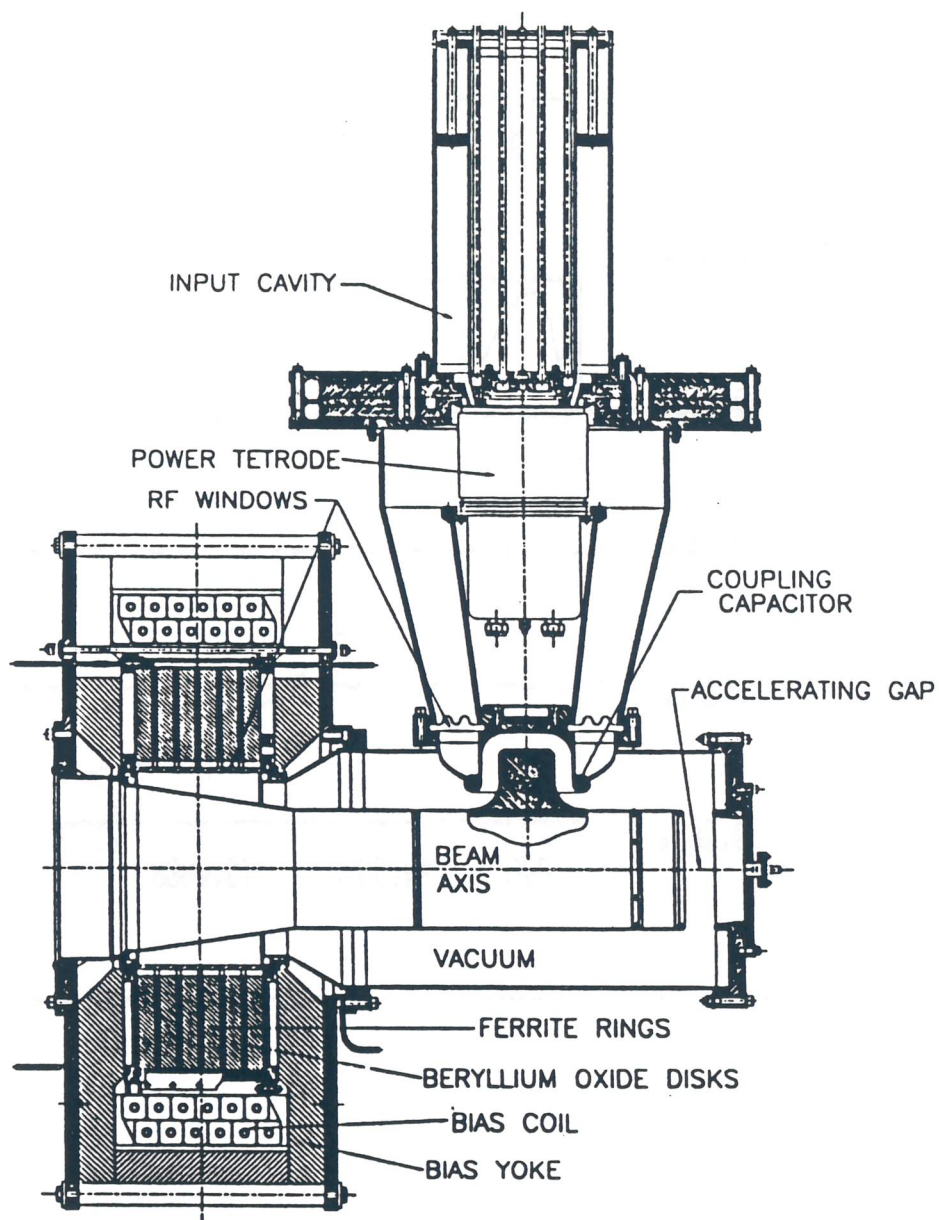Figure 3.7.10: Beam power requirements for the acceleration of Protons at 10 Hz.
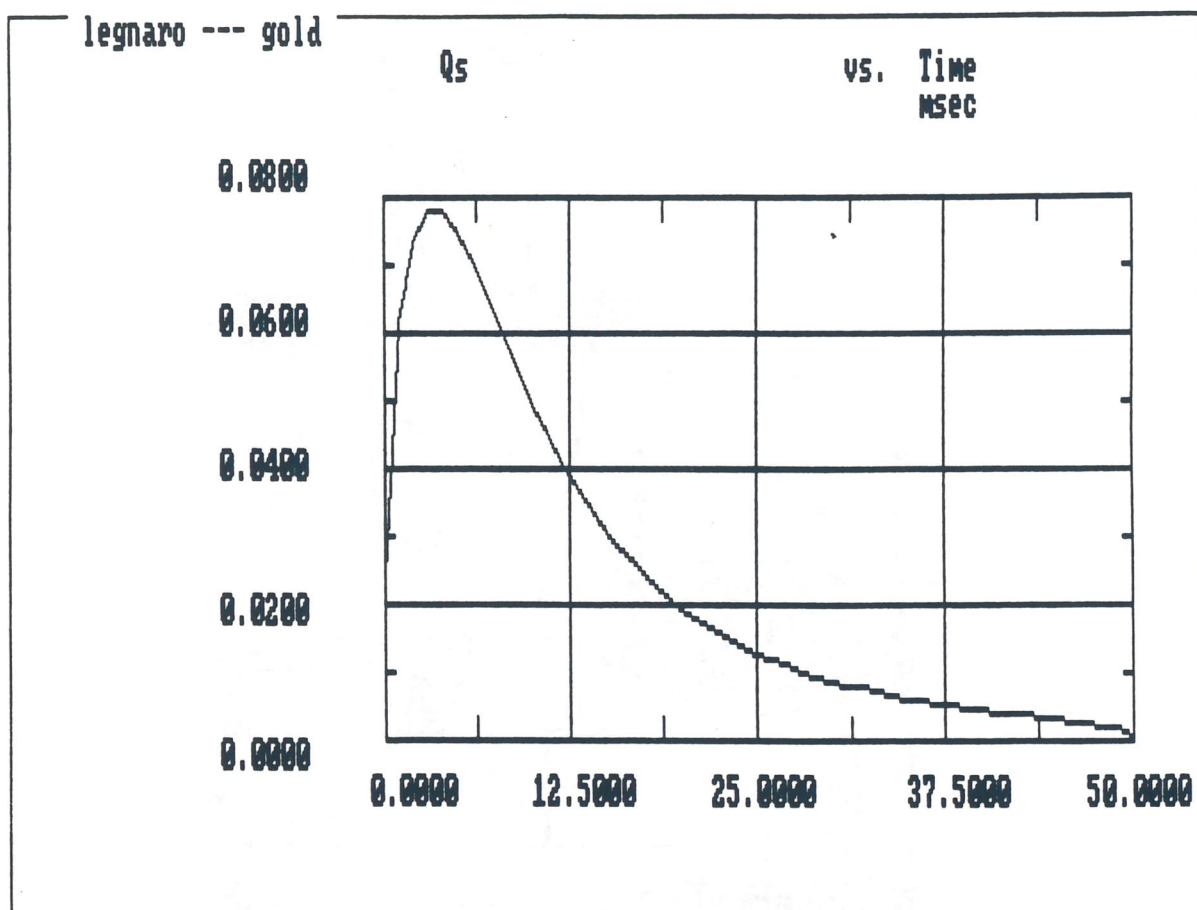
Figure 3.7.11: The LANL/TRIUMF rf cavity.

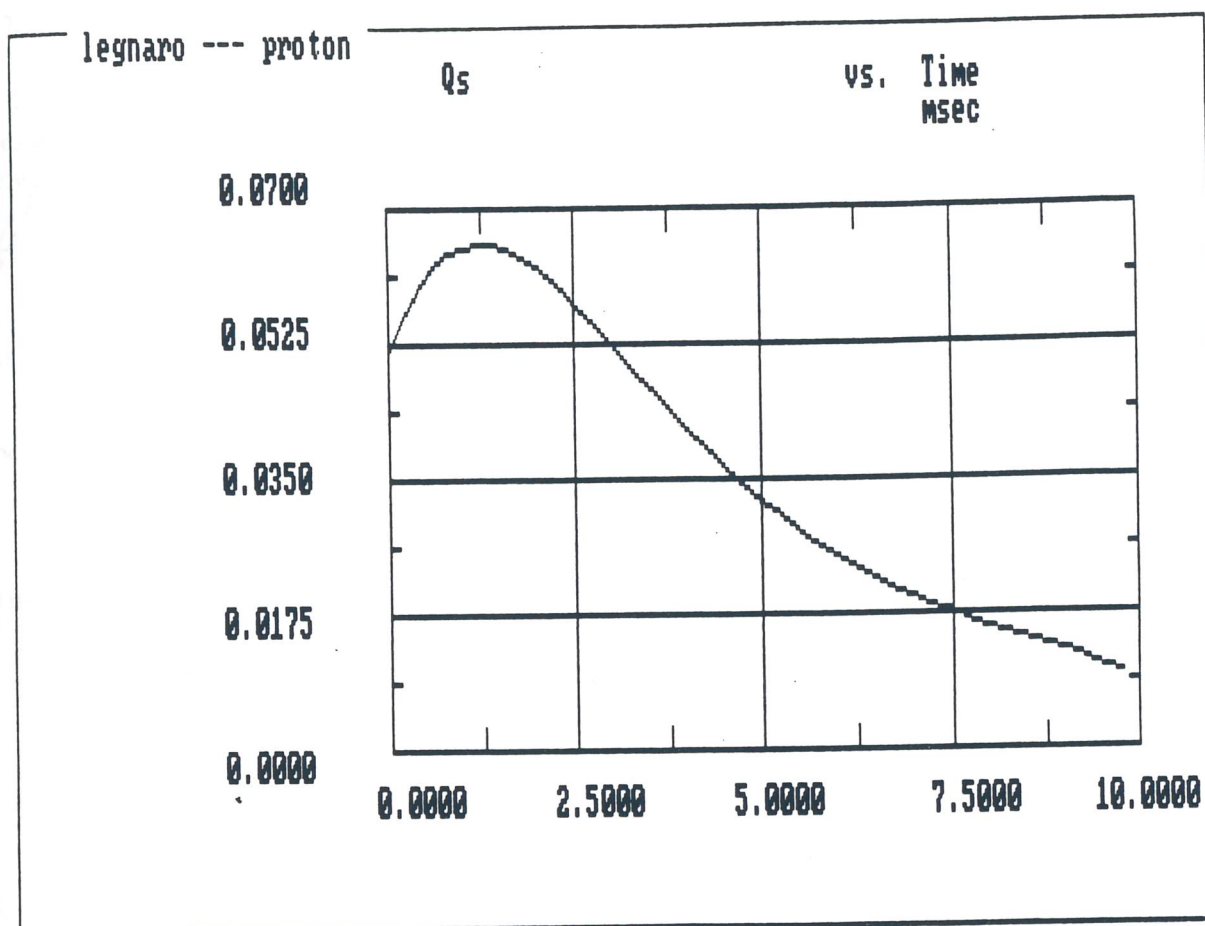Figure 3.7.12: Q_s in the acceleration Cycle for Au ions.

legnaro --- proton

Qs   vs. Time
                                           msec

0.0700

0.0525

0.0350

0.0175

0.0000

0.0000   2.5000   5.0000   7.5000   10.0000

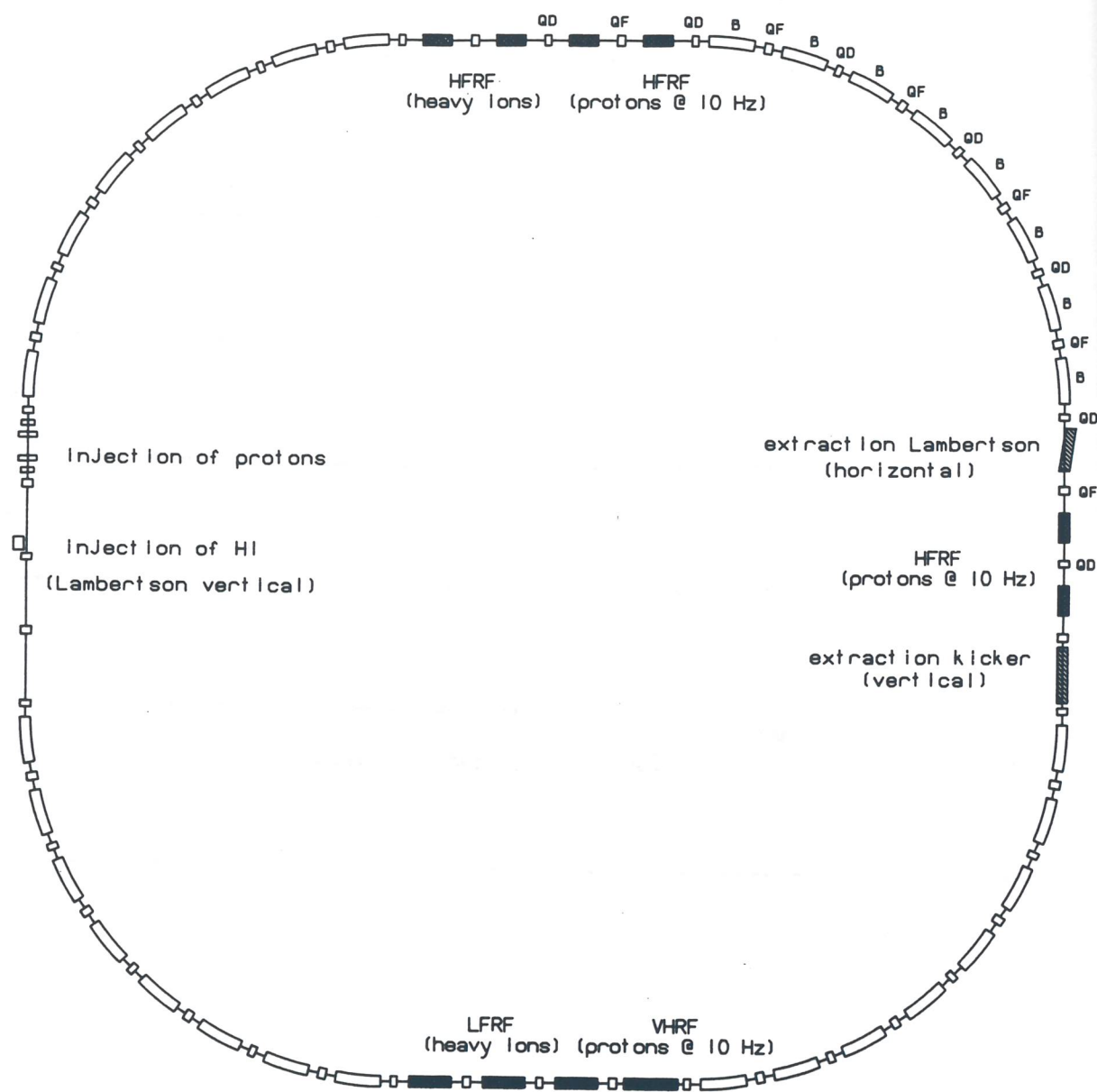Figure 3.7.13: Q_s in the acceleration Cycle for Protons at 50 Hz.

Figure 3.7.14: Arrangement of the rf cavities in the Booster.

3.8 The Vacuum System

The time spent by the beam in the accelerator is at most 50 msec, corresponding to the 10 Hz repetition rate; thus vacuum requirements are not expected to be very stringent. The two modes of operation with heavy ions and with protons present different requirements.

3.8.1 Heavy Ions

The most important effects during the acceleration of heavy ions are the loss, and the capture, of electrons by scattering on residual gas. These effects have a pronounced dependence on ion velocity, as shown by the cross-sections [20]:

$$\sigma_{loss} = 4\pi a_o^2 (\frac{\alpha}{\beta})^2 \frac{1}{B_n} Z_g (1 + Z_g) f_n \ln[\frac{(2\beta\gamma/\alpha)^2}{0.048 B_n}] \qquad (3.8.1)$$

for electron loss, and

$$\sigma_{capture} = \frac{X_b[(\gamma - 1) + B_n/m_e c^2]^2 \sigma_o}{(\gamma + 2B_n/m_e c^2)^2 - 1} \qquad (3.8.2)$$

for electron capture. Here α is the fine structure constant, a_o the Bohr radius of the Hydrogen atom, Z_g is the atomic number of the gas atomic species, B_n the binding energy of an n-shell electron in units of Rydbergs (1 Ry $\sim$ 13.6 eV), f_n is a constant times the oscillator strength for transitions from the n-shell to the continuum, and β and γ are the relativistic kinematic factors. In Equation (3.8.2) $m_e c^2$ is the rest energy of the electron, σ_o the photoionization cross section, and X_b the fraction of the shell of the projectile atom (in the beam) which is unoccupied. The depletion rate is given by

$$\lambda(t) = \beta(t)c \sum_i n_i \sigma_i \qquad (3.8.3)$$

where n_i are the densities of the atomic species in the vacuum gas, and σ_i is the sum of the two cross-sections given by Equations (3.8.1 and 3.8.2).

The worst case is represented by uranium ions, which thus set the vacuum requirement. In order to estimate the overall beam loss, one integrates Equation (3.8.3) over the whole accelerating cycle. Assuming a gas composition of 50% CO and 50% H_2, a nitrogen equivalent vacuum pressure of 10^{-8} mm Hg is required to keep the overall beam losses to less than 3%.

3.8.2 Protons

There are three effects of proton scattering on residual gas which may cause either particle losses or growth of the beam dimensions: nuclear scattering, Coulomb scattering, and ionization of the residual gas. The importance of the first two effects is minor; to keep the beam intensity loss to within 1% and the beam emittance increase to less than 15%,

a vacuum of 10^{-6} torr is required. The phenomenon of ionization is more important. By scattering with the atoms and molecules of the residual gas, positive ions and electrons are formed. The former are immediately removed by the beam by repulsive action; the latter can be trapped in the region occupied by the beam. When enough electrons have been accumulated, a coherent instability can be triggered whereby the centres of mass of the electrons and the beam protons oscillate against each other. At the same time, there is a partial neutralization of the charge of the proton beam which causes a betatron tune-shift and a tune-spread. If the beam intensity is large enough, electrons are not trapped, but kicked away from the beam. Some trapping is possible during the early stages of multi-turn injection when the beam intensity is low, nevertheless a vacuum of 10^{-7} torr has been estimated to be adequate to cope with the ionization effects without any other remedy. Thus proton acceleration demands less of the vacuum system than heavy ions.

The 3.8.3 The Vacuum Chamber

A vacuum of 10^{-8} mm Hg can be achieved and maintained in various ways. First of all, it is possible to do without a vacuum chamber in the dipole magnets, as is done in the Fermilab Booster, for example. vacuum chambers would be installed only between magnets and in the quadrupoles. This solution is the most economical, and eliminates the problems of heating and field distortion due to eddy currents. Nevertheless, the beam would be directly exposed to the magnet laminations, which can cause a beam instability. Further, conditioning and vacuum operation in the absence of a vacuum chamber is more difficult, though successfully demonstrated at Fermilab.

A second solution is a ceramic vacuum chamber. Not only is this more expensive, the required thickness of at least 5 mm reduces the available physical aperture unless the magnet gap is also increased correspondingly. Although the ceramic vacuum chamber eliminates eddy current problems, and makes vacuum operation easier, it does not shield the beam from the magnet laminations. This can be done with metal strips placed parallel to each other around the vacuum chamber, or with some sort of metallic mesh.

A solid metallic vacuum chamber made of either aluminium or stainless steel with a thickness of 1-2 mm provides very effective electro-magnetic shielding of the beam from the magnet laminations. It does however present problems associated with eddy currents. Field distortions, mostly sextupole and decapole components, can be compensated by pole-face windings properly located between the vacuum chamber and the magnet poles of the magnet, as it is done in the AGS Booster at BNL. The other problem is the power deposited as heat in the vacuum chamber. About 5.4 kW is dissipated in a full 3.5 m length of 1 mm thick stainless steel vacuum chamber with a width of 15 cm and a height of 10 cm. To absorb the heat dissipation water cooling of the vacuum chamber may be required. The metallic vacuum chamber solution is the most appealing, since it provides good vacuum operation conditions and subtracts only marginally from the physical aperture.

Another possibility is to use a very thin metallic vacuum chamber of 0.1 mm thickness which is transparent to the dipole field and does not trap eddy currents. This vacuum chamber is nevertheless very fragile and requires either to be corrugated or strengthened with supporting ribs, which would make the construction difficult and expensive. It might also be difficult to replace in the event of a breakage.

The 3.8.4 The Vacuum Pumps and Valve System

A vacuum of 10^{-8} mm Hg can be obtained with conventional pumping systems. Baking and conditioning of the vacuum chamber may not be required. The rectangular magnet aperture of 10×15 cm^2 has a good conductance over the 3.5 m length. Dipole magnets are connected by a cylindrical pipe of 7 cm radius which extends through the quadrupoles. The vacuum chamber in the 22 metre straight sections is also cylindrical with the same radius of 7 cm.

Vacuum ports are located about 5 metres apart next to each of the 48 quadrupoles, with an opening of about 10 cm to which conventional sublimation or ion pumps are attached. Vacuum pressure gauges can be located in the wall facing the vacuum port, in principle at every location, though probably two readings per arc and one per straight section will be sufficient. One or at most two gas analyzers are needed to determine the residual gas chemical composition.

Vacuum valves are located to provide easy access and operation, and to leave sections of beam pipe under vacuum when specific sections are open to atmospheric pressure for maintenance or repair. Considering the size of the ring and its geometry, it is sufficient to provide high quality remotely controlled vacuum valves at each end of the four long straight sections, for a total of eight vacuum valves.

3.9 Diagnostics and Instrumentation

The basic unit of the Booster ring is the half-cell, which includes a dipole magnet with a half-quadrupole at each end. There is a drift 0.78 m long between dipoles and quadrupoles as shown in Figure 3.9.1. The vacuum chamber is rectangular in the dipole magnets, and circular in the quadrupoles and drifts. Bellows about 10 cm long are located next to the dipole ends. On one side of the quadrupole there is room for a beam position monitor (BPM) and a vacuum port; and on the other side there is a steering dipole next to which a sextupole magnet can be located if required. All these elements are about 20 cm long. The BPMs and steering magnets next to QF quadrupoles work in the horizontal plane while those next to QDs operate in the vertical. This layout is also maintained in the long straight sections, where sextupole magnets will not be needed.

The most fundamental function of the beam diagnostics is to detect beam lateral displacement. This is done with the BPMs, which are essentially pairs of strip lines. The sum of the induced voltages on each plate gives a signal proportional to the beam intensity, and the difference a signal proportional to the beam displacement. The sensitivity of the strip lines has to be adequate to detect each bunch individually; this corresponds to at least 10^{11} protons at one extreme, and 10^8 gold ions with charge state 51 at the other, with an order of magnitude difference in the total bunch charge. Sensitivity requirements correspond to a fraction of a millimetre in beam displacement.

The steering magnets are required to correct detectable closed orbit distortions. For this purpose they are individually powered to a maximum current of 100 A, which yields a maximum field of 500 Gauss.

Other useful devices for beam instrumentation are: one longitudinal wide-band detector (wall current BPM) for measurements of individual bunch length, and a few monitors of the beam transverse dimensions, e.g. multi-wire ionized gas chambers or flying wires.
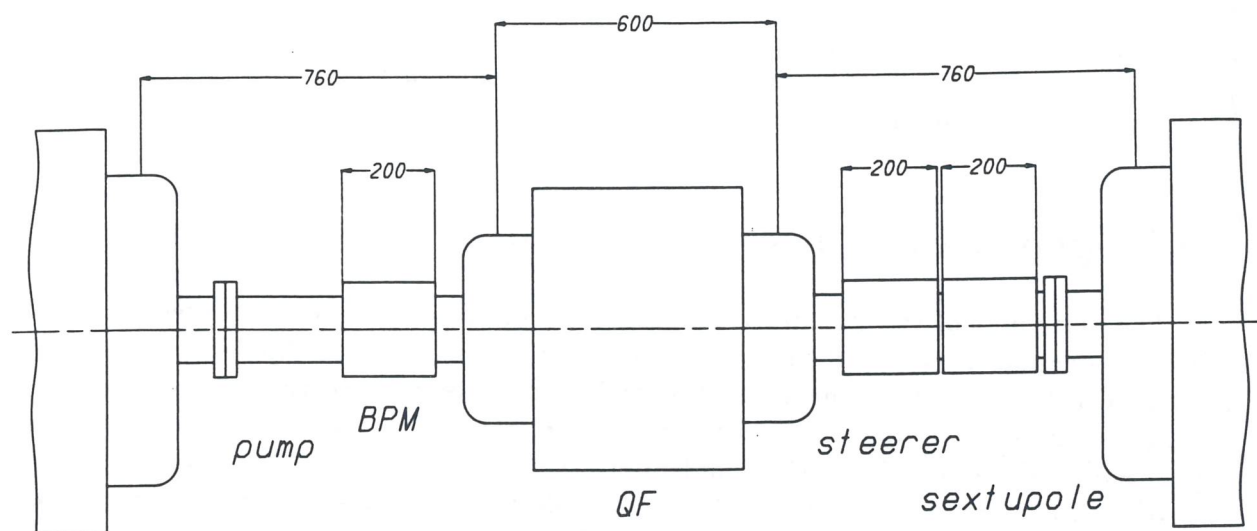
Figure 3.9.1: Hardware Arrangement in the Booster.

References

[1a] K. Reich, K. Schindl, H. Schönauer. "An Approach to the design of space-charge limited high-intensity synchrotrons", 12th Int. Conf. on High energy Accelerators, Fermilab, 1983.

[1b] L. J. Laslett, "On intensity limitations imposed by transverse space-charge effects in circular particle accelerators", Proc. of 1963 summer study on Storage Rings, BNL-Report 7534 (1963) 324-367.

[1c] B. Zotter, "Proc. of the CERN Accelerator School", Gif-sur-Yvette, September 1984, CERN 85-19.

[2] J. Wei and S. Y. Lee, Booster Technical Note No. 102/ Dec. 8, 1987/ BNL.

[3a] G. I. Budker and G. I. Dimov, "On the Charge Exchange Injection of Protons into Ring Accelerators", Intern. Conf. 1963, CONF-114, USAEC TID-4500, 1372-1377.

[3b] C. Hojvat et al., "The multiturn charge exchange injection system for the Fermilab Booster Accelerator", IEEE Trans. on Nucl. Sc. NS-26 No. 3, June 1979, 3149-3151.

[3c] V. C. Kempson, C. W. Planner and V. T. Pugh, IEEE Trans. Nucl. Sci., NS-28 No. 3, (1981) pp3085-3087.

[4] LAMPF II Proposal, Feb. 1986, Page 5-28 LANL, Los Alamos NM 87545, USA

[5] TRIUMF KAON Proposal, September 1985, UBC Congr., Vancouver, B. C. V6T 2A3, Canada

[6] R.L.York et al., Particle Accelerator Conf., San Francisco 1991.

[7] M.Froissart, R.Stora, Nucl. Instr. and Meth. 7 (1960) 297.

[8] E.D.Courant, R.D.Ruth, BNL Report 51270.

[9] "Proposal for a European Hadron Facility", edited by J.F. Crawford, EHF 87-18 (1987).

[10] M.R. Harold, "Magnet Systems", Proc. of the CERN Accelerator School", Gif-sur-Yvette, September 1984, CERN 85-19.

[11] G. Hemmie, Design and measurements of AC magnets at DESY II Proc. of the KAON PDS Magnet Design Workshop TRIUMF, Vancouver October 3-5, 1988.

[12] J.A. Fox, " Resonant magnet network and power supply for the 4 GeV electron synchrotron NINA", IEEE Proc. 112, No.6, June 1965.

[13] M.R. Harold, "The design, manufacture and testing of the ISIS fast-cycling magnets", Proc. of the KAON PDS Magnet Design Workshop TRIUMF, Vancouver October 3-5, 1988.

[14] A.J. Otter et al.," Magnet Design Studies for the TRIUMF KAON Factory Proposal", Proc. of the 11th Intern. Conf. on Magnet Technology (MT-11) Tsukuba, Japan, 1989.

[15] H. Allen, et al., "Design and operation of the Princeton-Pennsylvania Proton Synchrotron", Proc. of the Intern. Conf. on High Energy Accelerators, Dubna 1963.

[16] J. Kirchgessner, et al., "The rf system for the Princeton-Pennsylvania Accelerator", Proc. of the Intern. Conf. on High Energy Accelerators, Dubna 1963.

[17] J. Griffin, private communication, Lecce 1989.

[18] R. Carlini, et al., "rf cavities with transversely biased ferrite tuning", IEEE Trans. Nucl. Sci., NS-32 No. 5, October 1985, 2951-53.

[19] C. Friederichs, et al., "Test results of the Los Alamos ferrite tuned cavity", Proc. of the 1987 Particle Accelerator Conference, Washington 1987, 1896-8.

[20] H. Gould et al., Phys. Rev. Lett. 52 No. 3 (1984) 180-183.

4

Transfer Line

An important part of the complex turns out to be the Transfer Line between the two rings, which has been designed to transfer heavy ions, to be capable of producing, collecting and selecting exotic beams, and to transport protons.

The production of exotic beams requires a complex system of targeting and of beam species selection of elaborate design. In fact, the Transfer Line is a replica of half of the Booster, with suitable insertions for obtaining specified beam sizes and dispersions, for the ion fragmentation target, and for the degrader system for the mass separation of different species. The Transfer Line can also be operated at the magnetic rigidity of 22.25 Tm.

The physical location of the Line in the complex is dictated by the position of the experimental hall, which will be south of the rings, and by the position of the rings with respect to the injectors, namely ALPI and the Proton Linac. Extraction from the Booster, which is in the lower position, is on the west straight insertion of the ring, and injection into the Decelerator ring is on the opposite straight section, about 2.5 metres above the Booster. The Line lies between the two rings, and combinations of kickers and bending magnets bring the beam from the Booster to the Line, and from the Line to the Decelerator. The horizontal distance between the Transfer Line and the rings is large enough ($\sim$ 40 m) to allow space for radiation shielding.

4.1 Secondary Beam Production

Heavy-ion beams of energy $\sim$ 1 GeV/u have attractive features (compared to lower energies) for producing exotic nuclei and studying them after separation in an energy loss achromat like the one described below. These features are:

- production targets as thick as 1-2 g/cm^2,
- full stripping, even for very heavy products, with unambiguous isotope separation and assignment,
- strong forward peaking for projectile fragments from peripheral collisions.

The last feature is of particular importance, since it means that ion fragments are produced at essentially the velocity, and therefore the specific energy, of the primary particles.

For beam energies of the order of 1 GeV/u, the total cross-section for the fragmentation process depends essentially on the interaction radii according to

$$\sigma_I = \pi[R_p^2 + R_t^2] \tag{4.1.1}$$

where the subscripts p and t stand for projectile and target. The interaction radius of a nucleus with mass number A is $R \sim A^{1/3} \times 10^{-13}$ cm independent of the energy [1]. Typical values of σ_I are of the order of few barns (10^{-24} cm^2).

A great variety of fragments with different mass and charge values are produced in the process. The cross-section for a single isotope of given A and the most probable Z is of the order of ten to one hundred millibarns. Detailed calculations of the cross-section, performed within the framework of the abrasion-ablation model and GDR excitation followed by one evaporation stage, describe some of the principal features of the mass and charge distribution of the fragments, but slightly overestimate the experimental data [2,3]. The cross-section is simply given by

$$\sigma(A, Z) = \pi R^2 \frac{\binom{Z_1}{z}\binom{N_1}{n}}{\binom{A_1}{a}} \tag{4.1.2}$$

where A_1, Z_1 and N_1 are respectively the total number of nucleons, protons and neutrons in the target nucleus before interaction and a, z and n are respectively the number of nucleons, protons and neutrons removed in the interaction, so that $A = A_1 - a$ and $Z = Z_1 - z$ (J. O. Rasmussen et al., unpublished, see ref. [2]). Typically, a fragment nucleus has the same overall dimensions as the projectile, i.e. $z \ll Z_1$ and $a \ll A_1$. Thus, the secondary beam is likely to have a specific energy not very different from that of the primary beam.

The longitudinal momentum dispersion of the fragments in the projectile rest frame is well described by a Gaussian distribution of width given by

$$\Delta p_\parallel = \sigma_o \sqrt{\frac{A_f(A_p - A_f)}{A_p - 1}} \tag{4.1.3}$$

where A_p and A_f are the numbers of nucleons in the projectile and fragment nucleus [4]. The constant σ_o is related to the Fermi momentum p_F of the nucleons in the projectile by $\sigma_o = p_F/\sqrt{5}$. The experimental value of σ_o is 94 ± 5 MeV/c. It has also been shown [5] that, to within 10% error, the transverse momentum dispersion is given by:

$$\Delta p_\perp = \Delta p_\parallel \, . \tag{4.1.4}$$

4.2 Targetry

The Transfer Line and the fragment collection system are designed for the capture and transfer of a full momentum spread of 0.7%, which corresponds to the capture of almost all the ions of the required species. Similarly the production angle is taken to be 7.5 mrad, corresponding to a transverse momentum spread which matches the momentum width. The expected yield can then be as large as 10^{-4}, and typically 10^6 fragments of assigned mass number A and atomic number Z can be collected per Booster pulse.

The production target is placed at a waist in the Transfer Line where $\beta \sim 1$ m. The full emittance of the primary beam being about $6\,\pi$ mm-mrad, the beam size at the target is 2.5 mm. The production target is no more than few millimeters long, and therefore the emittance of the secondary beam is given by the product of the size of the primary beam

and the maximum angle at which secondaries are emitted; this implies a full value of 19 π mm-mrad. Based on these figures, the betatron acceptance of the Transfer Line and of the Decelerator ring is set conservatively to 40 π mm-mrad, and the momentum aperture to 2%.

The production target is located in a dispersion-free insertion to avoid correlations between the energy and position of an event. Looking backward at the target, the Transfer Line is to be matched to the beam phase-space ellipses which are upright with dimension 2.5 mm $\times$ 7.5 mrad, in the horizontal and vertical planes. The equivalent value of β at that location, which is to be regarded as the object point for the remainder of the transfer line, is 0.3 m. Thus the Transfer Line must be able to tune the section preceding the production target and the section following independently, with different matching values of β.

4.3 Description of the Line

Extraction from the Booster ring is by a vertical kicker followed by a horizontal Lambertson magnet located 90^0 downstream in vertical phase. The beam comes out of the ring with angles of 9.8 mrad vertically and 157 mrad horizontally from the straight closed orbit.

The Transfer Line, shown in Figure 4.3.1, starts with two doublets separated by a horizontal bending magnet similar to the lattice dipoles, to direct the beam orbit parallel to the ring straight section. The two doublets provide dispersion suppression and a waist in the horizontal and vertical planes at the fragmentation target, which is placed at the centre of a 3 metre long drift. The β value in the waist is 1 metre in both planes.

An insertion about 20 metre long overall is required to match the lattice parameters of the two standard FODO cells that follow. These provide the initial bending of the beam back towards the rings, and a phase advance of 180° in the horizontal plane between the fragmentation target and the selection region.

Momentum selection of the fragments is done with pairs of collimators and slits in an 8 metre long drift, which follows the two bending cells and has a large dispersion ($\sim$ 5 m). There is a double waist at the centre of the drift with $\beta \sim 1$ m, where the degrader is located. This has a variable thickness in the horizontal plane [6], and it is located in a large-dispersion region. Thus particles with different momenta will cross different thicknesses of the degrader material and lose different amounts of energy depending on their velocity. For the given momentum dispersion, the degrader is shaped to match the velocity dispersion for only one mass number, in such a way that the subsequent arc, made of two FODO cells, will exactly match the achromaticity condition (compensation of the previously produced velocity dispersion) only for the required species. At the centre of the 20 metre drift, half way along the transfer line, there is a waist with a large β ($\sim$ 10 m) where additional slits are located for the final selection of the required ion fragment.

The second half of the Line has two empty insertions corresponding to the degrader and to the target locations, which can be used for other applications. The latter insertion is long enough to accommodate the dipoles for the vertical displacement of the beam from the elevation of the Booster to the elevation of the Decelerator; vertical dispersion can also be corrected locally by means of properly placed quadrupoles.

The same Transfer Line, without the target and the degrader, can transport the proton beam from the Booster to the Decelerator (which acts in this case as a Holding Ring) with no losses and no emittance dilution.
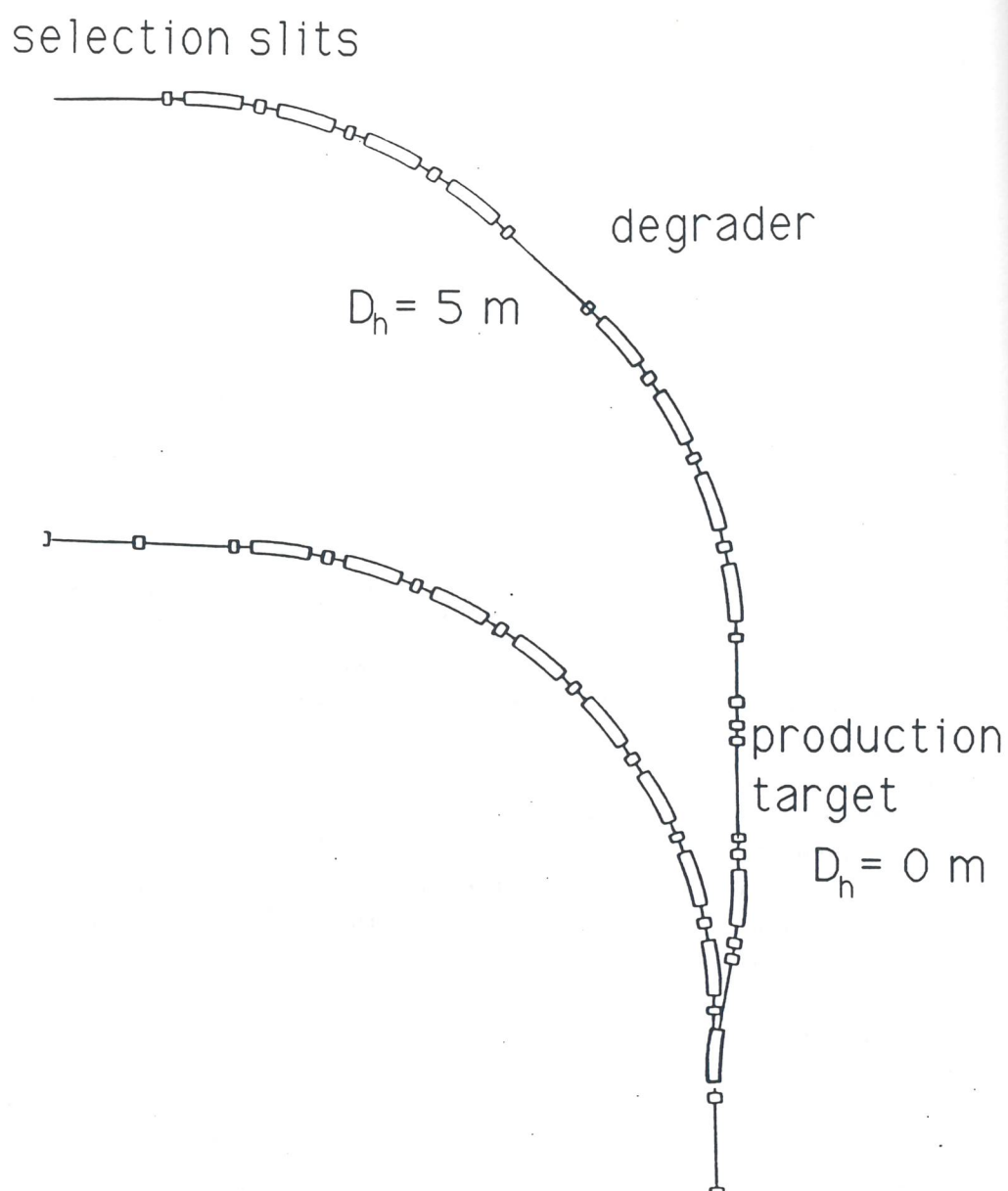
Figure 4.3.1: The Transfer Line for the production and selection of unstable fragments.

References

[1] H. Sato et al., Phys. Rev. C <u>34</u>, (1986) 2171.

[2] D. J. Morrissey et al., Phys. Rev. C <u>18</u> no. 3, (1978) 1267.

[3] L. F. Oliveira et al., Phys. Rev. C <u>19</u> no. 3, (1979) 826.

[4] A. S. Goldhaber, Phys. Lett. <u>53B</u>, (1974) 306.

[5] D. E. Greiner et al., Phys. Rev. Lett. <u>35</u> no. 3, (1975) 152.

[6] J. P. Dufour et al., Nucl. Instr. and Meth. <u>A248</u>, (1986) 267-281.

5
Decelerator Ring

5.1 Lattice and Operation Cycle

The main functions of the Decelerator are the accumulation and storage of many pulses of ion fragments, the cooling of the stored beam, and the deceleration of the beam to energies corresponding to the Coulomb Barrier. Moreover the ring can be used as a Stretcher for both heavy ion and proton beams, or as a Holding Ring for beam pulses to be accelerated in a larger future facility.

5.1.1 The Lattice of the Decelerator

To accommodate all these functions, the lattice of the Decelerator has to provide space for injection and extraction, dispersion-free locations for the rf cavities, and a drift space at least 10 metres in length for electron cooling. Moreover the ring must be able to match the rigidity of the Booster of 22.25 Tm. The space available on the LNL site suggests a solution in which both rings are housed in the same tunnel, one on top of the other. A convenient solution is to have exactly the same circumference and geometry for the two rings.

Like the Booster, the Decelerator has a superperiodicity of four, each superperiod being mirror symmetric and consisting of an arc and a straight section, as shown in Figure 5.1.1. The arc is identical to the Booster arc, with a basic FODO cell as shown in Figure 3.1.2 and the parameters listed in Table 3.1.2. The straight section of the Decelerator has the same length as the one in the Booster, about 22 metres; a different quadrupole configuration is used to provide a magnet-free central region 11.5 metre long for electron cooling. The main parameters of the lattice of the Decelerator are listed in Table 5.1.1, and the lattice functions for a superperiod (one fourth of the ring) are shown in Figure 5.1.2; the long straight sections are essentially dispersion-free.

In addition to the QF and QD quadrupole families in the arcs, quadrupoles Q1, Q2 and Q3 are provided at the ends of each long straight section to allow tuning and matching of the lattice. The phase advances in the FODO cells are about 90° and 60° in the horizontal and vertical planes respectively, and the total betatron tunes are set to $\nu_h = 5.8$ and $\nu_v = 3.8$ as in the Booster. The transition energy has the same value as in the Booster. The positions of other components, for injection, extraction, rf acceleration, and electron and stochastic cooling are shown in Figure 5.6.2.

The momentum aperture required for the stacking of several beam pulses is a total of 2% while the requirement on the betatron acceptance is 40 π mm-mrad in both planes.

Taking a linear combination of the two contributions to the beam size, the beam envelope in the ring is plotted in Figure 5.1.3.

Because of the presence of the two triplets at the ends of each long straight section, the natural chromaticity is somewhat larger than in the Booster, but it is still very easy to correct with a sextupole arrangement in two families, SF and SD, identical to the one for the Booster. The chromatic effects of the lattice are expected to be marginal and of no consequence for the stability of the beam motion. The addition of correcting sextupoles is foreseen only for a later phase, after beam performance experiments. Variation of the betatron tunes is plotted versus the off-momentum value in Figure 5.1.4, without and with sextupoles. Figure 5.1.5 shows a similar plot of lattice functions, without sextupoles, in the middle of a straight section. Sextupoles introduce a variation of the betatron tunes of no more than 0.001 over the betatron acceptance of $40 \, \pi$ mm-mrad.

5.1.2 The Operation Cycle

The two-second operation cycle is shown schematically in Figure 1.2.1. Twelve pulses of ion fragments are transferred to the Decelerator, separated by 100 ms. The bunches of each pulse are captured in stationary buckets which are then rotated in longitudinal phase space. The momentum spread of the beam will therefore change from 0.7% at capture to 0.1% after the rotation. The beam bunches are then displaced by a second system of rf cavities to a new momentum trajectory where they are stored. On the stacking orbit, electron and stochastic cooling operate on the beam, and continue for another 0.5 sec after all 12 pulses have been accumulated. Figure 5.1.6 illustrates the use of the momentum aperture and the location and relative dimensions of the beam during the cycle.

The cooling reduces the beam momentum spread and the betatron emittance by an order of magnitude. Finally, the beam stack is captured by one more system of rf cavities which decelerates it down to energies of about 5 MeV/u. The deceleration stage is linear and lasts 0.3 sec; during the subsequent 0.1 sec the guiding field is reset to its initial value. The cycle then repeats. The main beam parameters at injection into the Decelerator are listed in Table 5.1.2 where some stable fully stripped species have been taken as reference.

Table 5.1.1: Parameters of the Decelerator.

Ring Length		266.6667	m
Lattice Periodicity		4	
Maximum Magnetic Rigidity		22.25	Tm
Magnetic Bending Radius		17.6216	m
Total Number of Cells		24	
Number of Cells per Arc		4	
Phase Advance per Cell			
	Horizontal	90°	
	Vertical	60°	
Transition Energy (γ)		4.6	
Betatron Tunes			
	ν_h	5.8	
	ν_v	3.8	
Natural Chromaticity			
	ξ_h	-5.5	
	ξ_v	-5.98	
β_H,	max	16.1	m
β_V,	max	32.0	m
dispersion,	max	4.95	m

Table 5.1.2: Beam Parameters at Injection into the Decelerator.

	S	Cu	I	Au	U	
Mass Number, A	32	63	127	197	238	
Charge State,	16	29	53	79	92	
Kinetic Energy	2.53	2.08	1.37	1.03	0.85	GeV/u
β	0.963	0.951	0.914	0.880	0.852	
Harmonic number	24	30	39	45	49	
Bunch length (rms)	0.5	0.5	0.5	0.5	0.5	ns
Momentum spread	0.7	0.7	0.7	0.7	0.7	%
Intensity	$2.6 \cdot 10^8$	$1.3 \cdot 10^8$	$2.8 \cdot 10^7$	$8.1 \cdot 10^6$	$7.7 \cdot 10^6$	ions/pulse
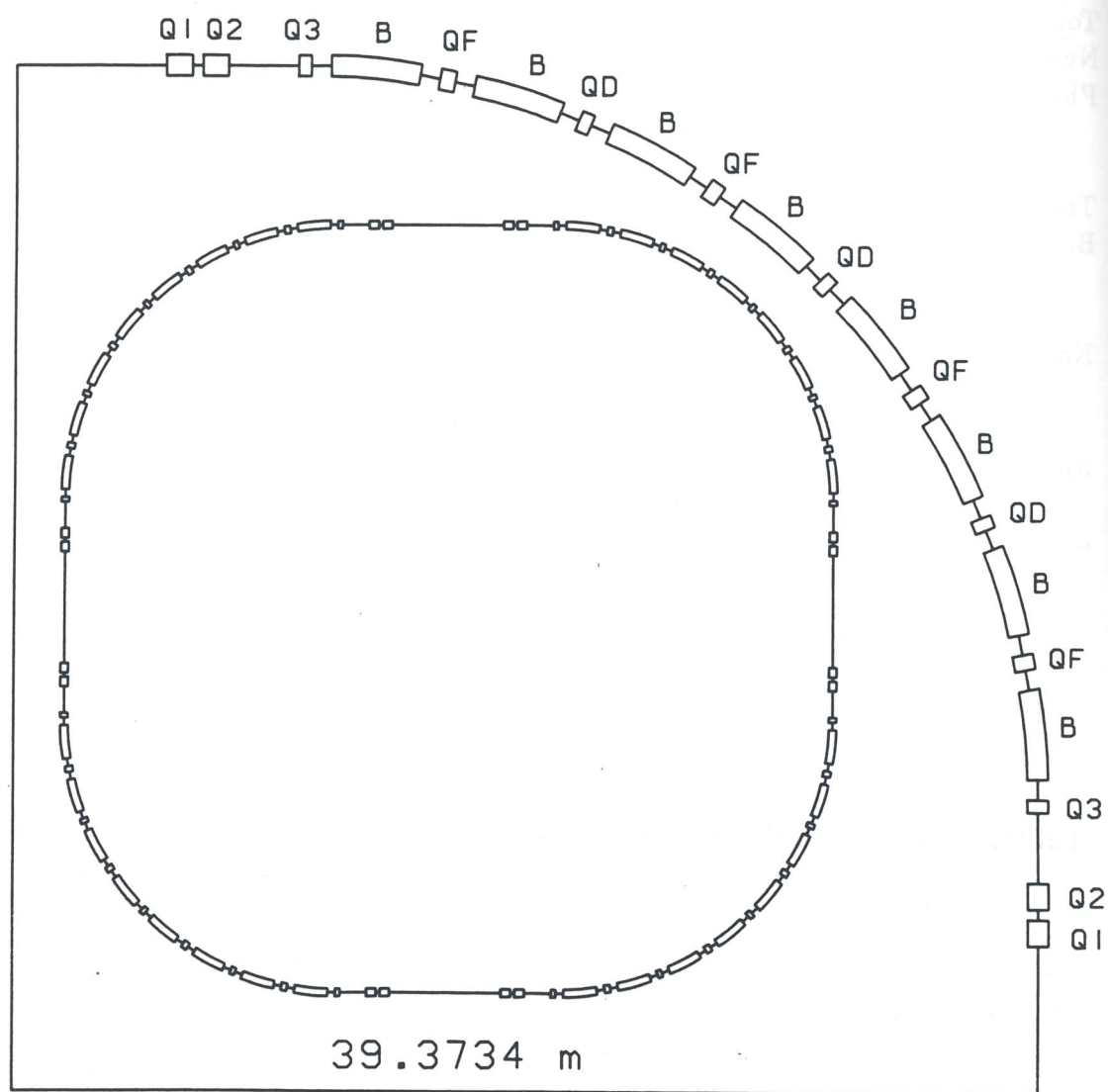
Decelerator : General layout of magnetic lattice

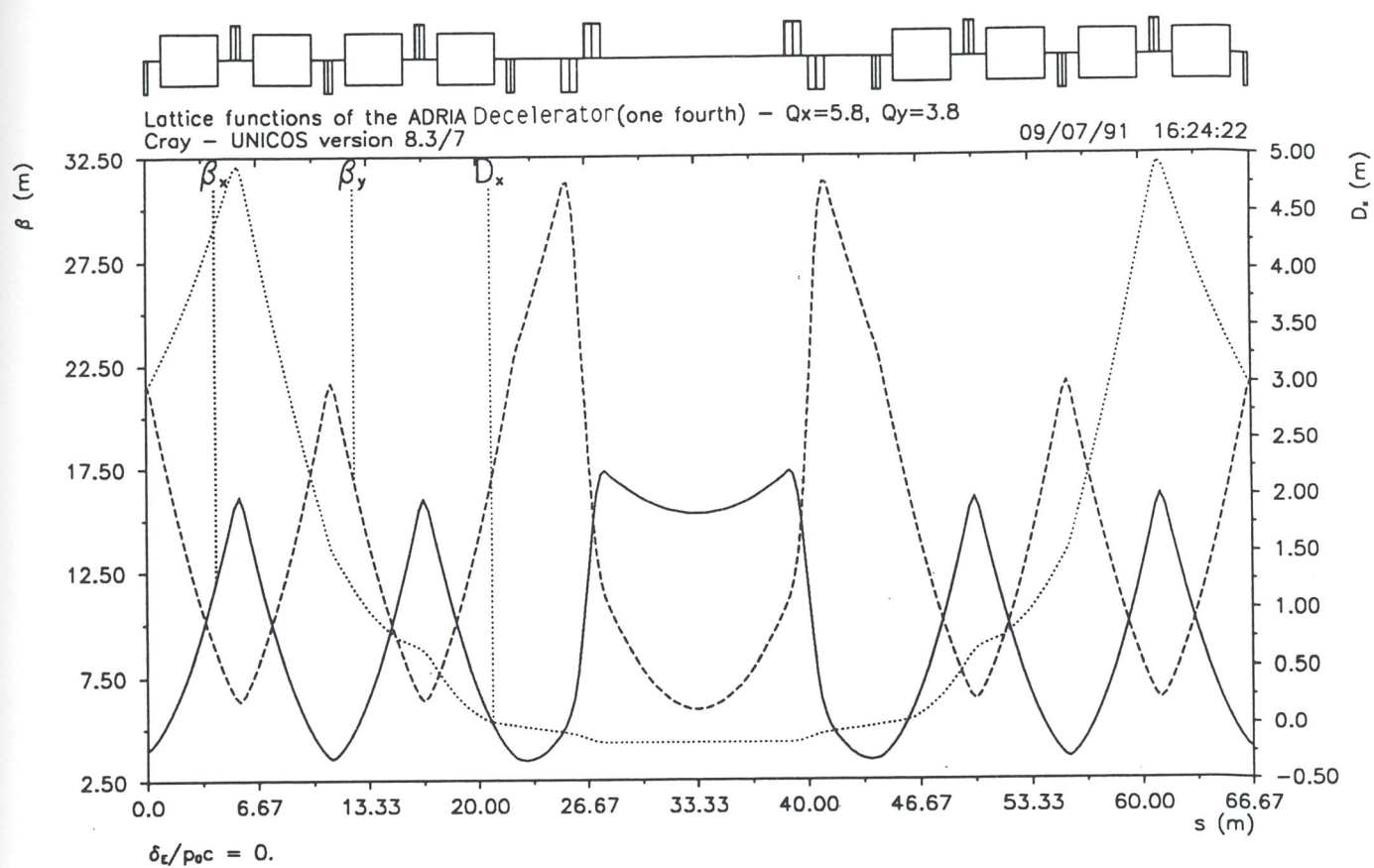Figure 5.1.1: The Layout of the Decelerator.

Figure 5.1.2: Lattice Functions of the Decelerator.

ADRIA Decelerator (one fourth)

11/07/91 10.30 MAD   ======> distance [m]

ADRIA Decelerator (one fourth)

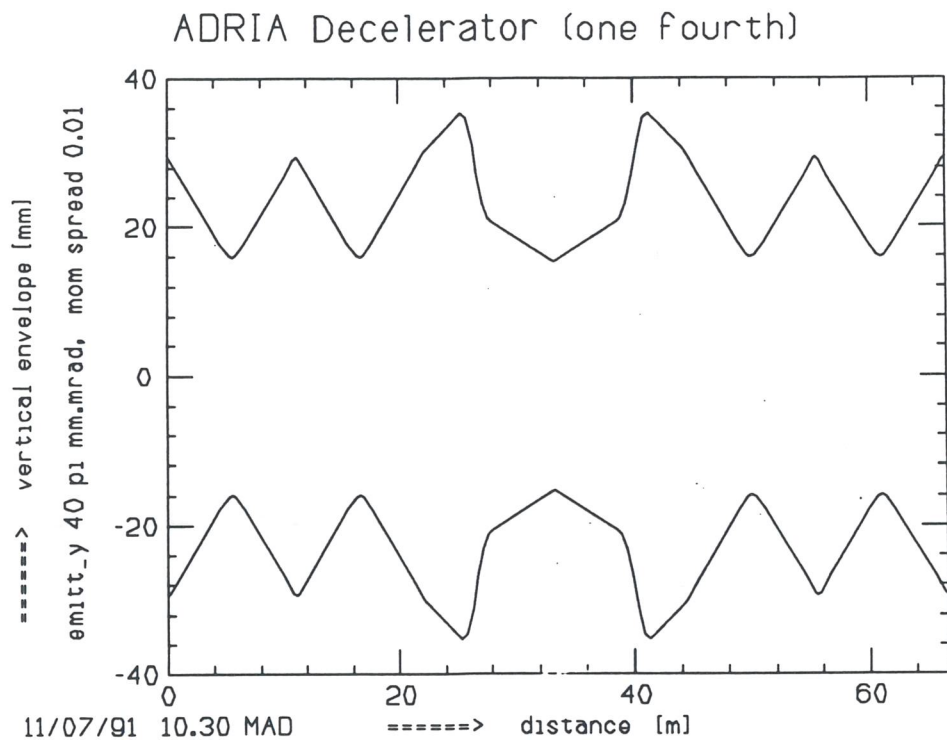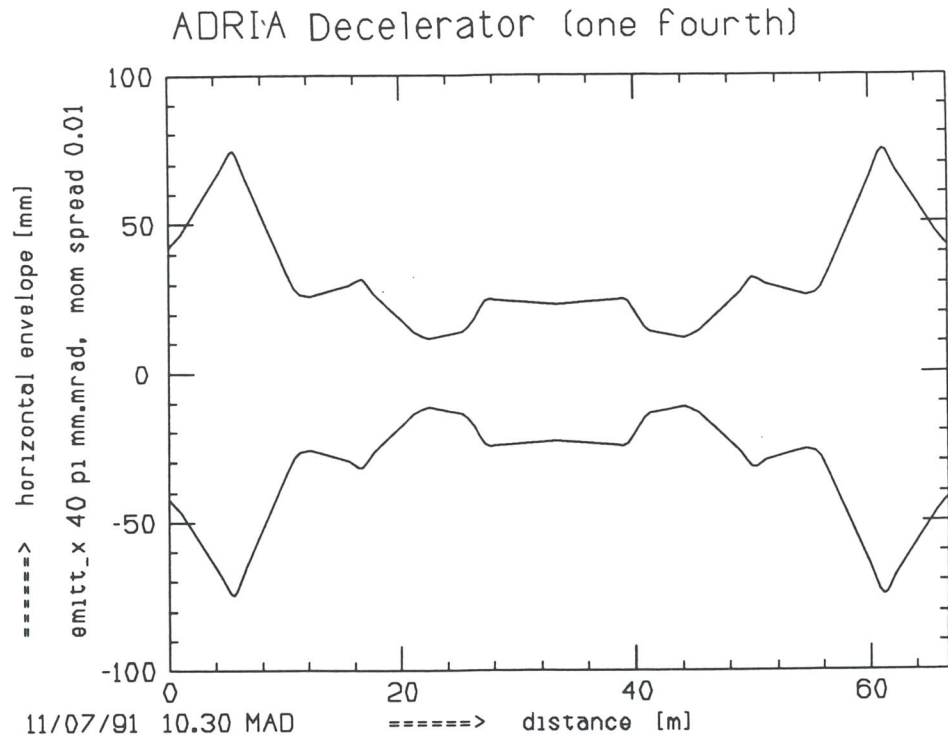11/07/91 10.30 MAD   ======> distance [m]

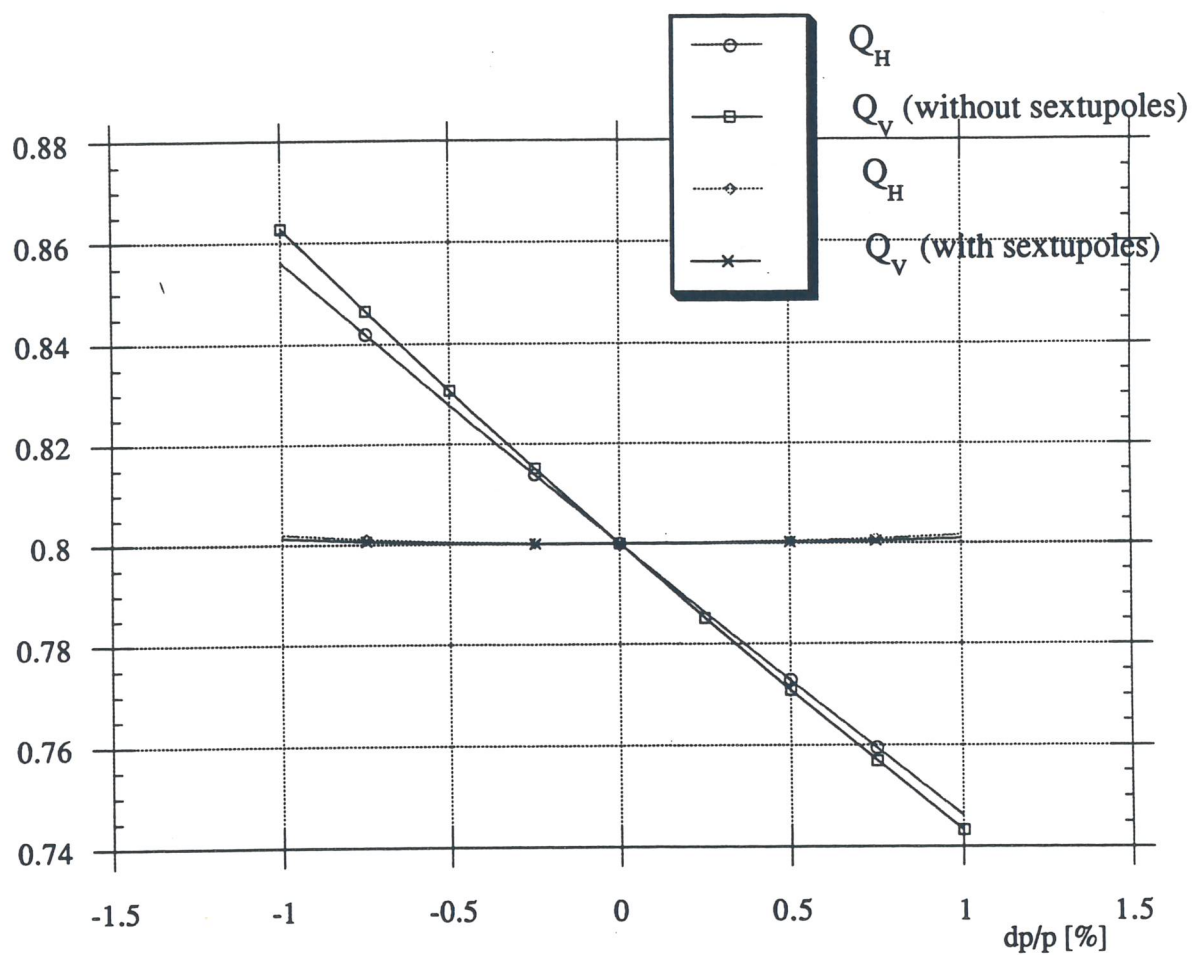Figure 5.1.3: Beam Envelopes in the Decelerator.

Figure 5.1.4: Betatron Tunes vs. momentum deviation for the Decelerator.
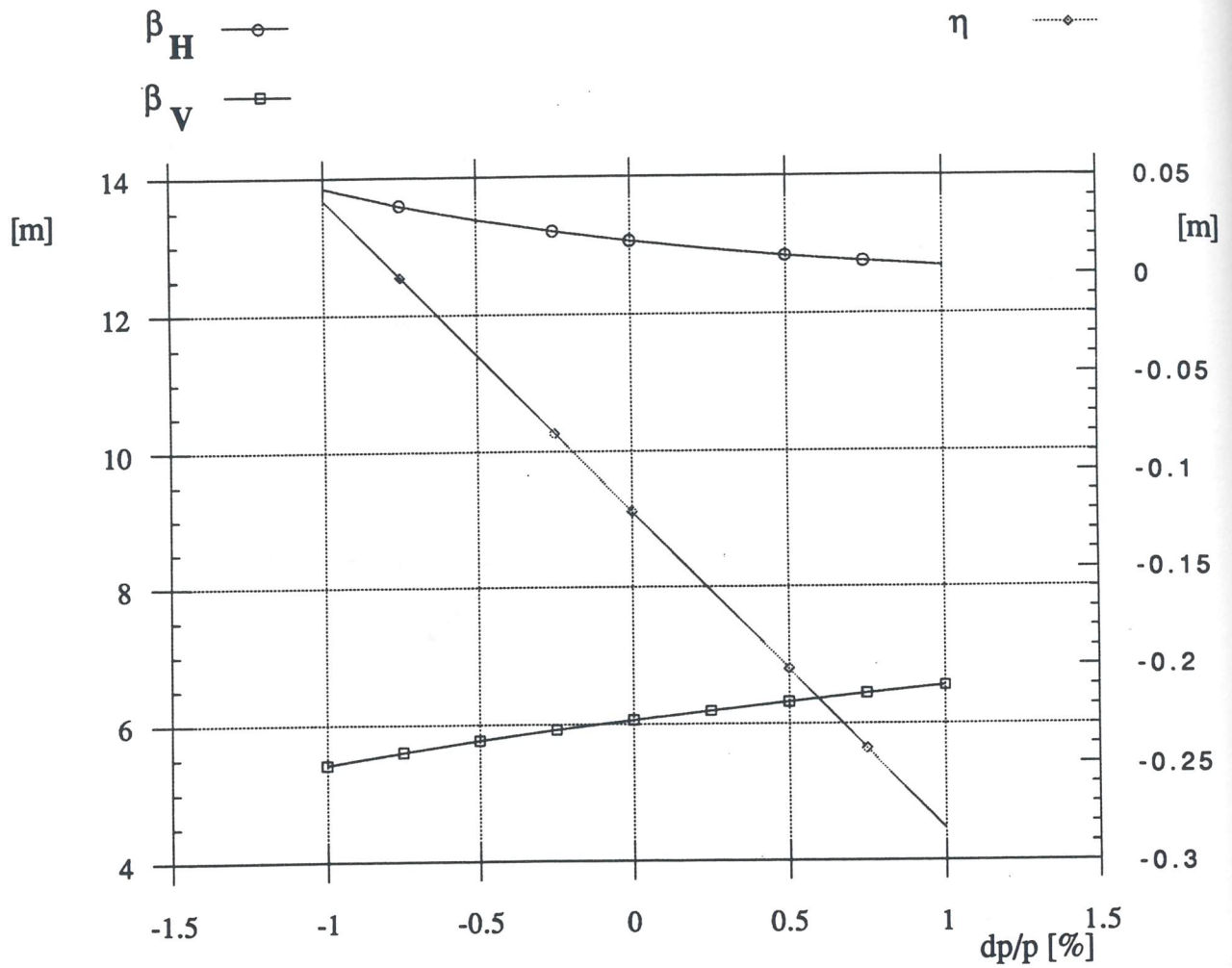
Figure 5.1.5: Variation of the Lattice Functions with momentum in the long straight section (symmetry point) of the Decelerator.
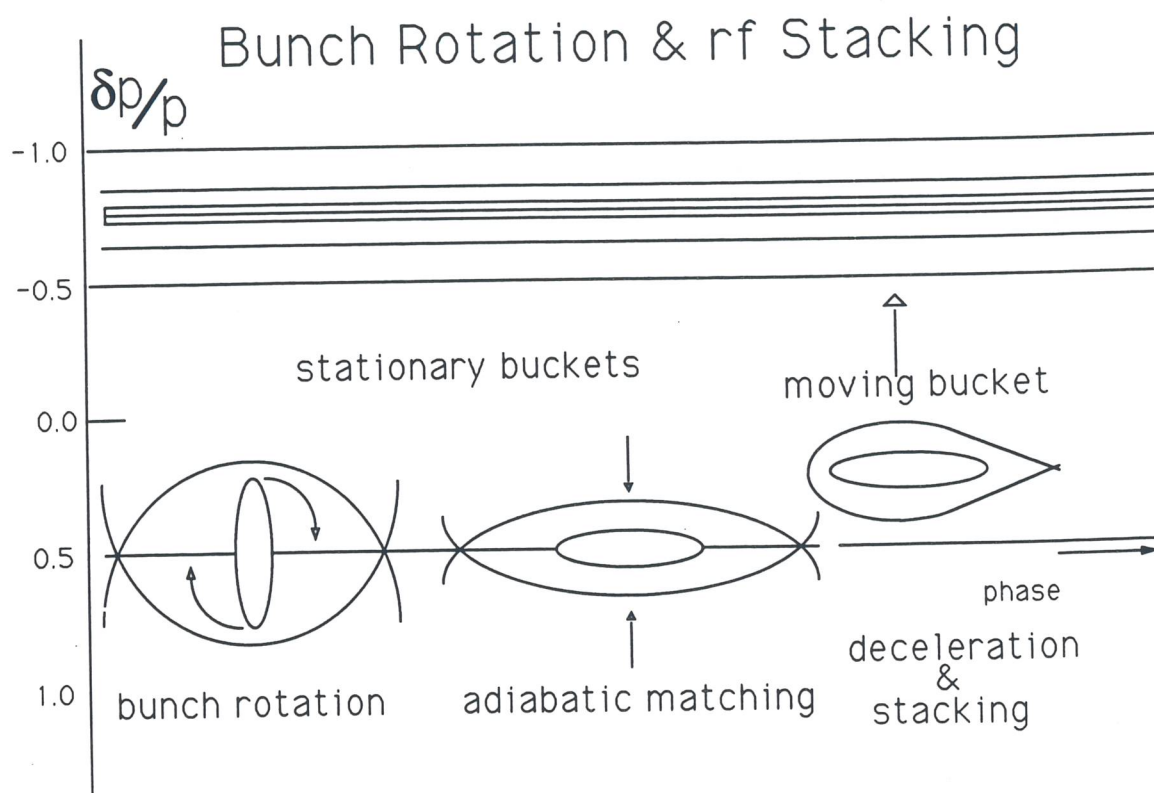
Figure 5.1.6: The Momentum Aperture of the Decelerator.

5.2 Injection

Injection into the Decelerator is the exact inverse of extraction from the Booster; because the rings are the same size, one turn is injected at a time, for both protons and heavy ions. The locations of the injection septum and kicker magnets are shown in Figure 5.2.1. These magnets are identical to those used for extraction from the Booster, and their parameters appear in the same Table 3.3.1. The beam enters the Decelerator with a vertical angle; the septum magnet moves the beam vertically inside the ring and places it on the median plane 60 mm away from the reference orbit. The kicker magnet finally kicks the beam horizontally onto the reference orbit. One can take advantage of the smallness of the transverse beam dimensions at the transfer energies and locate the 10 mm thick septum 40 mm away from the central orbit; this is enough to preserve the required betatron acceptance in the Decelerator.

For the case of heavy ions, with the typical cycle described in section 5.1, beam pulses are transferred to the Decelerator at intervals of 100 ms. After electron cooling, the circulating beam is smaller than the injected pulse. It is then preferable that injection of the new pulse does not perturb its dimensions and that, eventually, one allows the kicker to dilute the emittance of the stack. This is accomplished by first moving the circulating beam by 30 mm on a horizontally bumped orbit which is prepared slowly just before injection of the new pulse, bringing the stack closer to the septum.. As soon the new pulse is injected, the kicker is turned off in 150 ns, and the local bump is also turned off over a longer time corresponding to several revolutions. With this method the stack will initiate coherent oscillations which will dilute the beam emittance to the initial value, while the emittance of the injected beam is unchanged. The amplitude of the oscillations will be small enough to avoid hitting the septum on subsequent turns. Electron cooling will then reduce the emittance of the total beam down to the value acceptable for the injection of the subsequent pulse.
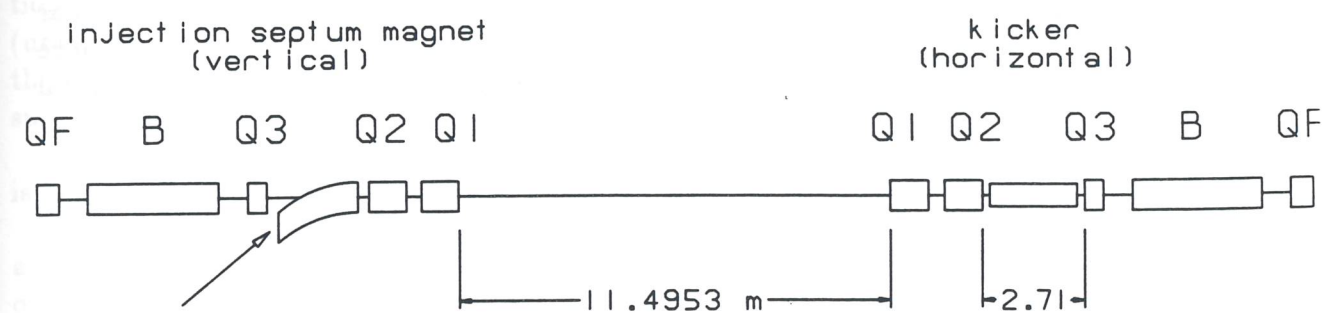
Figure 5.2.1: Layout of the Injection System in the Decelerator.

5.3 Extraction

Depending on the experimental program, the beam may be extracted from the Decelerator in a single turn, or over many turns to provide 100% duty cycle.

In the case of heavy ions, the Decelerator can be operated as a Stretcher at the Booster extraction energy, or, after deceleration of the accumulated fragments, at energies as low as 5 MeV/u. The duration of the spill may vary from 100 ms to a few seconds depending on the energy and the mode of operation. Fast extraction should also be possible for the production of secondary beams or for the transfer of the beam to a second accelerating stage.

The most immediate application for proton beams is slow-spill extraction at any energy up to 5.8 GeV, in which case the duration of the spill matches the 10 or 50 Hz repetition cycle depending on the final energy. Fast extraction is required when the beam has to be transferred to a possible future higher energy synchrotron. It is also required for neutrino production.

5.3.1 Fast Extraction

The components for fast extraction are shown in Figure 5.3.1. The procedure is similar to the one used for extraction from the Booster, and the septum and kicker magnets have similar characteristics to those shown in Table 3.3.1. The only relevant change, with marginal consequences, is that the lattice of the long straight section in the Decelerator is different.

5.3.2 Resonant Extraction

To accomodate resonant extraction from the Decelerator, a large horizontal beta function is required in the long straight section where the electrostatic septum is to be installed. A value of the beta function of about 50 m can easily be obtained by tuning the triplets at both ends of the insertion. Resonant extraction can then be done with either a half-integer or a third-order resonance.

The beam spill can be obtained with a half-integer resonance by adjusting the horizontal tune to a value just above 5.5 and then approaching the $2\nu_h = 11$ resonance from above. A diametrically opposed pair of perturbing quadrupoles, powered oppositely so as to create an 11th harmonic perturbation without exciting a 0th harmonic signal, is used to create a narrow stop-band centred about $\nu_h = 5.5$. At the same time, a pair of octupoles are powered so as to make the tune amplitude-dependent. During extraction the perturbing quadrupoles are ramped up while the octupoles are fixed in strength. Particles with large betatron amplitude will enter the half-integral stop-band first; their motion will be unstable and move away from the central orbit towards the electrostatic deflector. Parameters are adjusted so that, between two consecutive turns, a particle has a better than 99% chance to be extracted cleanly without hitting the wires of the electrostatic septum. The most demanding case corresponds of course to the extraction of a 6 GeV proton beam. The same configuration will work equally well for slower protons and for heavy ions at all energies.

Resonant extraction can also be executed with a third-order resonance. In this case, the betatron tune is first adjusted to just above the third-order value $\nu_h = 5.667$, and the

resonace is created with a pair of sextupoles located in such a way to generate the $3 \nu_h = 17$ harmonic. If the sextupoles which compensate for the natural chromaticity are turned off, the particles will acquire a betatron tune which is momentum dependent. During the spill, the sextupoles are ramped up so that the stable region shrinks; first the particles with lower momentum, i.e. higher tune, will leave the stable region. Seen from the electrostatic septum, the particles will move away from the centre along one of the separatrices towards the septum wires.

5.4 The Magnet System

The Decelerator lattice consists of 32 bending magnets, 16 horizontally focussing quadrupoles (QF) and 12 vertically focussing quadrupoles (QD). In addition there are 8 quadrupoles of Q1, Q2 and Q3 type, respectively of length 1000 mm, 1000 mm and 500 mm.

The magnet cycle of the Decelerator for heavy ion operation is shown in Figure 1.2.1. The flat top of the cycle, which lasts 1.6 seconds, accomodates multi-turn injection and time to cool the secondary beam coming out of the target in the Transfer Line. The magnetic rigidity of the beam is reduced following the charge state ratio before and after the production target; according to different species the injection magnetic field ranges between 0.74 T (uranium) and 1.26 T (sulfur) (see Figure 5.6.3). After deceleration down to a few MeV/u the required magnetic field is reduced to 0.042 T for the uranium case and to .069 T for the sulfur ion. Deceleration takes place in 0.3 sec and the reset time is 0.1 sec.

Because in proton operation the Decelerator is used as a storage ring, the magnetic field is held at a constant value of 0.36 T at 1.2 GeV and 1.26 T at 5.8 GeV.

A possible choice for the magnet design, driven by both economic and technical cosiderations, is to make use of the Booster design; because of the lower frequency, the number of the dipole subconductors is reduced to 3, as shown in Figures 5.4.1 and 5.4.2, maintaing the same coil dimensions. Consequently the specifications are the same as those described in section 3.5. Parameters for the bending magnets and the quadrupoles are listed in Tables 5.4.1-2-3.

5.5 Power Supply

Because of the special magnet cycle, the Decelerator is ramped with a digital power supply. A resonating system seem unsuitable because of the relatively slow variation of the guide field, and because of the form of the cycle.

Table 5.4.1: List of parameters Dipole magnets of the Decelerator .

Parameter	Unit	Heavy Ion	Proton
Type of magnet		Curved H	
Number of Magnets		32	
Bending Angle	degrees	11.25	
Bending Radius	m	17.60	
Core Length	mm	3360	
Magnetic Length	mm	3460	
Gap Height	mm	100	
No. Pancakes per Magnet		4	
No. Turns per Pancake		5	
Conductor Dimensions	mm^2	17.0×78.0	
Minimum Field	T	0.0690	——-
Maximum Field	T	1.2643	1.2643
Minimum Current	A	276.8	——-
Maximum Current	A	5085.7	5085.7
Max Current Density	A/mm^2	4.62	4.62
Max $\dot{I}$	kA/s	48.1	——-
DC Resistance	mΩ	2.91	
Inductance	mH	5.50	
Dissipated Power	kW	65.32	75.30
Copper Weight	ton	1.45	
Iron Weight	ton	13.6	
Dissipated Power,total	MW	2.10	2.41
Stored Energy,total	MJ	2.3	2.3

Table 5.4.2: List of parameters for the QF magnets of the Decelerator

Parameter	Unit	Heavy Ion	Proton
Type of magnet			QF
Number of Magnets			16
Core Length	mm		530
Magnetic Length	mm		600
Pole Tip Radius	mm		70
No. Turns per Pole			4
Conductor Dimensions	mm²		17.0×52.0
Minimum Gradient	T/m	0.479	——-
Maximum Gradient	T/m	8.772	8.772
Minimum Current	A	240.1	——-
Maximum Current	A	4419.2	4419.2
Max $\dot{I}$	kA/s	41.8	——-
Max Current Density	A/mm²	6.02	6.02
DC Resistance	mΩ		0.764
Inductance	mH		0.340
Dissipated Power	kW	13.00	14.92
Copper Weight	kg		185
Iron Weight	kg		680
Dissipated Power,total	MW	0.214	0.240
Stored Energy,total	kJ	53.4	53.4

Table 5.4.3: List of parameters for the QD magnets of the Decelerator

Parameter	Unit	Heavy Ion	Proton
Type of magnet		QD	
Number of Magnets		12	
Core Length	mm	430	
Magnetic Length	mm	500	
Pole Tip Radius	mm	70	
No. Turns per Pole		4	
Conductor Dimensions	mm^2	17.0×52.0	
Minimum Gradient	T/m	0.479	——-
Maximum Gradient	T/m	8.768	8.768
Minimum Current	A	240.1	——-
Maximum Current	A	4419.2	4419.2
Max $\dot{I}$	kA/s	41.8	——-
Max Current Density	A/mm^2	6.02	6.02
DC Resistance	mΩ	0.655	
Inductance	mH	0.280	
Dissipated Power	kW	11.0	12.8
Copper Weight	kg	160	
Iron Weight	kg	550	
Dissipated Power,total	MW	0.132	0.154
Stored Energy,total	kJ	33.	33.

extraction kicker
(vertical)

lambertson magnet
(horizontal)

QF   B   Q3   Q2 Q1   Q1 Q2   Q3   B   QF

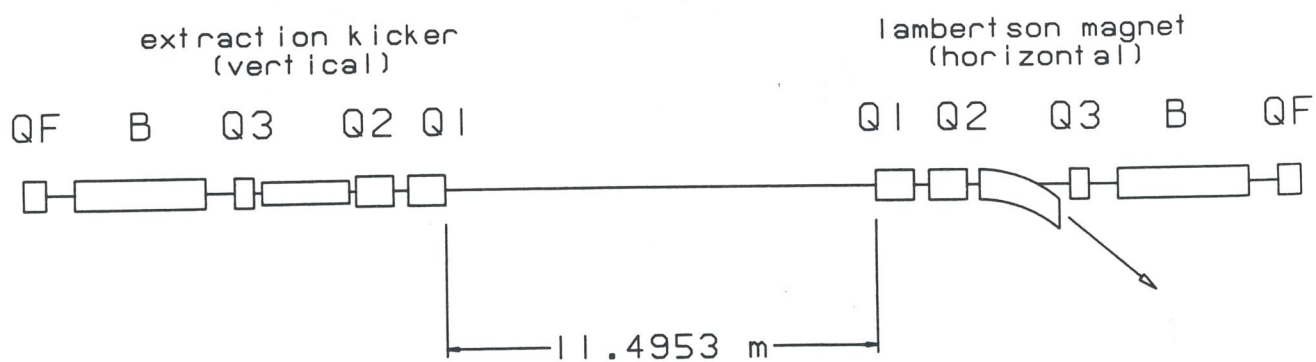|——————11.4953 m——————|

Figure 5.3.1: Layout of the Extraction System in the Decelerator.
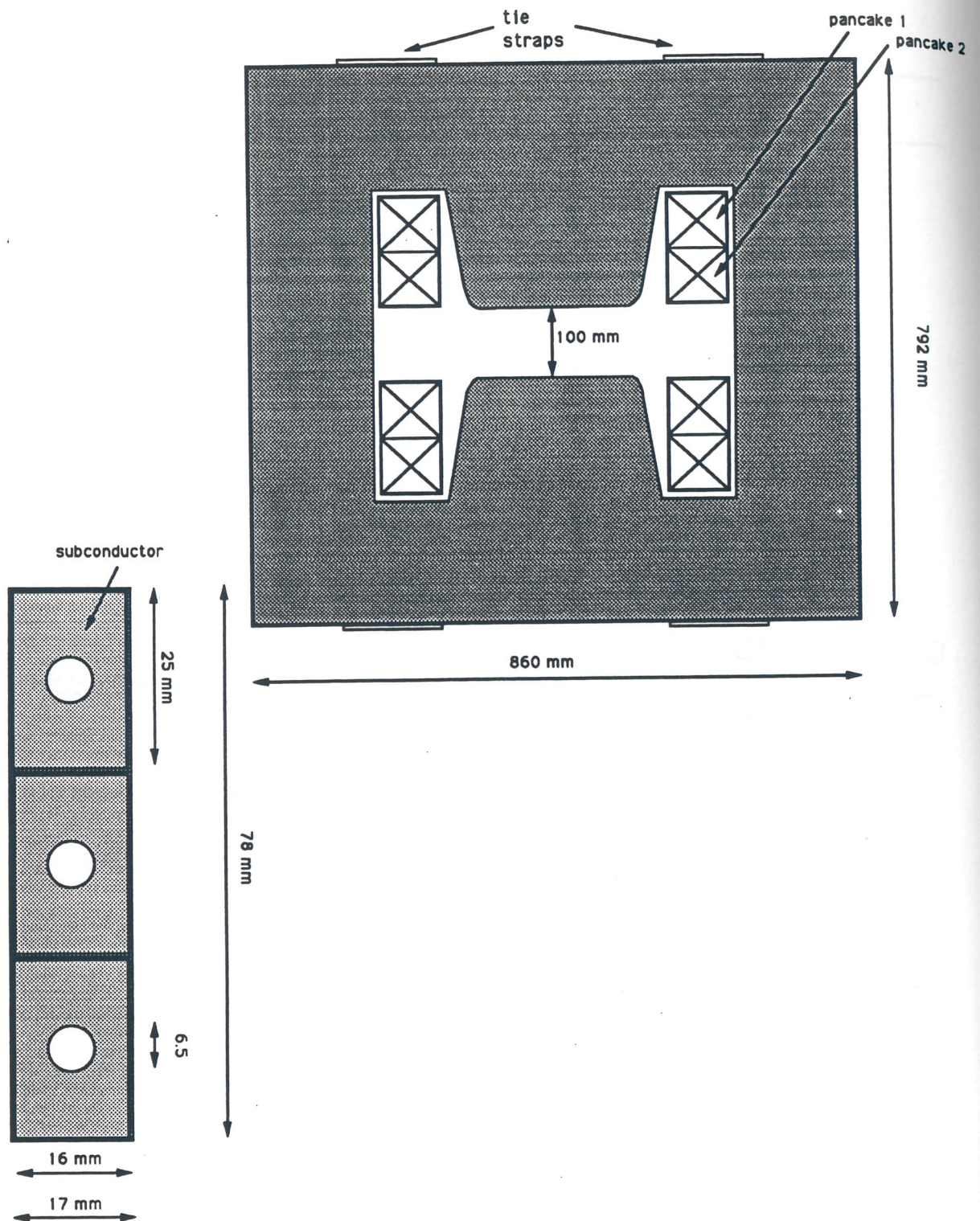
Figure 5.4.1: a) Cross-Section of the Dipole Magnets;
b) Cross-Section of the Dipole Conductor.

140 mm

155 mm

590 mm

25 mm

52 mm

6.5 mm

16 mm

17 mm
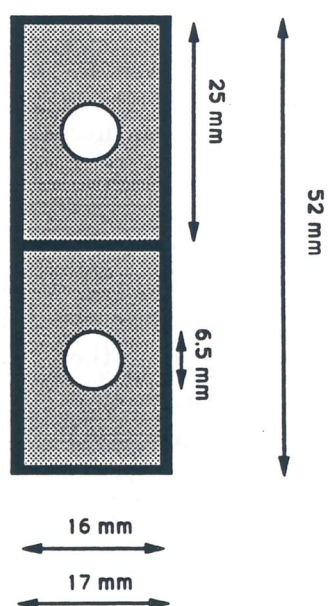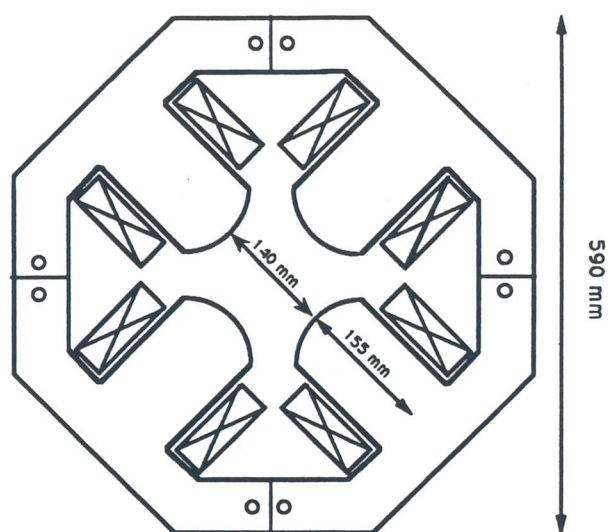
Figure 5.4.2: a) Cross-Section of the Quadrupole Magnets;
b) Cross-Section of the Quadrupole Conductor.

5.6 rf System

The rf system in the Decelerator has to fulfill three purposes: capture and bunch rotation, rf stacking, and deceleration. All these functions are accomplished with a dedicated rf system as explained below.

5.6.1 Bunch Rotation

After being produced at the target in the Transfer Line between the Booster and the Decelerator, bunches of heavy ion fragments are injected into the Decelerator in a single turn. The corresponding beam parameters are listed in Table 5.6.1. The nominal kinetic energy is roughly equal to that of the primary beam. The bunches are 0.5 ns long (rms) for all species, the same length as the bunches of primary particles before they hit the target. Fragments are captured with a full momentum spread of 0.7% for all species. Because the selected species have mass numbers fairly close to that of the primary beams, the operation can be described with reference to the isotopes listed in Table 5.6.1, fully stripped; there is indeed no requirement to accumulate exotic elements with mass number below 30.

After injection, the beams are captured in a sequence of stationary buckets, with a height chosen so that a mismatch will result between the shape of the bunches and the buckets. The bunches then rotate and, after one quarter of a synchrotron oscillation, they have traded momentum spread for bunch length; they are now longer and have a smaller momentum spread [1].

For efficient bunch rotation, it is important to select a bucket height that optimizes the reduction of the momentum spread without introducing unnecessary nonlinear distortions. Experience has shown that a bucket height 1.4 times the momentum spread is a good choice. If the frequency of the rf buckets is chosen equal to the bunch spacing then a reduction of the momentum spread, or equivalently an increase of the bunch length by a factor of seven can be expected.

Table 5.6.2 gives the required frequencies and voltages for different species. The most demanding case corresponds to the heaviest ions. The 'Rotation Period', i.e. the time needed to accomplish the rotation efficiently, is also shown; it is about one third of one synchrotron period. Towards the end of the rotation, the rf voltage must be quickly reduced to the smaller value required for matching the rf buckets to the shape of the bunches.

The cavity that performs the bunch rotation is a modification of the one used in the Fermilab Debuncher [2], shown in Figure 5.6.1. One of the main changes is that this cavity must operate at a wide range of discrete frequencies, listed in Table 5.6.2. The tuning range required for bunch rotation is 26 to 47 MHz, which can be achieved with a set of tuners at proper locations along the cavity.

The second critical task is to turn off the cavities in a very short time. This is done by abruptly inverting the loadline of the amplifier so that the tetrodes run at very high peak currents for a few cycles and absorb most of the energy from the cavity. With this scheme, it is possible to reduce the voltage to the desired value in about 20 μs [2]. Since for the operation of the Decelerator it is necessary to turn the rf off in about half that time, some improvements are required. For instance, it will be necessary to modify the loop that couples power into and out of the cavity: the rate at which the cavity can be turned off depends upon the rate at which flux is coupled into the driving loop. This is limited by current, voltage

and series inductance. Should an optimum trade-off between these parameters prove to be insufficient, a further improvement may be obtained with a dedicated loop activated by fast switching devices.

It is reasonable to assume two cavities for bunch rotation, each capable of producing 700 kV. It is then necessary to turn the voltage down to a low value of a few tens of kilovolts, as shown in Table 5.6.2, so that the rf buckets are matched in shape to the bunches at the end of rotation. After this point, to avoid problems with multipactoring, the voltage is maintained on each cavity; yet the total effective voltage as seen by the beam can be reduced essentially to zero in few milliseconds by driving the two cavities at opposite phases.

Figure 5.6.1 shows the Fermilab debuncher cavity; this can be reduced in length to 1.5 metres for present purposes, allowing two of them to fit comfortably in one of the long straight sections of the Decelerator as shown in Figure 5.6.2.

5.6.2 rf Stacking

Once the beam bunches have been rotated, they must be slightly decelerated to an inner orbit where they are released on top of the previously stored pulses. On this orbit the beam is cooled by an electron beam and by stochastic cooling. The operation of RF displacement is performed by a second rf system.

The rf displacement decelerates the beam by an amount corresponding to a momentum variation of -1.2%. The momentum spread of the beam at the end of bunch rotation is about 0.1 - 0.2% for all species, and the bunch length spans almost the full rf bucket length. As the bunch rotation system is turned off, the new rf system is turned on at the same frequency so that the beam bunches remain trapped by stationary buckets. By changing the synchronous phase angle of the second rf system, the rf buckets move and decelerate the beam. To minimize the amount of rf voltage, the synchronous phase is kept as low as possible; the deceleration to the inner orbit takes a time which is typically several milliseconds. All the major beam and rf parameters for the bunch displacement are shown in Table 5.6.3. At the end of the displacement, the rf cavities are turned off adiabatically, releasing the bunches.

The rf cavities required for this operation are a further modification of the Fermilab Debuncher cavity mentioned above. This system must be able to run at all the frequencies at which bunch rotation is done, to capture the beam and to decelerate it to a 1.2% lower momentum, which corresponds to a frequency swing of a fraction of one percent. To do this the stacking cavity uses a tuner that provides the frequency shift, in addition to the tuner used to set the initial frequency as done for the bunch-rotating cavities. This is possible because the voltage required is now considerably lower (see Tables 5.6.2-3).

The total voltage required can be provided with two cavities, again 1.5 metres long, which are located as shown in Figure 5.6.2. To turn effectively the voltage off and to vary the synchronous phase angle, the two cavities are operated at opposite phases.

5.6.3 Deceleration of Heavy Ions

The third system of rf cavities is required for the deceleration of the ion beams at the end of the stacking and cooling process. A final momentum spread of about 10^{-4} for all ion

species is expected after cooling. The rf is turned on adiabatically to bunch and capture the coasting beam, at the same harmonic number selected in the corresponding acceleration process in the Booster. The beam is decelerated from the initial kinetic energy of few GeV/u to about 10 MeV/u, which corresponds to the Coulomb potential barrier. The magnetic field cycle of the Decelerator is shown in Figure 5.6.3; during the deceleration proper, the field varies linearly over a period of 0.3 sec. The beam parameters and the rf requirements are listed in Table 5.6.4, while the frequency and voltage requirements are shown in Figure 5.6.4; they are approximately the same for all ion species and need a total of 50 kV being needed. Deceleration stops at the lowest rf frequency of 5 MHz. The end of the deceleration is chosen to correspond to the lowest rf frequency of 5 MHz.

The rf cavities for deceleration are similar to those employed for acceleration in the Booster since the same voltage per gap and frequency modulation are required. It is estimated that four of these cavities are needed, two of the LFRF and two of the HFRF type; their location is shown in Figure 5.6.2.

5.6.4 rf System for Protons

The Decelerator can be operated in two different ways for protons. It can be used as a Stretcher for slow-spill extraction, in which case the beam does not need to be bunched. It can also be used as a Holding Ring should the complex be used as an injector for a possible subsequent stage of a larger hadron facility. For this mode of operation, the beam needs to be kept bunched before it can be transferred. The voltage requirement is however very modest, being about 100 kV, and no frequency modulation is required. Two single-gap cavities of the VHRF type, tuned at 50.5 MHz are adequate. Their location in the ring is shown in Figure 5.6.2, and they can be added at a later stage if required.

Table 5.6.1: Beam Parameters at Injection into the Decelerator

	S	Cu	I	Au	U	
Mass Number, A	32	63	127	197	238	
Charge State	16	29	53	79	92	
Rest Energy, E_0	0.9305	0.9303	0.9307	0.9313	0.9316	GeV/u
Kinetic Energy	2.53	2.08	1.37	1.03	0.85	GeV/u
β	0.963	0.951	0.914	0.880	0.852	
No. Bunches/pulse	24	30	39	45	49	
Bunch length (rms)	0.5	0.5	0.5	0.5	0.5	ns
Momentum Spread	0.7	0.7	0.7	0.7	0.7	%
No. ions/pulse	$2.6 \cdot 10^8$	$1.3 \cdot 10^8$	$2.8 \cdot 10^7$	$8.1 \cdot 10^6$	$7.7 \cdot 10^6$	

Table 5.6.2: rf requirements for Bunch Rotation

Bunch length (rms)	0.5 ns
Bunch momentum spread (full)	0.7%
Bucket-to-bunch height factor	1.414

	S	Cu	I	Au	U	
Kinetic Energy	2.53	2.08	1.37	1.03	0.85	GeV/u
β	0.963	0.951	0.914	0.880	0.852	
Harmonic no.	24	30	39	45	49	
RF Frequency	25.99	32.07	40.09	44.53	46.91	Mhz
RF Voltage	0.147	0.329	0.805	1.17	1.43	MV
Bunch area (rms)	0.0072	0.0061	0.0043	0.0034	0.0029	eV/u-s
Synchrotron Period	629.	261.	86.5	51.0	37.9	μs
Rotation Period	189.	78.3	25.9	15.3	11.4	μs
Rotation Factor	12.7	10.3	8.3	7.4	7.0	

Table 5.6.3: Parameters for the rf Displacement
    (from $\delta p/p = 0.5\%$ to $\delta p/p = -0.7\%$)

	S	Cu	I	Au	U	
RF Phase Angle	20	10	5	5	5	degrees
Harmonic No.	24	30	39	45	49	
Bucket Area	0.087	0.073	0.052	0.041	0.035	eV/u-s
RF Frequency	25.99	32.07	40.09	44.53	46.91	MHz
RF Frequency Swing	0.030	0.058	0.140	0.213	0.273	%
Time Duration	27.8	29.9	17.7	8.5	5.7	ms
Stationary Bucket						
RF Voltage	1.8	6.2	23.6	42.3	57.5	kV
Bucket Height	0.11	0.14	0.17	0.19	0.20	±%
Synchrotron Period	5.67	1.91	0.51	0.27	0.19	ms
Moving Bucket						
RF Voltage	7.5	12.8	34.8	62.1	84.5	kV
Bucket Height	0.16	0.17	0.19	0.21	0.22	±%
Synchrotron Period	2.87	1.34	0.42	0.22	0.16	ms

Table 5.6.4: Parameters of the Deceleration ramp

|	S	Cu	I	Au	U	
Harmonic No.	24	30	39	45	49	
Bunch area (rms)	0.0073	0.0062	0.0043	0.0034	0.0029	eV/u-s
Normal. Emittance	12.8	10.5	7.9	6.7	6.0	πmm-mrad
Top of Cycle						
Kinetic Energy	2.53	2.08	1.37	1.03	0.85	GeV/u
β	0.963	0.951	0.914	0.880	0.852	
Magnetic Field	1.263	1.176	0.953	0.815	0.741	T
RF Frequency	25.99	32.07	40.09	44.53	46.91	MHz
Emittance	3.56	3.43	3.50	3.59	3.68	πmm-mrad
Bottom of Cycle						
Kinetic Energy	16.45	10.43	6.13	4.59	3.87	MeV/u
β	0.186	0.148	0.114	0.099	0.091	
Magnetic Field	0.0665	0.0574	0.0485	0.0437	0.0416	T
RF Frequency	5.00	5.00	5.00	5.00	5.00	MHz
Emittance	67.6	70.1	68.7	67.0	65.4	πmm-mrad
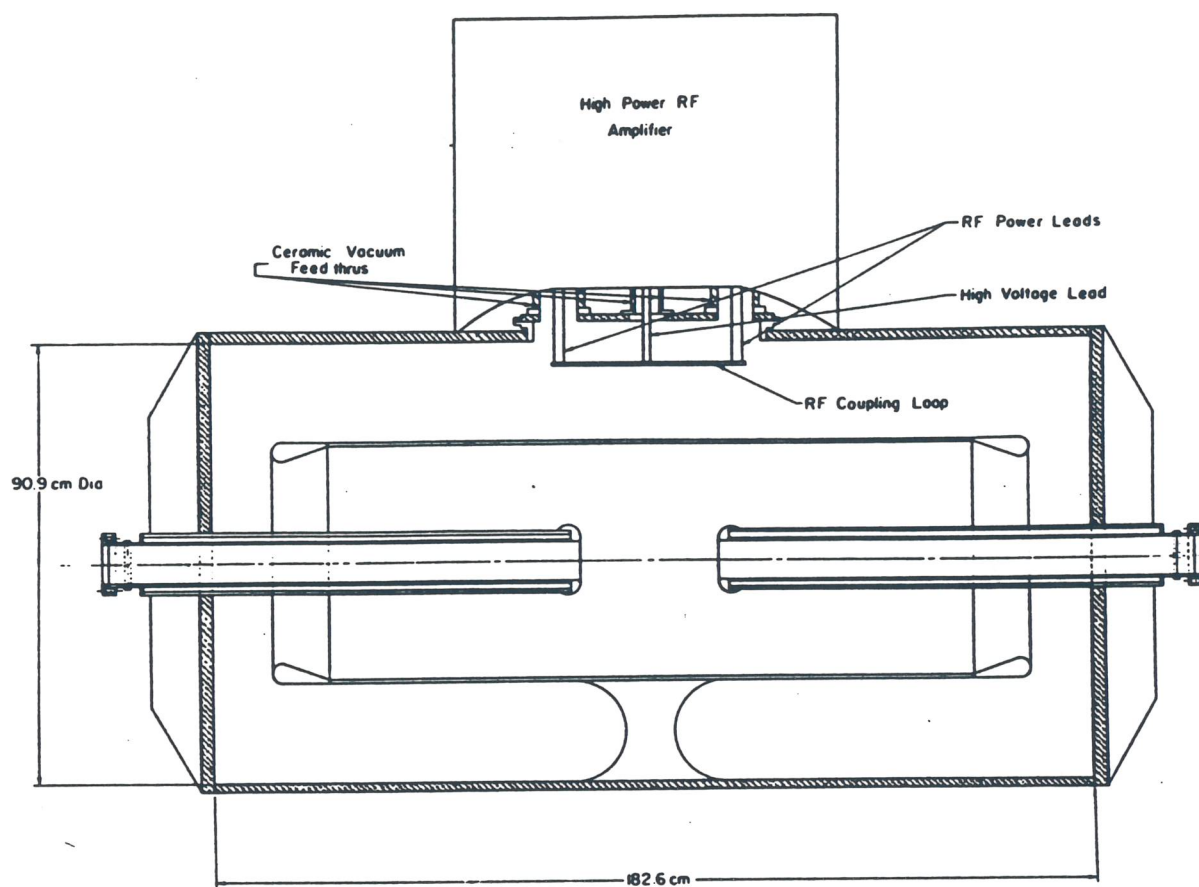
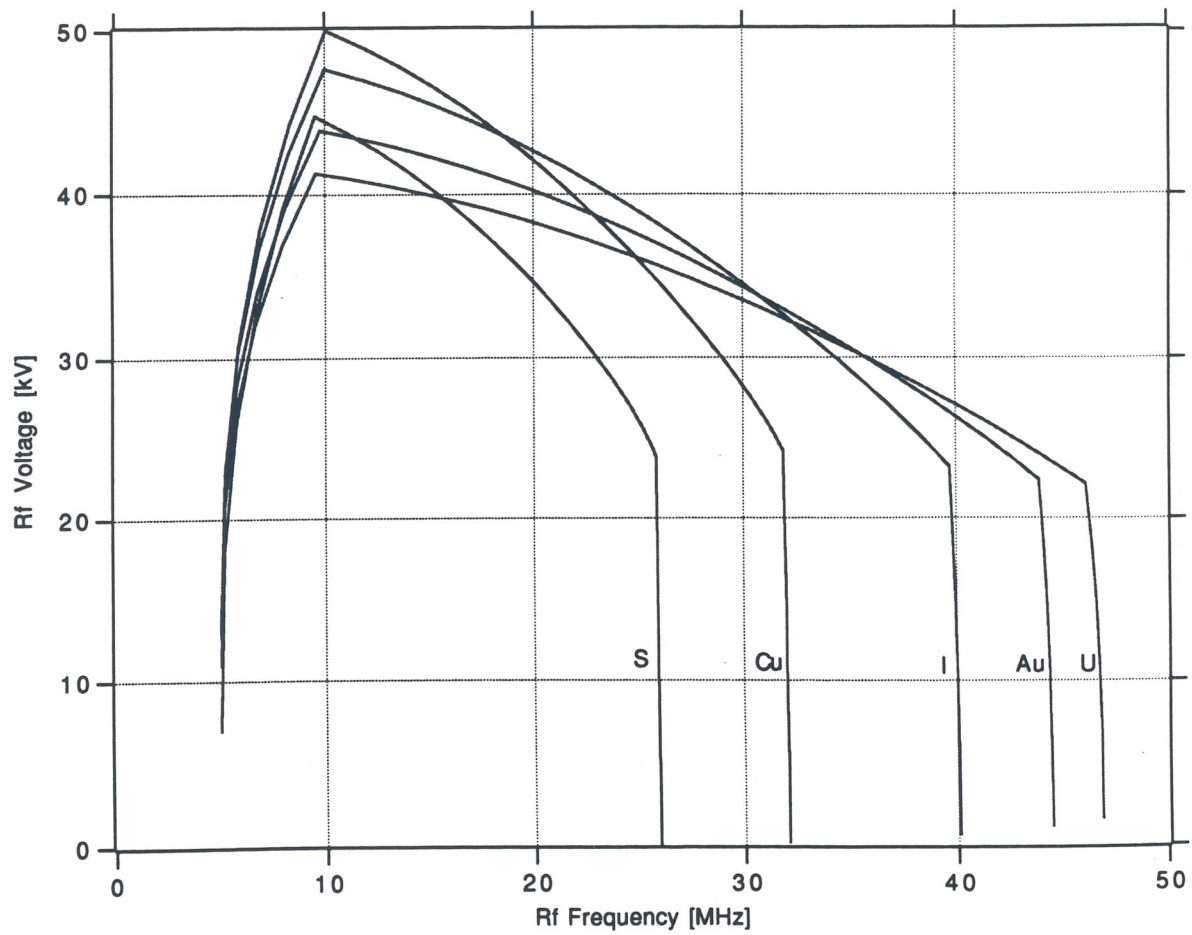Figure 5.6.1: The Fermilab Debuncher Cavity.

Figure 5.6.4: Voltage vs. Frequency during Deceleration.

5.7 The Vacuum System

The same considerations that applied to the vacuum in the Booster also apply to the vacuum in the Decelerator. The vacuum requirements are again different for the two cases of protons and heavy ions. Because the proton beam circulates in the Decelerator for at most 100 ms at a relatively high energy, no severe vacuum requirements are expected for this case, which will not be considered any further. On the other hand, heavy ion beams present more stringent conditions.

5.7.1 Vacuum Requirements

Heavy ions are stored in the Decelerator for as long as 2 seconds. For most of this time the particles circulate at maximum energy, but then they are decelerated down to about 10 MeV/u over a time of 0.3 sec; at the end of the deceleration, the velocity β is only ~ 0.1. Since the ions are completely stripped, the most important vacuum related effect is electron capture from the residual gas. This process has already been discussed in section 3.8; the cross-section is given by Equation (3.8.2) and the rate of the beam loss is estimated with the help of Equation (3.8.3), which can be integrated over the entire cycle to calculate the beam depletion. Again the heaviest ions demand the hardest vacuum. It is estimated that a nitrogen equivalent vacuum of 10^{-8} mm Hg will keep the beam loss below 3%.

5.7.2 The Vacuum Chamber

The variation of the guide field with time in the Decelerator is considerably slower than in the Booster. The field is constant for about 1.6 sec and then varies over a period of 0.3 sec for beam deceleration. The maximum rate of change is 13 T/s, occurring once every two seconds when the field is reset at the beginning of each accumulation cycle (see Figure 1.2.1).

The most convenient way to achieve and maintain a vacuum of 10^{-8} mm Hg is to employ a metallic vacuum chamber, made of either stainless steel or aluminium, with a thickness of 2 millimetres. This vacuum chamber subtracts little from the vertical magnet aperture of 10 cm, and provides good electromagnetic screening of the beam from the magnet laminations. Because of the lower rate of field variation during the deceleration cycle, heating and field distortions due to eddy currents are relatively small and can be tolerated. In principle, the required level of vacuum can be achieved without baking or conditioning the vacuum chamber; if in the future a vacuum upgrade should be found necessary, this can be easily achieved with a solid vacuum chamber in place.

As in the Booster, the vacuum chamber inside the dipole magnets is rectangular, 10 cm vertically × 15 cm horizontally; elsewhere the vacuum chamber is circular with 7 cm radius. The two vacuum chamber sections are joined by bellows at the dipole ends.

5.7.3 The Vacuum Pumps and Valve System

The arrangement of the vacuum pumps, flanges etc. in the Decelerator is the same as in

the Booster and is described in section 3.8.4. The two rings have in fact the same geometry and size; the vacuum requirements are about the same and the mode of operation is also expected to be the same.

5.8 Diagnostics and Instrumentation

The Decelerator and the Booster have the same geometry and size; the lattices are similar with the same arc configuration, differing only in the quadrupole arrangement in the long straight sections. It is thus reasonable to expect that both rings can be equipped with the same diagnostics and instrumentation, which is already described in section 3.9. To be more specific, one can opt for the same distribution of beam position monitors and closed orbit correctors, all located next to the quadrupoles and divided into two families. However, in the Decelerator, beam position monitors have a larger dynamic range, since they have to measure beam positions to a fraction of a millimetre with a beam intensity as low as 10^6 heavy ions per pulse. Figure 3.9.1 would still represent a reasonable configuration of the arc cell.

The components for stochastic cooling can also be valuable additions to the beam instrumentation; for fast cooling, a beam Schottky signal has also to be available.

Again, the sextupole arrangement in the Decelerator is the same as in the Booster. There is no important reason to include sextupoles at first; they can be added easily later if necessary. No sextupoles are required in the long straight sections.

5.9 Cooling Techniques

Two cooling techniques are planned for the Decelerator: electron [3] and stochastic cooling [4]. Both are needed since they have features which complement each other. Electron cooling does not depend on the beam intensity, is very effective at low energy, and affects mostly the core of the beam. Stochastic cooling works at any energy; it depends on the number of particles in the beam, and it effectively brings the tails to the centre of the distribution. Electron cooling is limited by the electron beam density and its temperature, stochastic cooling by the available electronic bandwidth and power. Electron cooling operates on the beam momentum spread and both betatron emittances at the same time; two different stochastic cooling systems are required for momentum and betatron cooling.

5.9.1 Cooling Requirements

The requirements for beam cooling in the Decelerator are as follows: the beam momentum spread has to be continuously reduced to make room for twelve pulses of fragments during the accumulation process. The beam momentum spread must be sufficiently small at the end of accumulation to allow it to be captured and decelerated by a reasonable amount of RF voltage. During deceleration the beam momentum changes by a factor of ten, so that momentum spread and betatron emittance will increase by the same factor; as a consequence the cooled beam must be small enough to avoid excessive growth during deceleration. Cooling may also be useful at the end of the cycle, to obtain a smaller momentum spread if required by users.

The most demanding requirements for cooling are imposed by the accumulation process. The momentum spread δ of the stack varies according to the following equation:

$$\frac{d\delta}{dt} = -\lambda\delta + D \tag{5.9.1}$$

where λ is the cooling rate and D is the increase of 0.2% in momentum spread due to the addition of a new pulse to the stack every 100 ms. By setting the overall cooling time to 150 ms, the average momentum spread in the stack during the accumulation procedure is maintained to 0.3%. To achieve the required cooling rate, both electron cooling and momentum stochastic cooling are required, each providing a cooling time of 0.3 sec. With a second cooling period of 0.5 sec at the same rate after the stacking cycle, the total beam momentum spread is finally reduced to about 10^{-4}.

Electron cooling alone is adequate for the reduction of the beam emittance. Betatron cooling proceeds at twice the rate of momentum cooling; thus, over a period of 0.5 sec, the betatron emittance can be reduced by at least an order of magnitude. Betatron stochastic cooling is not required; it is in any case more difficult to achieve because of the bad mixing situation due to the relatively small momentum spread of the beam.

5.9.2 Electron Cooling

The electron cooling apparatus, similar to the device at present operating at LNL [5], is shown schematically in Figure 5.9.1 and its location in the ring is shown in Figure 5.6.2. The design is based on the following formula for the cooling rate

$$\lambda = \frac{4\pi Q^2 r_e r_p L \eta J / e}{A \beta^4 \gamma^5 \theta^3} \tag{5.9.2}$$

where r_e and r_p are the electron and proton classical radii [6,7,8]; Q is the charge state and A the mass number of the particles being cooled; η is the ratio of the electron beam length to the ring circumference; L is the Coulomb logarithm; β and γ are respectively the velocity and the energy relativistic factors of the beam; J is the electron beam density

$$J = \frac{I}{\pi a^2} \tag{5.9.3}$$

with I the electron beam current and πa^2 the cross-section. Finally,

$$\theta^2 = \theta_{ion}^2 + \theta_{electron}^2 \tag{5.9.4}$$

where θ_{ion} and $\theta_{electron}$ are the relative velocity spreads in the ion and electron beams. For each, there are two contributions: a longitudinal one $\theta_{\parallel}$ and a transverse one $\theta_{\perp}$, so that:

$$\theta^2 = \theta_{\parallel}^2 + \theta_{\perp}^2 \tag{5.9.5}$$

Because of the high intensity, the electron beam is confined to the required dimensions by a solenoidal field along the entire interaction length. If the field is strong enough the trajectories of the electrons are essentially parallel lines directed along the main beam axis and the transverse temperature is effectively reduced, that is $\theta_{\perp} \sim 0$ for the electron beam.

Further, with a resonable cathode design we can expect $\theta_{\parallel} = 0.001$. The longitudinal temperature of the proton beam is given by its momentum spread

$$\theta_{\parallel} = \frac{1}{\gamma} \frac{\Delta p}{p} \tag{5.9.6}$$

and the transverse temperature by the beam emittance

$$\theta_{\perp}^2 = \epsilon / \beta^* \tag{5.9.7}$$

where β^* is the value of the lattice function at the centre of the interaction region.

The parameters corresponding to a cooling time of 0.3 sec are given in Table 5.9.1. The most important condition to be satisfied is that the electron beam velocity equals in magnitude and direction the velocity of the ion beam. For instance, to cool 1 GeV/u ions, the electron energy must be about 550 keV, which is the largest so far conceived for any application. Moreover, if one considers that the beam current is 12.5 A, it is seen that the beam power is 7 MW continuous; this is a very large value which places severe constraints on the energy recovery, system which requires an efficiency of better than 99%.

5.9.3 Stochastic Cooling

Momentum stochastic cooling is required to operate in parallel with electron cooling. Both systems are designed for a cooling time of 0.3 sec. The components for stochastic cooling are shown schematically in Figure 5.6.2. The Schottky current signal is detected by pickups consisting of pair of striplines located where the dispersion is zero [9]; the signal is amplified and filtered through a device called a "notch filter": a cable with length equal to half the ring circumference, shorted at the far end. The signal then travels to the next location, half of the ring circumference away, where it is distributed equally to a system of kickers which are also made of pairs of striplines identical to the pickups, and are located in dispersion-free regions.

An important parameter which describes the performance of stochastic cooling is the frequency bandwidth of the electronic system. This is chosen to optimize "mixing" between pickups and kickers; it depends on the ring transition energy γ_t and on the beam momentum spread. For the Decelerator the optimum bandwidth is 1-2 GHz, since the width of the Schottky band in the middle of this range is about half the revolution frequency, and there is overlapping between neighbouring Schottky bands at the upper end of the ampolifier bandwidth.

The main parameters of the stochastic cooling system are given in Table 5.9.2. Between pickups and kickers there is an variable cable delay of up to 150 ns to synchronize the kicker signal with the particle arrival at the kicker. The total power requirement of 1 kW is due to the Schottky signal after amplification; thermal power due to thermal noise at the exit of the pickups is low and of no consequences to the cooling performance.

Table 5.9.1: Electron Cooling Parameters

Specific Kinetic Energy	1.0	GeV/u
β	0.80	
Mass number	200	
Charge state	80	
Betatron emittance	20.0	π mm mrad
Momentum spread	0.28%	
β^* (h,v)	13, 6	m
Length of e-beam	8	m (3%)
Coulomb log	15	
e-beam semi-axis	10	mm
e-beam current	12.5	A
e-beam current density	4	A/cm^2
θ, total	1.3	mrad
Cooling time	0.3	s
e-beam energy	550	keV
e-beam power	7.1	MW
Final momentum spread	$\pm 0.01\%$	

Table 5.9.2: Stochastic Cooling Parameters

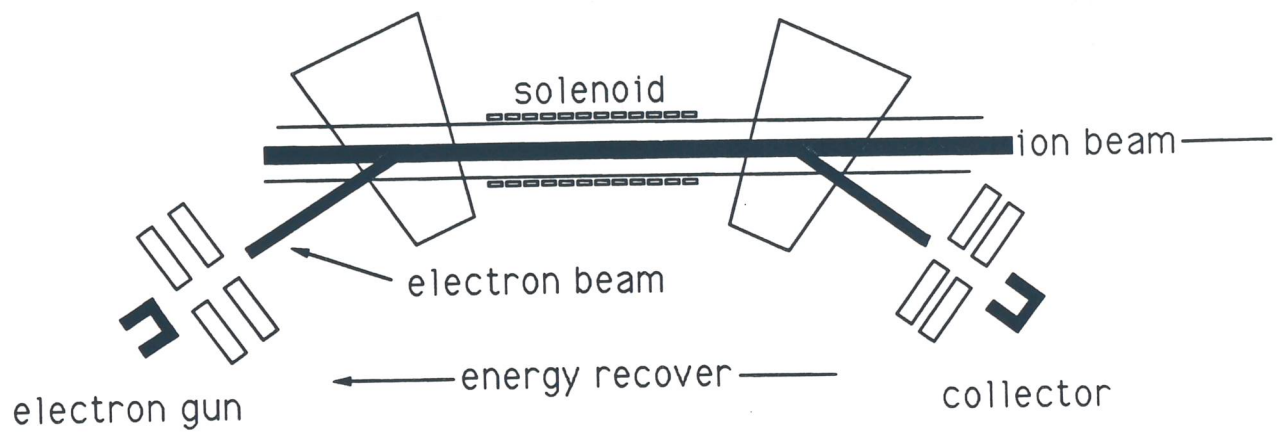|		
Number of Ions	$1 \cdot 10^7$	
Mass number	200	
Charge state	80	
Specific Kinetic Energy	1.0	GeV/u
β	0.80	
Bandwith	1-2	GHz
Method	Notch Filter	
No. of Pickups	16	
No. of kickers	32	
Schottky Power (initial)	1.0	kW
Thermal Power	negligible	
Amplifier Gain	160	dB

Figure 5.9.1: Schematics of the Electron Cooling Apparatus.

References

[1] J. Griffin et al., "Time and Momentum exchange for production and collection of Intense Antiproton Beams at Fermilab", IEEE tr. on Nu. Sci., NS-30, no. 4, August 1983.

[2] J. Griffin et al., "Design of th rf Cavity and Power Amplifier for the Fermilab Antiproton source", IEEE tr. on Nu. Sci., NS-30, no. 4, August 1983, 3435-7.

[3] G. I. Budker and A. N. Skrinsky, Sov. Phys. Usp. 21 (1978) 277.

[4] D. Möl, G. Petrucci, L. Thorndahl and S. van der Meer, Phys. Rep. 58, (1980) 75.

[5] L. Busso et al. "An Electron Cooling Device in the One-MeV Energy Range". Proceedings of the 13th HEPAC, Novosibirsk 1986. Page 344.

[6] T. Ogino and A.G. Ruggiero "The Physics of the Electron Cooling", Fermilab Internal Report p-bar 30 April 2, 1979.

[7] T. Ogino and A.G. Ruggiero, "Theory of Electron Cooling with Magnetic Field and Space Charge", Particle Accelerators 10, (1980) 197-205.

[8] T. Ogino and A.G. Ruggiero" Theory of Electron Cooling in Accelerators" Journal of the Physical Society of Japan, 49, No. 5, (1980) 1654-1664.

[9] A.G.Ruggiero and J.Simpson, "Momentum Precooling in the Debuncher Ring for the Fermilab Tevatron -I project", IEEE Trans. on Nucl. Sc., NS-30 No. 4, (1983).

[10] D.Möl, "Stochastic Cooling", CERN 87-03, p.453

6

Radiation Protection

While a full discussion of radiation protection considerations is premature for a feasibility study, space must be devoted to it because of its fundamental importance.

The main constraints on Radiation Protection for the complex are determined by the following energy fluxes:

- Heavy Ions beams with intensities of 10^{11} ions/s with specific energies in the GeV/u range;

- 100 μA of protons (6.25×10^{14} proton/s) with a kinetic energy of 1.2 GeV.

Because of the possible high intensity proton beams foreseen in the long term in the facility, and because of civil engineering and environmental constraints, the complex must be underground. Furthermore it is clear that the acceleration of such high intensity proton beams sets stringent constraints on all Radiation Protection items.

Following some recent studies on hadron facilities [1], a preliminary analysis of Radiation Protection can be made taking into account the three main items: active shielding, induced radioactivity, and radiation damage.

6.1 Active Shielding

Because so many subsystems are not yet fully defined, it is difficult at this stage of the proposal to finalise a design of the active shielding; furthermore it is still under discussion whether a tunnel or a large room (about 90 m in diameter) would be the better solution for the accelerator building. However, a rough evaluation of the active shielding can be based on the following assumptions:

a. In the worst possible accident, up to 20 pulses of 1.25×10^{13} protons at the maximum energy of 1.2 GeV may be dumped before the the acceleration cycle is aborted;

b. Short term local losses at any point in the ring, during tuning, may reach values of the order of 10^{-3} of the beam (6.25×10^{11} p/s) at 1.2 GeV;

c. Continuous losses of the order of 10^{-5} of the beam intensity in each metre of the vacuum chamber and of the order of 10^{-2} at some localized place, i. e. on a dedicated scraper in the injection section or on a septum magnet at the extraction;

d. The maximum dose rate at the surface must be limited to 10^{-2} mSv/h or to 10^{-2} mSv per accident event.

The amount of earth necessary to shield the accelerator housing can be evaluated by the following general expression for the dose rate at angles θ larger than 5° [2,3]:

$$H'(\theta) = 10^6 \times (kEI/R^2\theta^2)\, e^{-l(\theta)/\lambda} \quad (Sv/h) \qquad (6.1.1)$$

where k is the production factor of the target material (Be: 0.3, Fe: 0.5, W: 0.7), E the beam energy in GeV, I the beam loss in μA, R the distance in metres from the loss point, θ the angle in degrees between the detection direction and the beam axis, $l(\theta)$ the shielding thickness, and λ the effective attenuation length (iron: 20 cm, concrete: 50 cm, earth: 60 cm).

For the loss of 20 pulses at a single spot, the dose at a distance of 1 metre will be 10^3 mSv; the attenuation factor required to reduce the total dose per accident at the surface to 10^{-2} mSv is then 10^5, which corresponds to about 7.4 effective attenuation lengths or 4.4 metres of earth of average density 2.2 g cm^{-3}.

Continuous losses of 0.1 μA produce a dose rate of about 0.12 mSv/h at 8 metres, which implies at least about 10 attenuation lengths or 6 metres of earth, neglecting local shielding around the ring.

Continuous losses localized at some specialized devices (scrapers and collimators) produce a dose rate of about 1.2 mSv/h at the same 8 metres, which corresponds to 12 attenuation lengths; the required attenuation factor near these devices can be obtained by adding 2 attenuation lengths (0.4 m) of steel to the 6 metres of earth derived above.

A somewhat different approach to shielding calculation for this energy region has been adopted by Thomas and Stevenson [4], with results which are in agreement with equation (6.1.1).

At the full energy of 1.2 GeV, protons will enter the target area and be dumped after passing through the target. In the lateral direction a radiation level of 10^{-2} mSv/h requires about 15 attenuation lengths of shielding. For the present rough calculation for-forward shielding, the empirical equations described in ref [4] (page 216) are used (equation (4.4), with parameters extrapolated to 1.2 GeV using table 4.3, page 220). Given a proton beam of 6.25×10^{14} proton/s at 1.2 GeV, the total attenuation length required for forward shielding is about 18 attenuation lengths. Roof shielding of target areas will be dictated by skyshine radiation. Again 10^{-3} mSv/h can be taken as the limiting dose rate outside the laboratory fences at about 1 Km from the source. Using the semi-empirical model described in ref [4] the source term comes out to be about 20 Sv m^{-2} h^{-1} on the accelerator building roof. For a roof area of 100 m^2, the dose rate outside the roof will be 0.2 Sv/h. However, experience at PSI [1] shows that this level should be reduced by about two orders of magnitude. A roof about 10 attenuation lengths thick is necessary to reduce the dose equivalent rate to 2 M/Sv/h outside the roof, about 12 m away from the source.

When the complex is used to accelerate protons to 6 GeV at the repetition rate of 10 Hz the average intensity is a factor five lower than in the 50 Hz case; following the assumptions given above (a,b,c,d) where now about 4 pulses are lost in the same fixed time interval ($\approx$ 0.5 s) before the cycle abort, the required shielding thickness becomes 4.2 metres of earth, i.e. 20 cm less than for the high intensity operation mode at 1.2 GeV.

Active shielding will be also of paramount importance in the Fragment Production Area, where the primary beam of 10^{11} heavy ions/s hits the target. An empirical model for shielding calculation has been developed at Berkeley [5], where neutron production by Ne and Si ions on a thick Cu target at 670 Mev/u has been investigated. The dose equivalent for θ between 20° and 120° is given by the following semi-empirical law:

$$H(\theta) = 0.48 \times 10^{-12} N e^{-0.038\ \theta} r^{-2} e^{-l^*(\theta)/\lambda^*} \quad (Sv) \tag{6.1.2}$$

and for θ between 0 and 20° is given by:

$$H(\theta) = 12.0 \times 10^{-12} N e^{-0.20\ \theta} r^{-2} e^{-l^*(\theta)/\lambda^*} \quad (Sv) \tag{6.1.3}$$

where H is in Sv, r in metres, and N the number of ions stopped in the target. For a loss of 10^{11} ions/s and a dose equivalent rate of 10^{-2} mSv/h at 8 metres of distance and 90° from the source, the required shield thickness is 9 attenuation lengths. For forward angles (less than 10° and the same conditions, the required shield thickness is 14 attenuation lengths.

Finally the attenuation length for concrete (multiplied by the concrete density; $\lambda^* = \lambda \times \rho$) is given by the following:

$$\theta\ <\ 75° \quad \lambda^*(\theta) = 115.0\ e^{-0.01\theta} \quad g\ cm^{-2} \tag{6.1.4}$$

$$\theta\ >\ 75° \quad \lambda^*(\theta) = 55.0 \quad g\ cm^{-2} \tag{6.1.5}$$

The shielding thickness at 8 m of distance and 90° away from the beam line is then 2.3 m, and the shielding thickness in the forward direction is 6.6 m.

6.2 Induced Radioactivity

Maintenance workers receive an unavoidable radiation dose from radioactivity induced inside the beam lines and ring components. A "rule of thumb" which gives an induced gamma dose rate of 10^{-1} Gy/h at one metre of distance per μA of proton beam lost in an iron component 1 attenuation length long irradiated for 5-10 years [1] can be used to estimate the beam losses which will produce the maximum tolerable radiation levels for hands-on maintenance areas, namely 10^{-4} Sv/h. The result is a maximum continuous uncontrolled beam loss of less than 10^{-5} m^{-1}, or 10^{-3} of the beam at some localized points for short periods amounting to less than 1% of operating time.

Recent studies at TRIUMF [6] show that all beam defining collimators and scrapers require substantial local shielding. For example the 3 Gev Booster synchrotron of the KAON proposal has a scraper/catcher collimator system locally shielded by 80 cm of iron and 25 cm of borated concrete. According to TRIUMF estimate the scraper/catcher collimators are the only devices which will probably require shielding during transport to maintenance facilities.

6.3 Radiation Damage

According to [1] beam line components will be exposed to dose rates ranging from $1\,Gy/h$ up to $10^5\,Gy/h$. Continuous losses of the order of 10^{-5} of the beam per metre of the vacuum chamber, and local losses of the order of 10^{-2}, can be lethal for conventional installations. The local shielding described above also play an important role in reducing radiation damage; they will reduce the radiation dose rate in surrounding components (cables, electronics, etc.) inside the accelerator tunnel to about $10^5\,Gy$ in 10 years of operation (5000 h/year). Special care has to be taken with the components of the Isotope Separation Line where unstable fragments are produced and selected. In particular the magnets downstream of the production target and the profiled degrader (see chapter 4) have to be shielded from the radiation source. Further, magnet coils in the high radiation regions have to be made with mineral insulated cable [1].

6.4 Other Risks

Dedicated studies must be devoted to the understanding of associated risks of activation such as:

- Cooling Water activation
- Air activation
- Soil/Ground Water activation

Radioactivity produced in earth and groundwater can represent a few percent of the total radioactivity produced by a high intensity accelerator [4]. In particular, soil/ground water activation may be important because of the peculiar geology and hydrology of the Legnaro site. Because of air activation produced by short-lived isotopes coming from interactions near the primary beam lines, a closed circuit air system must be included.

References

[1] Proposal for a European Hadron Facility, edited by J.F. Crawford EHF-87-18, 18 May 1987.

[2] H. Sullivan, "Experience with target area shielding around the CERN 26 GeV proton synchrotron". Paper presented at the TRIUMF KAON Factory workshop, June 1986.

[3] G. R. Stevenson,"The determination of shielding for high energy proton accelerator", CERN HS-RP/010/CF (1976).

[4] R. H. Thomas and G. R. Stevenson, "Radiological safety aspects of the operation of proton accelerators", International Atomic Energy Agency, Vienna, 1988.

[5] J. B. McCaslin, P. R. LaPlant, A. R. Smith, "Neutron production by Ne and Si ions on a thick Cu target at 670 MeV/u with application to radiation protection", IEEE Trans. Nucl. Sci. NS-32 No. 5 (1985) 3104-3106.

[6] KAON Factory study, Accelerator Design Report, 1990.